PhD-FSTC-3-2008
The Faculty of Sciences, Technology and Communication

DISSERTATION

Defense held on 28/05/2008 in Luxembourg

in candidature for the degree of

DOCTOR OF THE UNIVERSITY OF LUXEMBOURG

IN SCIENCES DE L'INGÉNIEUR

by

Alexander Arkhipov
Born on 18 June 1974 in Dubna/Moscow

IFDMA FOR UPLINK MOBILE RADIO COMMUNICATION SYSTEMS

Dissertation defense committee:

Dr. Ulrich Sorger, dissertation supervisor
Professor, University of Luxemburg

Dr. Alex Gershman
Head of Communication Systems Group
Darmstadt University of Technology

Dr. Jürgen Sachau, Vice Chairman
Professor, University of Luxemburg

Dr. Michael Schnell
Head of Aeronautical Communications Group
German Aerospace Center (DLR)

Dr. Pascal Bouvry, Chairman
Professor, University of Luxemburg

Foreword

The present thesis was performed during my work as a researcher at the Communication Systems research group of Institute of Communications and Navigation at the German Aerospace Center (DLR) in Oberpfaffenhofen.

I would like to thank all those who supported me during this period. Special thanks go to Dr.-Ing. Michael Schnell for his support and permanent willingness for discussions. I am especially grateful to colleagues of DLR for the fruitful exchange of ideas during our involvement in research projects and for the pleasant working environment. The special thanks go to Dr.-Ing. Snjezana Gligorevic for reviewing an early version of the thesis and providing me with useful and valuable inputs.

Furthermore, I would like to thank the chairman of the examination committee Prof. Dr. Pascal Bouvry, second examiner Prof. Dr. Alex Gershman from the Darmstadt University of Technology and the supervisor of this thesis, Prof. Dr.-Ing. Ulrich Sorger from the University of Luxemburg. Their advises and hints contributed considerably to the quality of this thesis.

Munich, February 2008 Alexander Arkhipov

Contents

Chapter 1

Introduction

During the 1860s, Scottish physicist James Clerk Maxwell predicted the existence of radio waves. In 1886, the German physicist Heinrich Rudolph Hertz demonstrated that rapid variations of electric current could produce radio waves similar to those of light and heat.

In 1892, Serbian inventor Nikola Tesla delivered a widely reported presentation before the Institution of Electrical Engineers of London in which he noted, among other things, that intelligence would be transmitted without wires. Later, a variety of Tesla's radio frequency systems were demonstrated during another widely known lecture, presented to meetings of the National Electric Light Association in St. Louis, Missouri and the Franklin Institute in Philadelphia. According to the Institute of Electrical and Electronics Engineers (IEEE), "the apparatus that he employed contained all the elements of spark and continuous wave that were incorporated into radio" [Cen06].

On May 7, 1895, the Russian scientist Alexander Popov demonstrated a wireless receiver consisting of a metal "coherer" - a device that detected electromagnetic waves - an antenna, a relay, and a bell to signal the presence of these waves. Popov could send and detect them up to 64 meters away. Although not initially intended as a means of transmitting information, Popov's device proved that radio communication was feasible [Cen05].

The Italian inventor Guglielmo Marconi is generally recognized to have been the first to demonstrate the practical application of electromagnetic waves. In 1896, Marconi applied for a patent for his wireless work that gained him the credit for the invention of the radio.

In the next years, the development of the radio gives rise to television broadcasting, satellite and mobile radio communication systems. The latter are investigated in this thesis and basic principles of communication systems and their state of the art are shortly summarized in the following text.

Modern communication systems can be subdivided into two categories - single-carrier and multi-carrier systems. All these systems are characterized by the spectral efficiency which is the amount of information that can be transmitted over a given bandwidth in a specific time. A single-carrier system utilizes all available transmission bandwidth for one subcarrier and only one data stream can be transmitted. The spectral energy density (SED) of a single-carrier system is shown schematically in Fig. 1.1a.

Multi-carrier systems can be subdivided into frequency-division multiplexing (FDM) systems and orthogonal FDM (OFDM) systems. FDM subdivides the transmission bandwidth into multiple subcarriers and several data streams can be transmitted in parallel, each data stream on an isolated subcarrier. These subcarriers are non-overlapping, do not have any influence on each other and can be demodulated independently. However, to be able to separate different subcarriers at the receiver, large

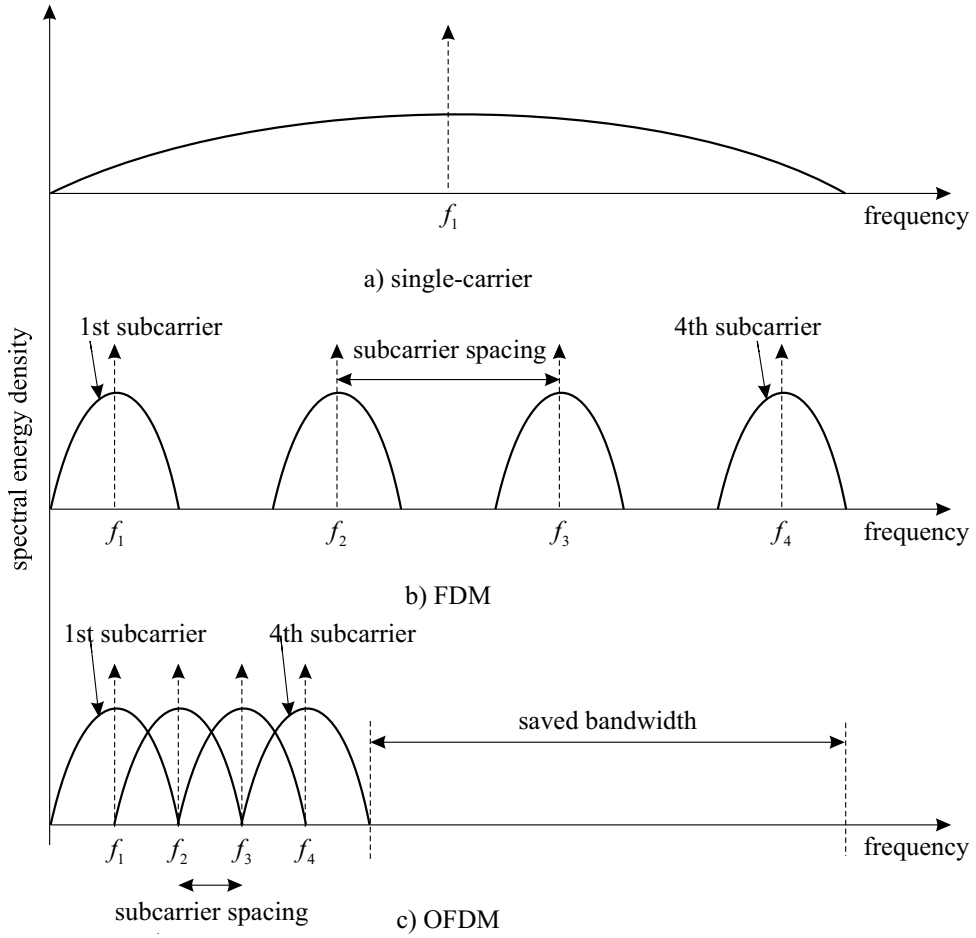

Figure 1.1: The spectral energy density of a) single-carrier, b) FDM, c) OFDM systems.

subcarrier spacings between adjacent subcarriers are required, hence reducing spectral efficiency of FDM systems in comparison to single-carrier systems. Fig. 1.1b illustrates the SED of the FDM modulation scheme.

OFDM makes it possible to increase the spectral efficiency of FDM by employing overlapping subcarriers as shown in Fig. 1.1c. The subcarrier spacing can be decreased and bandwidth is saved, that can be filled with additional subcarriers. Although the subcarriers overlap, they do not interfere with each other since the subcarrier waveforms in OFDM are chosen to be orthogonal [WE71]. At the receiver it is possible to separate individual subcarriers due to their orthogonality, while keeping the complexity of the receiver at a tolerable level.

The mobile communication systems have a common cellular structure [Pro00], first introduced in the early 1980s, where each cell includes one base station (BSs) and several mobile terminals (MTs) also referred to as users. The BS is a central radio transmitter/receiver for a network within a given area with a known fixed location and MT is a portable electronic device for personal communications over long distances. The communication link between the BS and one MT is referred to as downlink. Whereas the communication link between several MTs and a BS is defined as uplink.

The topic of this thesis is focused on the uplink of future mobile communication systems. Modern communication systems are based on several multiple-access techniques which allow MTs to access BS in the uplink. These include the following:

- frequency-division multiple-access (FDMA)
- time-division multiple-access (TDMA)
- code-division multiple-access (CDMA)
- orthogonal FDMA (OFDMA)

FDMA was the initial multiple-access technique for mobile communication systems. FDMA utilizes FDM where each user occupies one or more isolated subcarriers and the signals of different users can be received independently.

In TDMA, users are separated in time, meaning that each user transmits its data over all available transmission bandwidths only during the assigned time slot. Different users use different time slots, thus making multiple-access possible [Pro00].

The CDMA technique allows many users to simultaneously access the available frequency band. User separation at the receiver is possible because each user spreads its transmit signal over the available bandwidth using unique spreading codes. As other users do not use completely orthogonal spreading codes, there is residual multiple-access interference (MAI) present in the receiver [Vit95]. Usually, the CDMA technique is combined with single-carrier systems, however, the combination of CDMA with multi-carrier possible.

OFDMA is based on OFDM, where each user occupies its own set of isolated subcarriers. In contrast to FDMA, OFDMA uses overlapping subcarrier spectra and utilizes the transmission bandwidth more efficiently.

The history of modern communication systems has started in 1979, when the first cellular communication system has been employed in Japan. Since then, three generations of such systems have been deployed and each generation resulted in improved capacity and quality of service. The short description and technical characteristics of the first two generations can be found in [C̀05]. As already mentioned, this thesis is focused on the uplink of future mobile communication systems, therefore, the state of the art in the modern wireless communications is shorty described.

Third Generation of Mobile Communication Systems: Third generation cellular systems (3G) have been proposed with the goal of providing a seamless integration of mobile services into a single global network infrastructure. International Mobile Telecommunications-2000 (IMT-2000) is the global standard for 3G defined by the International Telecommunications Union (ITU) as a set of interdependent recommendations. IMT-2000 includes: Wideband CDMA (W-CDMA), CDMA-2000 and Time Division - Synchronous CDMA (TD-SCDMA). W-CDMA is used in Japan and Europe, CDMA-2000 is employed in America [TC99], whereas TD-SCDMA was launched in China. All these standards employ CDMA for multiple-access.

W-CDMA represents a part of the Universal Mobile Telecommunication System (UMTS) standard and operates with cells of different sizes. By using the radio spectrum in bands identified and provided by the ITU, 3G systems use uplink and downlink channels with a 5 GHz bandwidth to deliver 384 kbit/s for high mobility scenarios and 2 Mbit/s for low mobility scenarios.

The first commercial 3G service based on W-CDMA technology named Freedom of Mobile multimedia Access (FOMA) was launched in October 2001 in Japan. In April 2007, the number of FOMA subscribers exceeded 68.9 millions and corresponded to 67.5% of all mobile subscribers in Japan [Ono07].

Increasing demands on data rate have forced the development of transmission standards capable to provide higher data rates. A host of technologies enabling commercial mobile broadband services is known as 3.5G.

3.5G: The most significant 3.5G standards are: High Speed Packet Access (HSPA) and Evolution-Data Optimized (EV-DO) of Revision B and Revision C. HSPA is an extension of UMTS, whereas EV-DO is a part of the CDMA-2000 family of standards. Note that EV-DO Revision C is also known as Ultra Mobile Broadband (UMB).

Other commercial technologies such as FLASH-OFDM, and iBurst will have commercial traction in certain markets and applications [GSM07]. However, according to the research report of the ”Strategy Analytics”, there will be 518 million mobile broadband users worldwide by 2010. The competitors of HSPA and EV-DO will account for only 30 million of those [Str06].

EV-DO employs CDMA to maximize the throughput and supports a 9.3 Mbit/s downlink and a 5.4 Mbit/s uplink (EV-DO Revision B). HSPA is the set of technologies standardized by the 3rd Generation Partnership Project (3GPP) that defines the migration path for UMTS operators worldwide. HSPA includes High Speed Downlink Packet Access (HSDPA), High Speed Uplink Packet Access (HSUPA) and HSPA Evolved. These are also known as 3GPP Releases 5 through 8.

Both HSPA and EV-DO Revision C (or UMB) will introduce antenna array technologies such as beamforming and Multiple Input Multiple Output (MIMO). Beam forming can be described as focusing the transmitted power of an antenna in a beam towards the users direction. MIMO uses multiple antennas at the sending and receiving side. The deployment of HSPA and UMB is scheduled on 2008.

As an alternative to HSDPA, the new standard termed as High Speed OFDM Packet Access (HSOPA) is introduced, which uses OFDM. HSOPA is a technology under development for specification in 3GPP Release 8, which is called the Long Term Evolution (LTE) initiative. It aims to achieve data rates of up 200 Mbit/s for the downlink and 100 Mbit/s for the uplink.

1.1 Fourth Generation of Wireless Communication Systems

The ITU Recommendation ITU-R M.1645 ”Framework and overall objectives of the future development of IMT and systems beyond IMT-2000” [ITU03] defines the basic requirements to the systems beyond 3G. It is envisioned that development of such systems will proceed according to the following trends:

- Encompassing of the capabilities of the previously developed systems and standards.
- Developing of the new complementary multiple-access, fully packet based, wireless systems with hierarchical cell structure with an objective to provide global roaming of the mobile users according to the principle ”optimally connected anywhere, anytime”.
- Supporting of 100 Mbits/s between high mobility users with high speed on highways or fast trains (up to 250 km/h and more) and 1 Gbit/s for the low mobility users with a pedestrian speed.

Currently, many institutions and research consortiums are investigating possible technical solutions for the 4G radio interface. In the following, several different 4G initiatives are presented.

NTT DoCoMo Initiative: In May 2003, the NTT DoCoMo carried out a field trial of the 4G mobile communications system. The tests used Variable Spreading Factor Orthogonal Frequency and

Code Division Multiplexing (VSF-OFCDM) and Variable Spreading Factor CDMA (VSF-CDMA) technologies [AMAS02]. VSF-OFCDM, also known as Multi-Carrier CDMA (MC-CDMA) [Kai98] with variable spreading factor, enables downlink connections. The VSF-CDMA, also known as Multi-Carrier Direct-Sequence CDMA [FK00], realizes high-speed packet transmissions for the uplink. Note that for the small cells, Variable Spreading and Chip Repetition Factors CDMA (VSCRF-CDMA) known as Interleaved Frequency-Division Multiple-Access (IFDMA), is applied [AS03]. The proposed communication scheme uses adaptive modulation and coding scheme and MIMO. Recently, DoCoMo reports that 5 Gbits/s in the downlink is achieved at the MT speed equal to 10 km/h [Ono07].

4MORE Project: In January 2004, within the European Information Society Technology (IST) programme, 11 European partners have started the 4G MC-CDMA Multiple Antenna System on Chip for Radio Enhancement (4MORE) project [4MO06]. The 4MORE air interface is mainly based on a refinement of the MATRICE air interface proposal [MAT03].

The objective of the 4MORE project is to design the mobile radio system beyond 3G using multiple-antennas, adaptive modulation and coding schemes [BDN05]. The downlink is based on MC-CDMA, whereas the uplink is realized using OFDMA code division multiplexing (OFDMA-CDM) [KDL$^+$04] and IFDMA [Con06a]. The 4MORE demonstrator has a 50 MHz bandwidth. The peak data rates in downlink are 100 MHz and 20 MHz for the high and low mobility scenarios, respectively.

WIGWAM Project: In 2004, a consortium of partners led by Alcatel, DaimlerChrysler, Infineon, Nokia and Siemens launched a research project WIreless Gigabit With Advanced Multimedia (WIGWAM) [Wig07]. The goal of the WIGWAM consortium is to design a system concept with a peak data rate 1Gbit/s in the downlink, thus satisfying the ITU requirements and contributing to the standardization of 4G.

The system design considers different mobility scenarios [ZF04], scalable system bandwidth up to 100 MHz, MIMO and advanced scheduling [Fet03]. The WIGWAM air interface is based on MC-CDMA in downlink and OFDMA in uplink. The modulation schemes vary from binary phase shift keying (BPSK) to 256-quadrature amplitude modulation (QAM).

WINNER I and WINNER II Projects: The key objective of the WINNER I/II projects [WIN03] is to develop a totally new concept in radio access. These projects are built on the recognition that developing disparate systems for different purposes is no longer sufficient in the future converged wireless world. This concept is realized in the ubiquitous radio system concept.

Both uplink and downlink use chunk based TDMA/OFDMA for all propagation scenarios. In the uplink, Block IFDMA (B-IFDMA) is chosen, whereas downlink uses Block Equidistant Frequency Division Multiple Access (B-EFDMA) [Con06b]. Several key technologies such as adaptive modulation and coding schemes, MIMO and enhanced radio protocols are defined.

An analysis of industrial initiatives, European and international projects leads to the conclusion that OFDM based multi-carrier techniques are seriously considered as a basis for 4G air interface.

In the downlink, the tendency is to combine OFDM with TDMA/FDMA in different ways instead of using CDMA. The combination of OFDM and CDMA (known as MC-CDMA) has a serious drawback: it introduces MAI. However in some mobility scenarios, MC-CDMA has an advantage over conventional OFDM [Kai98]. From the practical point of view, the adaptive modulation and coding schemes, scheduling and MIMO make an additional bit error rate (BER) performance gain brought by the MC-CDMA over OFDM insignificant.

In the uplink, there is a clear tendency to use OFDMA schemes in order to assign to users separated subcarriers and avoid MAI. An absolute favorite for 4G uplink is IFDMA since it brings the advan-

tages of OFDMA and has an additional code division multiplexing (CDM) component. It is shown in this thesis that IFDMA provides the lowest peak-to-average power ratio (PAPR) among all known multi-carrier systems.

1.2 State of the Art in the Field of IFDMA

The application of interleaved frequency-division multiple-access (IFDMA) for mobile communications has become an active field of research since 1998. IFDMA can be applied to the downlink and the uplink. However, special interest has been given to the uplink since other multi-carrier systems show some deficiencies for the uplink.

This section gives an overview on the state of the art in the field of IFDMA with respect to data detection, PAPR of multi-carrier systems and the effects of frequency time offsets. Contributions to these topics made by the author of the thesis are not mentioned in this section. These contributions will be presented in Chapters 2 to 5.

IFDMA was introduced in [SBS98, SBS99] as a special kind of a multi-carrier spread-spectrum scheme, where the property of a repeated data sequence has been used for multiple-access. The multiple-access capability is achieved by assigning to each user a different set of orthogonal subcarriers as in the conventional OFDMA. The next contribution to IFDMA has been done in [Bro03], where

Table 1.1: Contributions to fundamental IFDMA topics - invention, basic description, and equivalence to OFDMA-CDM

references	contribution
[SBS98] [SBS99]	IFDMA invention
[Bro03]	time-domain equalization, DFE
[Kai02] [Kai98] [FK00]	OFDMA-CDM, LE, SIC
[Bur01] [GR00] [XZG03]	equivalence between IFDMA and OFDMA-CDM

maximum-likelihood (ML) and decision-feedback equalizers (DFE) have been compared.

Coincident with the first IFDMA publications, a novel multiple-access technique, named OFDMA-CDM, has been introduced in [Kai02] as a promising candidate for the 4th generation of mobile communications. In OFDMA-CDM, each user transmits its data on a fixed set of orthogonal subcarriers. Therefore, MAI is avoided. In contrast to conventional OFDMA, transmitted data symbols in OFDMA-CDM are spread with orthogonal Walsh-Hadamard (WH) codes, which provide additional robustness against non-ideal channels with frequency selective fading. However, this robustness is achieved at the cost of self-interference (SI) [FK00, Kai02, Kai98].

In [Kai02], different linear equalization (LE) techniques such as minimum mean square error (MMSE), equal gain combining (EGC), zero-forcing (ZF), and maximum ratio combining (MRC) have been investigated. In addition, an effective soft interference cancelation (SIC) technique has been proposed which allows the complete elimination of the SI.

Numerous contributions investigate different types of spreading codes for multi-carrier transmission systems. The WH spreading has been combined with pseudo-noise sequences in multi-carrier uplink [DK99], low-rate convolutional codes as spreading codes have been investigated in [Vit90] and Golay and Zadoff-Chu codes have been considered in [Bur01, NHM02]. Fourier codes have been

proposed as spreading codes in [BR98]. In this contribution, the size of the spreading Fourier codes is chosen equal to the size of the inverse discrete Fourier transform (IDFT) operation at the transmitter. Thus, the resulting scheme is a single carrier system with cyclic extension and frequency domain linear equalizers, which has a PAPR of a single-carrier system. The computationally efficient

Table 1.2: Contributions to the field of PAPR and BER performance of multi-carrier systems with Fourier and WH spreading

references	contribution
[Bur01] [BL00] [NHM02]	PAPR and MAI reduction
[BEL03] [RD05]	BER performance
[BV98] [GA02]	signal space diversity

implementation of the more general case, where the Fourier spreading is performed over group of subcarriers which are interleaved equidistantly, is described in [Bur01, GR00, XZG03]. In this case, the Fourier codes for spreading and the rotation factors of the IDFT transform cancel out and the transmit time-domain signal reduces to a repeated data sequence.

Comparing the results obtained in [GR00] with [SBS98, SBS99], it may be concluded that IFDMA is equivalent to OFDMA-CDM with equidistant allocation of subcarriers and the Fourier spreading. Important contributions concerning IFDMA detection techniques and equivalence between OFDMA-CDM and IFDMA are summarized in Table 1.1.

The PAPR distributions for Fourier and WH spreading has been investigated in [BL00] for the up- and downlink. For both cases, Fourier spreading delivers a lower or equal PAPR. The superiority of Fourier spreading increases significantly for larger spreading factors.

The BER performance of multi-carrier transmission systems with Fourier and WH spreading is compared in [BEL03, RD05]. It is shown that the performance of the most commonly used WH transform is asymptotically bad for a high signal-to-noise ratio (SNR). The Fourier spreading as an alternative offers slightly better performance since it spreads transmitted data symbols more efficiently over the complex plane. In this case, the Fourier spreading efficiently exploits signal space diversity [BV98, GA02], thus providing better BER performance than the conventional WH spreading. However, if LE techniques are applied, an application of the Fourier codes for spreading improves BER performance only if the BPSK alphabet is used. In contrast, if modulation alphabet of higher cardinality is applied, e.g. quadrature phase-shift keying (QPSK), the achieved BER performance gain is remarkable only if ML equalizer is used. Important contributions to the fields of PAPR and BER performance of multi-carrier systems with Fourier and WH spreading are recapitulated in Table 1.2.

Being a special kind of a multi-carrier system, IFDMA inherits the sensitivity of the OFDMA to carrier frequency time offsets. The performance of the OFDMA uplink in the presence of the frequency offsets is studied in [TLP00, Ste00]. Three methods to combat MAI in the OFDMA uplink have been developed. The first method employs a frequency allocation scheme, where the data of a particular user is transmitted on a specific subset of adjacent subcarriers as described in [LH05]. The second method includes time-domain windowing [Mus96, MW01]. This method is developed for OFDM but can also be applied for OFDMA uplink systems and applies windowing at the receiver [BT07, SL05, YH03] in front of the discrete Fourier transform (DFT) operation. The third method makes it possible to correct the frequency offsets at the BS (reverse link receiver). These estimates can be used to correct the sampling time instances at the BS receiver or can be sent back to the MT where they are used to pre-compensate the frequency offsets before transmission. Another

Table 1.3: Contributions to the filed of frequency offsets in uplink of OFDMA and OFDMA-CDM

references	contribution
[TLP00] [Ste00]	analysis of influence of frequency offsets
[LH05]	sub-band transmission for OFDMA-CDM
[BT07] [Mus96] [MW01] [SL05]	windowing in the receiver side
[Mor04]	estimation of frequency offsets

algorithm for the frequency offset estimation in OFDMA was proposed in [Mor04]. The most important contributions to the field of frequency offset in uplink OFDMA and OFDMA-CDM are presented in Table 1.3.

1.3 Goals of the Thesis

The overview of the state of the art, given in Sec. 1.2, reveals that some aspects of IFDMA are thoroughly investigated and advantages of IFDMA are widely recognized. However, some issues are still open and further optimizations of the IFDMA receiver and the IFDMA transmit signal are necessary. The main goals of this thesis can be formulated as follows:

- The first objective of this thesis is to develop the IFDMA receiver with frequency domain equalization, low complexity and possibility to separate users in the frequency domain. Note that at the time the work on this thesis was started, efficient IFDMA receiver was not developed and the relationship between OFDMA and IFDMA systems were not yet understood.

- The BER performance of IFDMA and OFDMA systems should be compared in a frequency-selective channel with minimum-mean square error equalizer and self-interference in IFDMA systems to be understood, described analytically and compared to the self-interference of OFDMA-CDM. The closed form solution for the BER performance of uncoded IFDMA systems to be obtained.

- One of the most significant problems in IFDMA uplink are frequency offsets which cause SNR degradation of the received signal and MAI. Effective countermeasures against frequency offsets in the IFDMA uplink are required. Tradeoff should be found between minimization of the negative impact of frequency offsets and the complexity of the receiver. Moreover, identified countermeasures should keep the BER performance and spectral efficiency of IFDMA uplink systems at a tolerable level. An algorithm for the frequency offset estimation shall be developed and evaluated and its theoretical bounds shall be derived. In the presence of frequency offsets, the received signals of mobile users are not orthogonal to each other which complicates an estimation procedure. In order to reduce the estimation efforts and improve the quality of estimates, MAI should be suppressed.

- With the frequency offset, the inter-carrier interference in OFDM and OFDMA systems is reduced if one applies a window with better spectral characteristics than the rectangular one. By varying the window function, the spectrum of each individual subcarrier can be chosen so that it causes less interference to neighboring subcarriers. Other types of windows require, however, the introduction of cyclic prefix and postfix into time domain OFDM symbol. In its turn, an

insertion of the prefix and postfix leads to losses in the spectral efficiency, since prefix and postfix do not transmit any information. The solution should be proposed which allows utilizing a power invested into the prefix and postfix.

- The PAPR distribution of IFDMA and OFDMA systems with pulse-shaping should be compared. The reduction of PAPR in OFDMA and IFDMA systems is one of the most significant problems, since high PAPR values require an expensive power amplifier at the MT. In practical amplifiers, the output power of the signal depends on the input power and this dependence is usually non-linear. Therefore, high PAPR values cause non-linear distortions of the signal. The spectral properties of an OFDMA uplink system can be improved if pulse-shaping filters of the high cost and complexity are applied. However, an application of the pulse-shaping filters lead to the higher PAPR.

- In order to improve the spectral properties of IFDMA, the combination of IFDMA with continuous phase modulation schemes should be performed.

1.4 Contents and Important Results

The thesis consists of 7 Chapters. Chapter 1 and Chapter 7 are introductory and concluding chapters, respectively. The contents of Chapters 2 to 6 deal with the goals mentioned in Sec. 1.3.

In Chapter 2, the basic principles of multi-carrier systems are described and OFDM is introduced. The conventional OFDM model is extended in order to take into account the effects of pulse-shaping on the spectral properties of OFDM. The receiver structure proposed in Chapter 2 makes it possible to demodulate the OFDM signals with a variety of window functions without interference. The IFDMA technique is introduced as a special case of the OFDMA-CDM. The proposed transmitter does not have the computationally intensive DFT operation and thus is more preferable than the conventional OFDMA transmitter.

The concept of minimum shift keying (MSK) and Gaussian-shaped offset QPSK (GOQPSK) IFDMA is proposed. As a result of GOQPSK and MSK combination with IFDMA, the MSK/GOQPSK-IFDMA transmit signal is generated without phase transitions and has better spectral properties than the OFDMA transmit signal.

In Chapter 3, the PAPR of OFDMA, IFDMA and introduced GOQPSK- and MSK-IFDMA are compared. The cumulative distribution function of the PAPR is analyzed for the GSMK/MSK-IFDMA. As a reference, the conventional OFDMA and OFDMA-CDM systems are used. Finally, the circumstances under which PAPR distribution of GOQPSK-IFDMA outperforms the PAPR distribution of the conventional IFDMA are identified.

In Chapter 4, the effect of frequency offsets on the performance of IFDMA uplink system is investigated using raised cosine (RC) window. It is shown that MAI caused by the frequency offsets can be reduced significantly if RC window is applied instead of the conventional rectangular window.

Generally, frequency offset estimation in the uplink of multi-carrier systems is a complicated task, since the received signal at the BS comprises received signals from many users and each user can have its own frequency offset. Moreover, received signals from different users are distorted by different transmission channels which makes the problem of channel estimation complicated.

A frequency domain algorithm for frequency offset estimation is proposed and its performance is investigated in the mobile radio channel. This algorithm utilizes pilot symbols and provides joint

frequency offset and channel estimation. A special construction of pilot symbols with additional spreading in time domain is proposed which allows reduction of the frequency offset estimation error.

A practical time domain algorithm is evaluated which uses the repetitive structure of the IFDMA transmit signal in time domain. The time domain algorithm is independent of the transmission channel and modulation alphabet. Statistical properties of the estimate are analyzed and proven analytically and by Monte-Carlo simulations. As a result, the obtained estimate is unbiased and is able to provide a reliable result at SNR values of practical interest. The proposed algorithm is compared with existing techniques and its superiority is proven.

In Chapter 5, the optimum equalization techniques for OFDM and IFDMA are presented. As shown in Chapter 2, the application of the window in the receiver changes the received spectrum of each individual subcarrier. Varying the roll-off factor of the DFT window function and, therefore, changing the length of the prefix and postfix, MAI caused by the frequency offset can be reduced. A method that allows demodulating the information transmitted on individual subcarriers without interference and by using the DFT of double size was proposed in [BT07].

In Chapter 5, we describe the MMSE algorithm which utilizes part of the energy invested into prefix and postfix for the equalization. As a result, the BER can be improved. Thus, the proposed algorithm improves the spectral efficiency of an OFDM system described in Chapter 2.

Additionally, the SI of IFDMA systems is investigated in an independent Rayleigh channel and it is shown that IFDMA has significantly less SI than conventional OFDMA-CDM.

In Chapter 6, an IFDMA uplink system with non-linear amplifier is investigated and compared with OFDMA and OFDMA-CDM techniques in terms of passband interference, out-of-band radiation and BER performance. Finally, the performance of IFDMA systems is simulated in the mobile radio channel.

Chapter 2

Fundamentals of Uplink OFDMA

2.1 Introduction

As already mentioned in Chapter 1, the main focus of this thesis is IFDMA, applied to uplink mobile radio systems. Since IFDMA can be viewed as a special kind of OFDMA, this introductory chapter describes the basic principles of uplink OFDMA.

As a basis of uplink OFDMA, orthogonal frequency-division multiplexing (OFDM) is introduced in Sec. 2.2. The conventional OFDM model [FK00, Kai98, NP02] is briefly reviewed and extended in Sec. 2.2.1 in order to take into account the effect of pulse-shaping on the spectral properties of OFDM. Discrete-time signal processing in the OFDM transmitter is explained in Sec. 2.2.2. It is shown that pulse-shaping is required to perform an interpolation between individual samples of the discrete OFDM signal. The mobile radio fading channel models which are used in this thesis are presented in Sec. 2.2.3. The receiver proposed in Sec. 2.2.4 makes it possible to demodulate the OFDM signals with a variety of window functions without interference. Technical assumptions which are made throughout this thesis are summarized in Sec. 2.2.5 and the mathematical notations are given in Sec. 2.2.6.

Sec. 2.3 covers uplink OFDMA and its extensions. The characteristics of uplink communications are presented in Sec 2.3.1. Due to its high relevance for IFDMA, the OFDMA uplink system is described in detail in Sec. 2.3.2. Special emphasis is given to OFDMA with block-interleaved frequency allocation, where different users utilize separated and interleaved sets of subcarriers. Since IFDMA is a special case of OFDMA code-division multiplexing (OFDMA-CDM), this extension of OFDMA is presented in Sec. 2.3.3. OFDMA-CDM has been introduced in [Kai02, Kai98] and it is shown that OFDMA-CDM provides better robustness against the negative impact of the multipath channel than conventional OFDMA [Kai98].

The computationally efficient implementation of the IFDMA transmitter is described in Sec. 2.3.4 where the Fourier spreading of the transmit data is performed over the group of subcarriers which are interleaved equidistantly. As a result of the Fourier spreading, the IFDMA transmit signal reduces to a repeated data sequence.

The concept of minimum shift keying IFDMA (MSK-IFDMA) and Gaussian MSK-IFDMA (GOQPSK-IFDMA) is developed in Sec. 2.3.5. As a result of combination MSK/GOQPSK with IFDMA, the MSK/GOQPSK-IFDMA transmit signal is generated without phase transitions. As indicated in Sec. 2.3.6, the MSK/GOQPSK-IFDMA transmit signal has better spectral properties and smaller out-of-band radiation than the transmit signal of OFDMA and OFDMA-CDM systems

The M-modification for OFDMA based systems is described in Sec. 2.3.7. The intention of the M-modification is to increase the data throughput of each user by reducing the number of active users in the OFDMA uplink. The M-modification allows to increase the robustness of the OFDMA uplink in presence of frequency offsets [AS03] and reduces pilot symbols overhead [SFF+07]. Moreover, link adaptation requires link quality estimation and M-modification makes it possible to reduce the amount of link quality information transmitted to the BS, since the link quality of a group of adjacent subcarriers needs to be estimated and transmitted, instead of the link quality of each individual subcarrier [SFSA05].

The LK-modification introduced in Sec. 2.3.8 makes it possible to obtain the IFDMA system with arbitrary data rate while keeping the same PAPR as by single-carrier systems.

2.2 Orthogonal Frequency-Division Multiplexing

2.2.1 Time and Frequency Domain Properties of an OFDM signal

An OFDM modulator maps a sequence of complex-valued source data symbols $S_\kappa, \kappa = 0, \ldots, N_\mathrm{c}-1$, on N_c subcarriers. Throughout the thesis, variables representing values in the frequency domain such as the source symbols S_κ, are written with capital letters. The duration of each data symbol S_κ, is denoted as T_c. The symbol rate per subcarrier is defined as $1/T$ and the following expression holds true

$$\frac{1}{T} = \frac{1}{N_\mathrm{c} T_\mathrm{c}}, \tag{2.1}$$

i.e., the symbol rate per subcarrier $1/T$ is N_c times smaller than the source symbol rate $1/T_\mathrm{c}$. The N_c parallel modulated source symbols $S_\kappa, \kappa = 0, \ldots, N_\mathrm{c} - 1$, form an OFDM symbol.

Throughout the thesis, signals are considered in the equivalent lowpass domain [Pro00] and complex-valued notation is used for the description of the signals in time and frequency domain. The infinite complex-valued envelope of an OFDM symbol in time domain is defined as

$$x_\infty(t) = \frac{1}{\sqrt{N_\mathrm{c}}} \sum_{\kappa=0}^{N_\mathrm{c}-1} S_\kappa e^{j2\pi f_\kappa t}. \tag{2.2}$$

The factor $1/\sqrt{N_\mathrm{c}}$ normalizes the power in (2.2). The N_c subcarrier frequencies $f_\kappa, \kappa = 0, \ldots, N_\mathrm{c}-1$, are located at

$$f_\kappa = \frac{\kappa}{T}, \tag{2.3}$$

and the center of the frequency spectrum is located at $N_\mathrm{c}/2T$. Such definition of the center of the frequency spectrum and subcarrier frequencies f_κ simplifies mathematical modeling. The subcarrier spacing Δf is given as

$$\Delta f = \frac{1}{T}. \tag{2.4}$$

The infinite complex-valued envelope $x_\infty(t)$ of an OFDM symbol in time domain with N_c subcarriers has a bandwidth of

$$BW = \Delta f N_\mathrm{c} = \frac{N_\mathrm{c}}{T} = \frac{1}{T_\mathrm{c}}. \tag{2.5}$$

Since $x_\infty(t)$ has an infinite duration it cannot be realized in practical systems. By multiplying $x_\infty(t)$ by the rectangular function

$$\mathrm{rect}(t) = \begin{cases} 1 & \text{if } 0 \le t \le T \\ 0 & \text{otherwise} \end{cases} \tag{2.6}$$

the duration of (2.2) can be limited.

In order to improve the spectral properties of the time limited envelope $\mathrm{rect}(t)x_\infty(t)$ of an OFDM symbol, the pulse-shaping function $g(t)$ is applied. If not explicitly stated otherwise, it is assumed throughout this thesis that a Nyquist waveform [Pro00] is used as pulse-shaping function

$$g(t) = \mathrm{sinc}\left(\frac{t}{T_\mathrm{c}}\right)\frac{\cos(\pi\alpha t/T_\mathrm{c})}{1-4\alpha^2t^2/T_\mathrm{c}^2}, \tag{2.7}$$

where $\mathrm{sinc}(t)$ is defined as

$$\mathrm{sinc}(t) = \begin{cases} \frac{\sin(\pi t)}{\pi t} & \text{if } t \neq 0 \\ 1 & \text{if } t = 0. \end{cases} \tag{2.8}$$

The roll-off factor $\alpha, 0 \le \alpha \le 1$, in (2.7) defines the spectral characteristics of the pulse-shaping function $g(t)$ as described in [Pro00].

Applying the rectangular function (2.6) and the pulse-shaping function $g(t)$, the complex-valued envelope $x(t)$ of an OFDM symbol has a length T and is defined as

$$x(t) = \mathrm{rect}(t)\Big(x_\infty(t) * g(t)\Big) = \mathrm{rect}(t)\left[\frac{1}{\sqrt{N_\mathrm{c}}}\sum_{\kappa=0}^{N_\mathrm{c}-1} S_\kappa e^{j2\pi f_\kappa t}\right] * g(t), \tag{2.9}$$

where $'*'$ denotes linear convolution

$$a(t) * b(t) = \int_{-\infty}^{\infty} a(\tilde{t})b(t-\tilde{t})d\tilde{t}. \tag{2.10}$$

The transmit spectrum $X(f)$ of the complex-valued envelope $x(t)$ of an OFDM symbol is obtained by performing a Fourier transform as

$$X(f) = \frac{1}{\sqrt{2\pi}}\int_{-\infty}^{\infty} x(t)e^{-j2\pi ft}dt. \tag{2.11}$$

The SED $|X(f)|^2$ of an OFDM symbol is then given as

$$|X(f)|^2 = \left|\frac{1}{\sqrt{N_\mathrm{c}}}\sum_{\kappa=0}^{N_\mathrm{c}-1} TS_\kappa\,\mathrm{sinc}((f-f_\kappa)\,T)G(f)\right|^2, \tag{2.12}$$

where $\mathrm{sinc}(f)$ and $G(f)$ are Fourier transforms of $\mathrm{rect}(t)$ and the pulse-shaping function $g(t)$, respectively.

As can be seen from (2.12), the SED $|X(f)|^2$ is different for different OFDM symbols, since the source symbols $S_\kappa, \kappa = 0, \ldots, N_\mathrm{c}-1$, influence $|X(f)|^2$. However averaging over the set of different

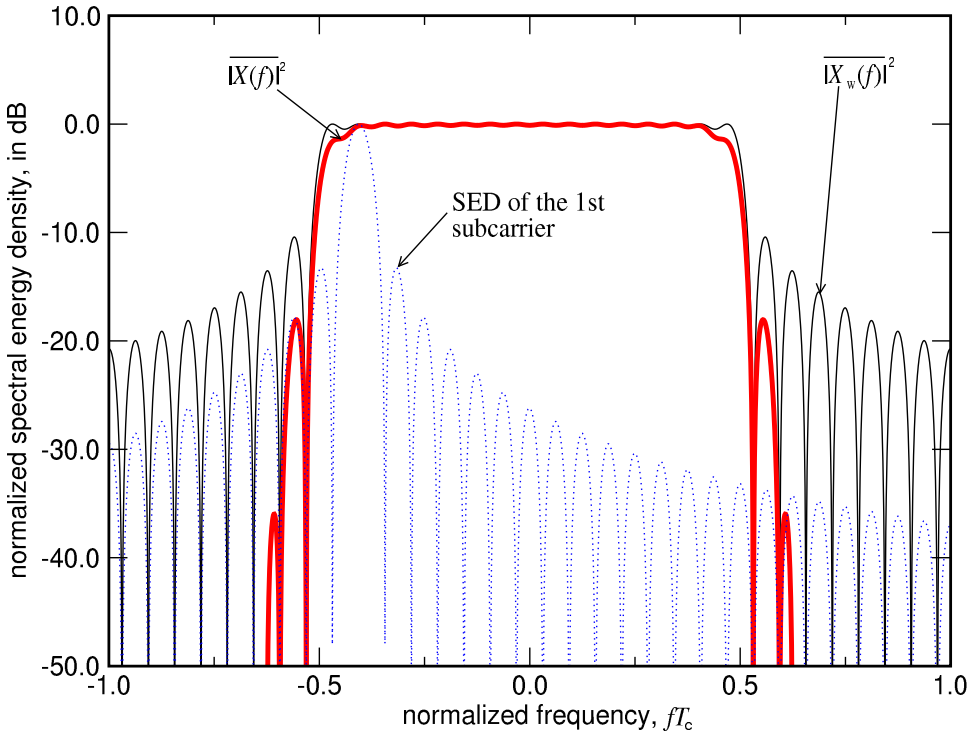

Figure 2.1: Average normalized SEDs versus normalized frequency fT_c: $\overline{|X(f)|^2}$ is the average normalized SED of an OFDM symbol with $N_c = 16$ subcarriers, and Nyquist pulse-shaping function with $\alpha = 0.25$; $\overline{|X_w(f)|^2}$ is the normalized SED $|X_w(f)|^2$ of an OFDM symbol with $N_c = 16$ subcarriers and the Kronecker delta function $\delta(t)$ used as pulse-shaping function; the dotted line refers to the normalized SED of subcarrier $\kappa = 1$.

OFDM symbols, by taking the expectation $E\{.\}$, allows deducing a more convenient representation which is independent of the source symbols S_κ

$$E\left\{|X(f)|^2\right\} = \overline{|X(f)|^2} = \frac{1}{N_c}\sum_{\kappa=0}^{N_c-1}\left|T\,\mathrm{sinc}((f-f_\kappa)\,T)G(f)\right|^2. \tag{2.13}$$

In (2.13), the assumptions that the source symbols $S_\kappa, \kappa = 0,\ldots,N_c-1$, are uncorrelated and have zero mean has been applied, i.e., for every $p = 0,\ldots,N_c-1$,

$$E\left\{|S_\kappa S_p^*|^2\right\} = \begin{cases} 1 & \text{if } \kappa = p \\ 0 & \text{if } \kappa \neq p \end{cases} \tag{2.14}$$

is fulfilled. Note that $|T\,\mathrm{sinc}((f-f_\kappa)\,T)|^2$ in (2.13) denotes the transmit SED of the κth modulated subcarrier. The frequency domain representation $G(f)$ of the pulse-shaping function $g(t)$ is also denoted as the frequency response of the pulse-shaping function and is given as [Pro00]

$$G(f) = \begin{cases} T_c & \text{if } 0 \le |f| \le \frac{1-\alpha}{2T_c} \\ \frac{T_c}{2}\left\{1+\cos\left[\frac{\pi T_c}{\alpha}\left(|f|-\frac{1-\alpha}{2T_c}\right)\right]\right\} & \text{if } \frac{1-\alpha}{2T_c} \le f \le \frac{1+\alpha}{2T_c} \\ 0 & \text{if } |f| > \frac{1+\alpha}{2T_c}. \end{cases} \tag{2.15}$$

In numerous publications, e.g. [Kai98, NP02, FK00], the effect of the pulse-shaping function in OFDM systems is not taken into account and it is assumed that the transmit pulse-shaping function

$g(t)$ is equal to the Kronecker delta function $\delta(t)$ which is defined as

$$\delta(t) = \begin{cases} 1 & \text{if } t = 0 \\ 0 & \text{otherwise.} \end{cases} \tag{2.16}$$

The Kronecker delta function $\delta(t)$ can be considered as a pulse-shaping function with an infinite passband, i.e.,

$$G(f) = 1. \tag{2.17}$$

If $g(t) = \delta(t)$, the average normalized SED in (2.13) simplifies to

$$\overline{|X_{\mathrm{w}}(f)|^2} = \frac{1}{N_{\mathrm{c}}} \sum_{\kappa=0}^{N_{\mathrm{c}}-1} \left| T \operatorname{sinc}\left(\left(f - f_\kappa \right) T \right) \right|^2 . \tag{2.18}$$

The average normalized SED $\overline{|X(f)|^2}$ for $N_{\mathrm{c}} = 16$ subcarriers versus the normalized frequency fT_{c} for the case of Nyquist pulse-shaping with the roll-of factor $\alpha = 0.25$ is depicted as thick solid line in Fig. 2.1. For comparison, the average normalized SED $\overline{|X_{\mathrm{w}}(f)|^2}$ with $N_{\mathrm{c}} = 16$ subcarriers for the case of a Kronecker delta function as pulse-shaping function is depicted as a thin solid line. The dotted line illustrates the normalized SED of the subcarrier $\kappa = 1$.

The normalized frequency range $-0.5 \leq fT_{\mathrm{c}} \leq 0.5$ is denoted as passband in the following, because all information transmitted within one OFDM symbol is located within this frequency range. The out-of-band frequency range is defined for normalized frequencies $|fT_{\mathrm{c}}| > 0.5$. Design rules for multi-carrier systems target at the minimization of energy emitted in the out-of-band frequency range in order to reduce interference to adjacent transmission systems. As a consequence, the transmit energy within passband is maximized in order to improve the SNR of the received signal. If the Nyquist pulse-shaping function defined in (2.7) is applied, out-of-band radiation can be reduced as illustrated in Fig. 2.1.

The subcarriers on the edges of the transmit spectrum are slightly faded because of the pulse-shaping function $g(t)$. Thus, some subcarriers on the edges of the spectra carry less energy than subcarriers located in the middle of the spectrum. However, any phase ambiguity on different subcarriers introduced by the transmit pulse-shaping function can be compensated in the equalization process, since the pulse-shaping function $g(t)$ has linear phase characteristics [Pro00].

In this thesis, we add postfix and prefix to the beginning and end of $x(t)$, respectively, as shown in Fig. 2.3a. The prefix and postfix are the cyclic extension of $x(t)$ which are used at the receiver for the windowing operation as explained in Sec. 2.2.4. The length of the prefix and postfix is $\beta T/2$, where β denotes the roll-off factor of the applied window.

With prefix and postfix the duration of the complex-valued envelope $x(t)$ of an OFDM symbol is $T + \beta T$, which is larger compared to the maximum delay $\tau_{\max}$ of the channel impulse response (CIR) [Kai98, FK00]. In order to avoid interference between succeeding OFDM symbols, maintain the orthogonality between the N_{c} subcarriers, and avoid inter-carrier interference [FK00], a guard interval with duration T_Δ is added at the beginning of the OFDM symbol [AL87, Bin90, NP02] as shown in Fig. 2.3a. The duration of the guard interval is chosen in order to fulfill

$$T_\Delta \geq \tau_{\max}. \tag{2.19}$$

By adding prefix, postfix and guard interval, the OFDM symbol duration extends to

$$T' = T + \beta T + T_\Delta. \tag{2.20}$$

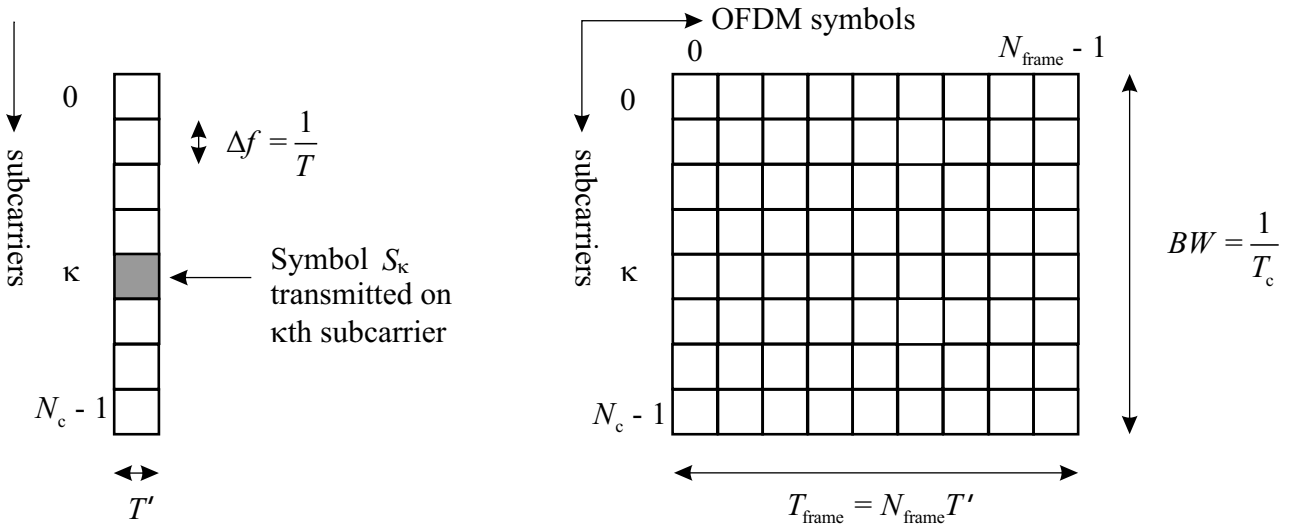

a) OFDM symbol b) OFDM frame

Figure 2.2: Time/frequency representation of an OFDM symbol and an OFDM frame.

The guard interval, prefix and postfix consume transmission energy and induce an energy loss of

$$V_{\mathrm{g}} = 10 \log_{10} \left(\frac{T + T_\Delta + \beta T}{T} \right) \text{ dB} . \tag{2.21}$$

An OFDM frame is defined as N_{frame} subsequent OFDM symbols which are transmitted serially, one after another. The duration of an OFDM frame T_{frame} is defined as

$$T_{\text{frame}} = N_{\text{frame}} T'. \tag{2.22}$$

The time/frequency representation of an OFDM symbol is depicted in Fig. 2.2a and an OFDM frame is shown in Fig. 2.2b.

2.2.2 Discrete-Time Signal Processing in OFDM Transmitter

In the following, we describe the baseband discrete-time signal processing procedure in an OFDM transmitter which allows to generate the complex-valued envelope $x(t)$ of an OFDM symbol in time domain.

Sampling extended complex envelope $x(t)$ at the time instances $t = \upsilon T/(N_{\mathrm{c}}+2N_{\mathrm{w}}), \upsilon = 0, \ldots, N_{\mathrm{c}}+2N_{\mathrm{w}}-1$, as shown in Fig. 2.3a, the discrete length N_{w} of the prefix and postfix can be defined as

$$N_{\mathrm{w}} = \left\lceil \frac{N_{\mathrm{c}} \beta}{2} \right\rceil , \tag{2.23}$$

where $\lceil x \rceil$ represents the smallest integer larger or equal to x. The discrete length of the guard interval is given by

$$N_\Delta = \left\lceil \frac{\tau_{\max} N_{\mathrm{c}}}{T} \right\rceil . \tag{2.24}$$

As shown in Fig. 2.3b, sampling $x(t)$ produces elements

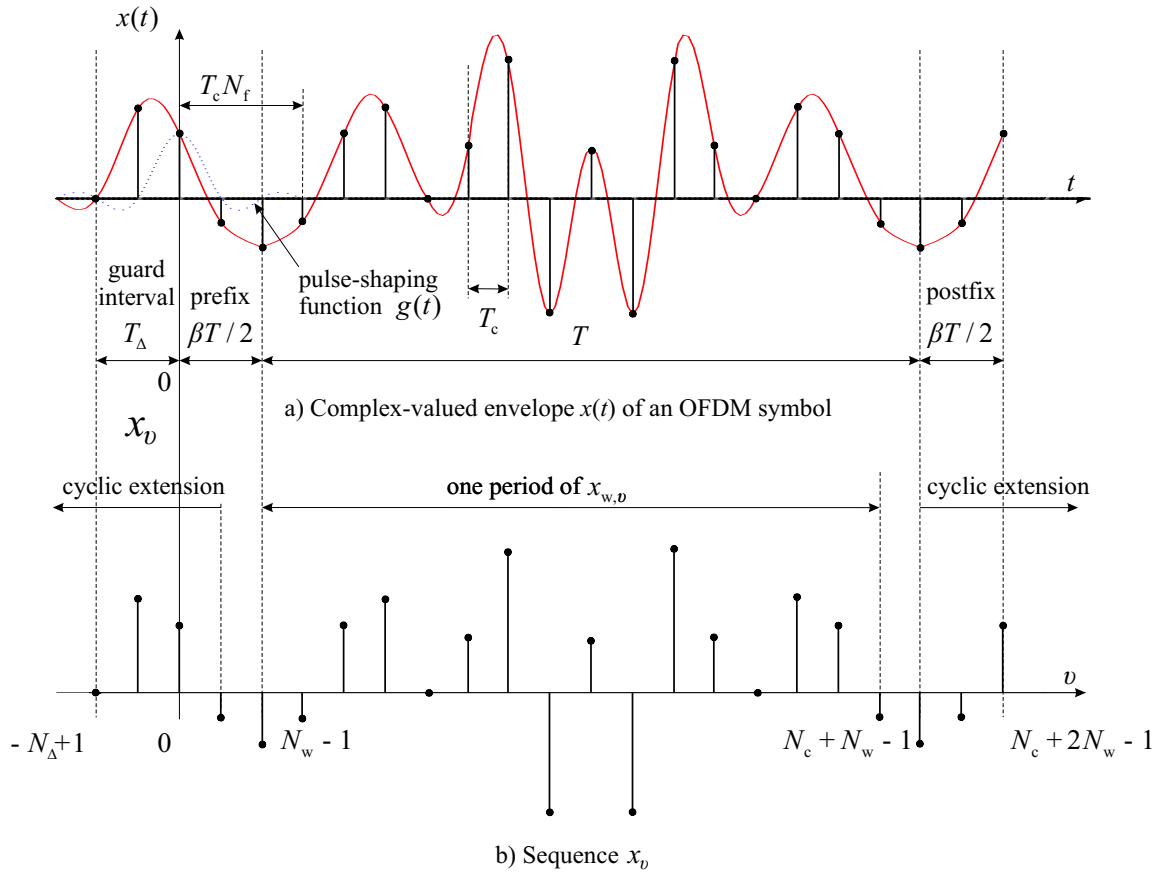

Figure 2.3: Illustration to the generation of the complex-valued envelope $x(t)$ of an OFDM symbol: a) complex-valued envelope $x(t)$ of an OFDM symbol in time domain sampled with the rate $1/T_\mathrm{c}$; as an example, the pulse-shaping function $g(t)$ is depicted, b) the sequence $x_\upsilon, \upsilon = -N_\Delta, \ldots, N_\mathrm{c} + 2N_\mathrm{w} - 1, N_\mathrm{c} = 16; \alpha = 0.25; \beta = 0.25; N_\Delta = 2$.

$$x_\upsilon = \frac{1}{\sqrt{N_\mathrm{c}}} \sum_{\kappa=0}^{N_\mathrm{c}-1} S_\kappa e^{j2\pi\kappa(\upsilon-N_\mathrm{w})/N_\mathrm{c}}, \upsilon = -N_\Delta, \ldots, N_\mathrm{c} + 2N_\mathrm{w} - 1. \tag{2.25}$$

Since the pulse-shaping function $g(t)$ satisfies the Nyquist criterion [Pro00], i.e.,

$$g(\upsilon T_\mathrm{c}) = \begin{cases} 1 & \text{if } \upsilon = 1 \\ 0 & \text{otherwise,} \end{cases} \tag{2.26}$$

$g(t)$ disappears in (2.25).

The block diagram of a multi-carrier modulator employing OFDM based on an IDFT and a multi-carrier demodulator based on DFT is illustrated in Fig. 2.4. An advantage of using OFDM is that the multi-carrier modulation can be implemented in the discrete domain by using an inverse discrete Fourier transform (IDFT), or the more efficient inverse fast Fourier transform (IFFT) [WE71]. As seen in (2.25), the samples of the sequence x_υ are obtained as IDFT of the complex-valued source data symbols $S_\kappa, \kappa = 0, \ldots, N_\mathrm{c} - 1$.

After IDFT operation in the OFDM block, cf. Fig. 2.4, one obtains the sequence $x_{\mathrm{w},\upsilon}$ in time domain

$$x_{\mathrm{w},\upsilon} = \frac{1}{\sqrt{N_\mathrm{c}}} \sum_{\kappa=0}^{N_\mathrm{c}-1} S_\kappa e^{j2\pi\kappa\upsilon/N_\mathrm{c}}, \upsilon = -\infty, \ldots, \infty, \tag{2.27}$$

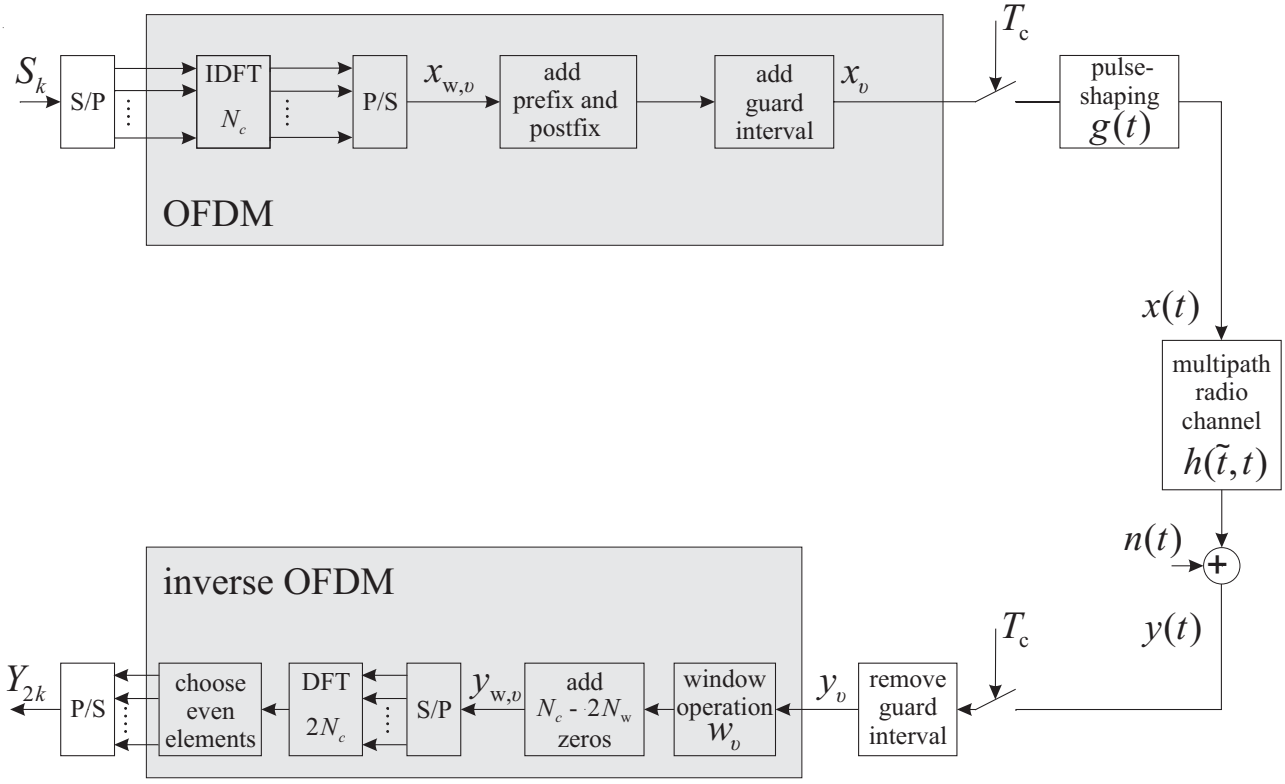

Figure 2.4: Multi-carrier transmission system with OFDM.

which has a period N_c. Note that the IDFT operation is a cyclic operation [PM96], and IDFT block supplies only one period of $x_{w,\upsilon}$. This cyclic property is used to obtain the elements within the guard interval, prefix and postfix. The guard interval, prefix and postfix are formed by cyclic extension in the "add guard interval" and "add prefix and postfix" blocks, respectively. The elements of sequence x_υ are mathematically obtained by

$$x_\upsilon = x_{w,\upsilon}, \upsilon = -N_\Delta, \ldots, N_c + 2N_w - 1. \tag{2.28}$$

Then, the pulse shaping is performed by convolution of x_υ with the pulse-shaping function $g(t)$. Usually, this convolution is performed in the discrete-time domain by using a discrete pulse-shaping filter [OS89, PM96]. Throughout this thesis, the impulse-response of this pulse-shaping filter is modeled as the function $g(t)$, which is non-zero only within $|t| \leq N_f T_c$, where N_f denotes the length of the pulse-shaping filter. The example of $g(t)$ is given in Fig. 2.3a. Note that in the pulse-shaping function $g(t)$, T_c is chosen in such a way that no interference between any two successive elements x_υ and $x_{\upsilon-1}$ occurs. The extended complex-valued envelope $x(t)$ of an OFDM signal at the output of the pulse-shaping filter is given by

$$x(t) = \sum_{\upsilon=-N_\Delta}^{N_c+2N_w-1} x_\upsilon g(t - \upsilon T_c). \tag{2.29}$$

2.2.3 Multipath Channel Model

The multipath propagation environment for mobile radio transmission can be described by the time variant CIR $h(\tilde{t}, t)$. In this thesis, we assume that $h(\tilde{t}, t)$ follows the commonly used wide sense

stationary uncorrelated scattering (WSSUS) assumptions [Kai98]. Hence, $h(\tilde{t},t)$ can be modeled by a tapped delay line of length M_{ch} with coefficients $h_m, m = 0,\ldots,M_{\text{ch}}-1$. Each propagation path of the channel corresponds to a complex-valued coefficient h_m [Pae02, SA00]. The amplitude of the coefficient h_m represents the amplification/fading of the mth received replica of the transmit signal $x(t)$ at the input of the receive antenna. Channel modeling is described in detail in [Pae02, SA00, Kai98].

Throughout this thesis it is assumed that coefficients h_m remain time-invariant for at least one OFDM symbol duration and the power of the received signal $y(t)$ in average is equal to the power of the transmit signal $x(t)$, if averaging is performed over a long period of time. This assumption leads to the condition that the mobile radio channel should not amplify or fade the received signal, i.e., the following condition holds true

$$E\left\{\sum_{m=0}^{M_{\text{ch}}-1}|h_m|^2\right\}=1. \tag{2.30}$$

Another channel model which is used in this thesis is the independent Rayleigh fading channel model, see e.g. [Kai98]. This is a frequency domain channel model without line-of-sight component and there is no correlation between the fading coefficients which are generated independently for each subcarrier and OFDM symbol. The independent Rayleigh channel allows to save simulation time and is easy to implement.

2.2.4 Discrete-Time Signal Processing in OFDM Receiver

The output of the multipath fading channel is the signal waveform $y(t)$ as shown in Fig. 2.4. The signal waveform $y(t)$ is a linear convolution of $x(t)$ and the CIR $h(\tilde{t},t)$ [Pae02] plus additive-white gaussian noise (AWGN) signal $n(t)$. The signal $n(t)$ has zero mean and variance σ^2. The received waveform $y(t)$ at the input of the receive antenna is represented as

$$y(t)=\int_0^{\tau_{\text{max}}}x(t-\tilde{t})h(\tilde{t},t)d\tilde{t}+n(t). \tag{2.31}$$

At the receiver, $y(t)$ is sampled with the rate $1/T_{\text{c}}$ as shown in Fig. 2.4 and the received sequence $y_\upsilon, \upsilon = 0,\ldots,N_{\text{c}}+2N_{\text{w}}-1$, is obtained. The elements $y_\upsilon, \upsilon = -N_\Delta,\ldots,0$, represent guard interval and are not used in the data detection in the following and are discarded. Then, a windowing operation is performed. Before proceeding with the windowing operation, the window function needs to be introduced. Without loss of generality, only the commonly used RC window is considered in this thesis which is defined as [Pro00]

$$w(t)=\begin{cases}\frac{1}{2}+\frac{1}{2}\cos\left(\pi+\frac{t\pi}{\beta T}\right) & \text{if } 0\le T\le \beta T\\ 1 & \text{if } \beta T<t<T\\ \frac{1}{2}+\frac{1}{2}\cos\left(\frac{(t-T)\pi}{\beta T}\right) & \text{if } T\le t\le (1+\beta)T\\ 0 & \text{else,}\end{cases} \tag{2.32}$$

where β is the roll-off factor already defined in Sec. 2.2.2. Note that the window function $w(t)$ has a duration $T+\beta T$. For $\beta=0$, the window function in (2.32) simplifies to the rectangular window

$$w(t)=\text{rect}(t) \tag{2.33}$$

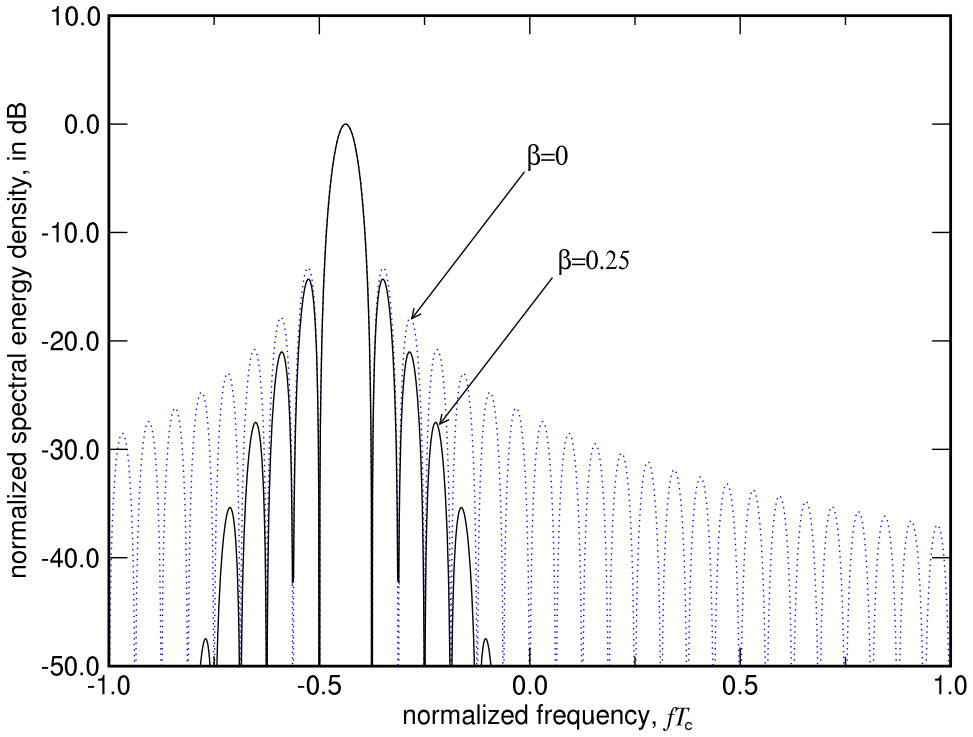

Figure 2.5: The normalized received SEDs of the modulated subcarrier $\kappa = 1$ versus normalized frequency fT_c for $\beta = 0$ and $\beta = 0.25$; $N_\mathrm{c} = 16$.

of duration T. If $W(f)$ is the Fourier transform of $w(t)$, then $|W(f - f_\kappa)|^2$ denotes the received SED of the modulated subcarrier κ. In the case of a RC window, the SED of the kth subcarrier is given as

$$|W(f - f_\kappa)|^2 = \left| T \operatorname{sinc}\left((f - f_\kappa)\, T\right) \frac{\cos(\beta\pi\,(f - f_\kappa)\, T)}{1 - 4\beta^2\,(f - f_\kappa)^2\, T^2} \right|^2 \tag{2.34}$$

and for $\beta = 0$ simplifies to

$$|W(f - f_\kappa)|^2 = |T \operatorname{sinc}\left((f - f_\kappa)\, T\right)|^2 . \tag{2.35}$$

The effect of the window function on the received SED of a modulated subcarrier is shown in Fig. 2.5. It is clearly seen that by increasing β the sidelobes of the subcarriers can be reduced, without introducing any interference.

The windowing operation is performed in the discrete-time domain as illustrated in Fig. 2.6, where the received waveform $y(t)$ is shown in Fig. 2.6a and the window function $w(t)$ is illustrated in Fig. 2.6b. The beginning of the window function must lie within the guard interval, in the area which is free from the interference with the previous OFDM symbol. For simplicity, but without loss of generality, it is assumed that the beginning of the window function is located ideally just after the end of the guard interval.

Sampling the RC window function $w(t)$ given in (2.32) at the time instances $t = \upsilon T/N_\mathrm{c}, \upsilon = 0, \ldots, N_\mathrm{c} + 2N_\mathrm{w} - 1$, with sampling rate $1/T_\mathrm{c}$ one obtains $N_\mathrm{c} + 2N_\mathrm{w}$ elements $w_\upsilon, \upsilon = 0, \ldots, N_\mathrm{c} + 2N_\mathrm{w} - 1$.

After windowing operation, which is simply the multiplication of elements y_υ and w_υ, the sequence $y_\upsilon w_\upsilon, \upsilon = 0, \ldots, N_\mathrm{c} + 2N_\mathrm{w} - 1$, is obtained as shown in Fig. 2.6c. In order to transfer the sequence

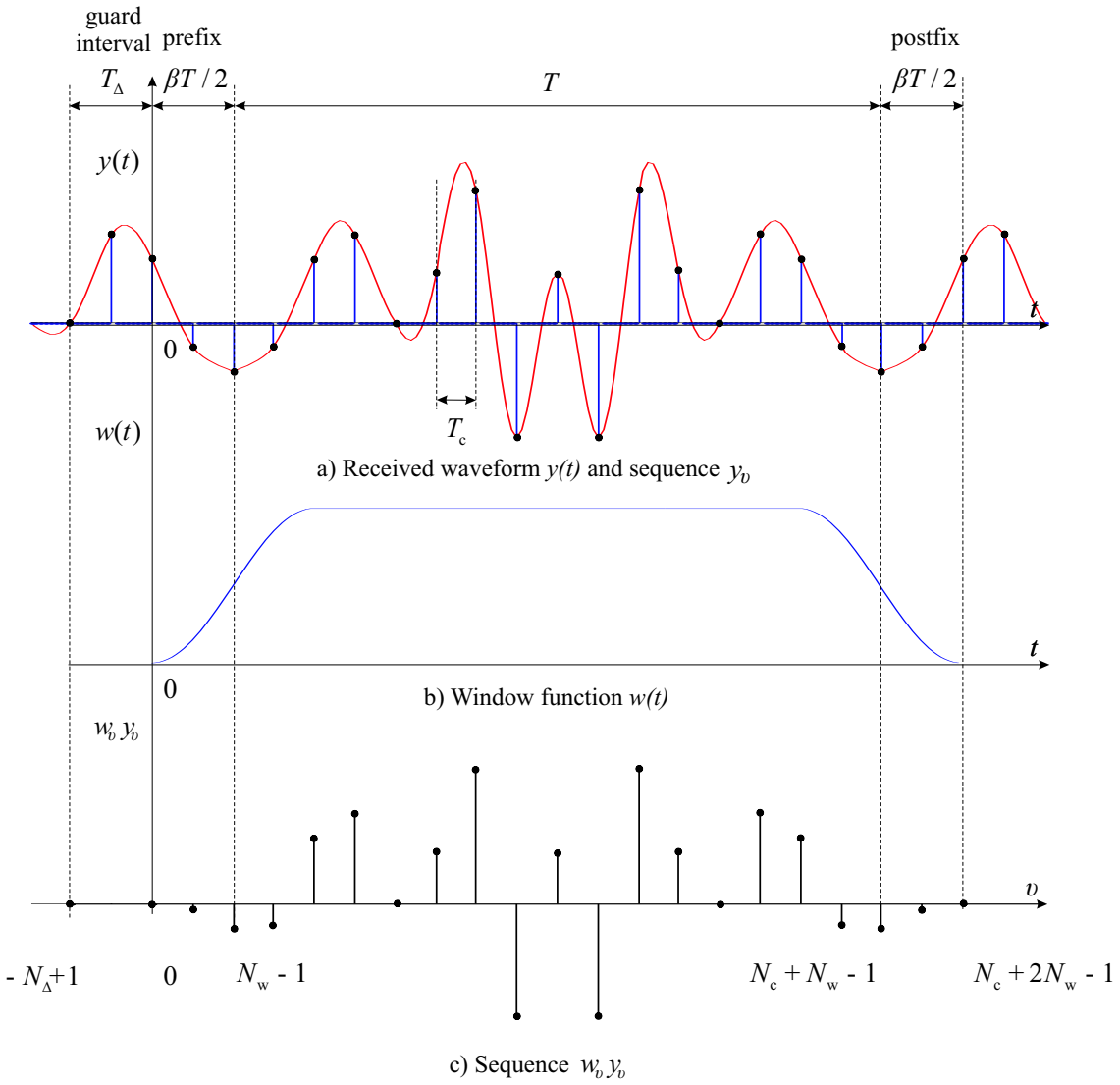

Figure 2.6: Illustration to the windowing operation at the OFDM receiver: a) received waveform $y(t)$ and sequence $y_\upsilon, \upsilon = 0, \ldots, N_c + 2N_w - 1$ b) window function $w(t)$ c) sequence $w_\upsilon y_\upsilon, \upsilon = 0, \ldots, N_c + 2N_w - 1$, obtained after windowing operation; $N_c = 16$; $\alpha = 0.25$; $\beta = 0.25$; $N_\Delta = 2$.

$y_\upsilon w_\upsilon$ in the frequency domain, the DFT operation of size $2N_c$ is applied. In doing so, $N_c - 2N_w$ zero elements are added to the end of the obtained sequence $y_\upsilon w_\upsilon$ in order to adjust the length of the sequence to the DFT length. Then, obtained sequence $y_{w,\upsilon}, \upsilon = 0, \ldots, 2N_c - 1$, is given as

$$y_{w,\upsilon} = \begin{cases} w_\upsilon y_\upsilon & \text{if } \upsilon = 0, \ldots, N_c + 2N_w - 1 \\ 0 & \text{if } \upsilon = N_c + 2N_w, \ldots, 2N_c - 1. \end{cases} \tag{2.36}$$

At the output of inverse OFDM, one obtains the frequency domain sequence $Y_{\kappa'}, \kappa' = 0, \ldots, 2N_c - 1$,

$$Y_{\kappa'} = \frac{1}{\sqrt{2N_c}} \sum_{\upsilon=0}^{2N_c-1} y_{w,\upsilon} e^{-j\frac{2\pi}{2N_c}\upsilon\kappa'}. \tag{2.37}$$

For an interference free reception of an OFDM symbol three conditions have to be fulfilled. First, the OFDM symbol duration $T + \beta T$ should be smaller than the coherence time of the channel and the

subcarrier spacing Δf should be smaller than the coherence bandwidth of the channel as described in [Kai98]. Second, the duration of the guard interval T_Δ should be larger than the maximum delay $\tau_{\max}$ of the channel. Third, the received signal $y(t)$ should not have any frequency and time offsets at the receiver. If these conditions are satisfied, the output of the DFT block is represented by the sequence

$$Y_{\kappa'} = H_{\kappa'} S_\kappa + N_{\kappa'}, \kappa' = 2\kappa, \kappa = 0, \ldots, N_\mathrm{c} - 1 \tag{2.38}$$

of length $2N_\mathrm{c}$, where $H_{\kappa'}, \kappa' = 2\kappa$ are the fading coefficients on the subcarriers $\kappa = 0, \ldots, N_\mathrm{c} - 1$,

$$H_{\kappa'} = \frac{1}{\sqrt{2}} e^{\frac{j\pi N_\mathrm{w}}{N_\mathrm{c}}\kappa'} \sum_{m=0}^{M_\mathrm{ch}-1} h_m e^{-j\frac{2\pi}{2N_\mathrm{c}}m\kappa'} \tag{2.39}$$

and $N_{\kappa'}$ denote AWGN elements. For a more detailed information, refer to (A.1).

As shown in (A.1), only even elements, $\kappa' = 2\kappa, \kappa = 0, \ldots, N_\mathrm{c} - 1$, of the sequence $Y_{\kappa'}, \kappa' = 2\kappa, \kappa = 0, \ldots, 2N_\mathrm{c} - 1$, represent the received values on the subcarriers $\kappa = 0, \ldots, N_\mathrm{c} - 1$. Each element $Y_{\kappa'}$ is equal to the multiplication of the fading coefficient $H_{\kappa'}$ and transmit source symbol S_κ plus an additive white Gaussian noise sample $N_{\kappa'}$. The real and imaginary parts of the noise elements $N_{\kappa'}, \kappa' = 2\kappa, \kappa = 0, \ldots, N_\mathrm{c} - 1$, in (2.38) are assumed to be statistically independent, Gaussian distributed random variables with zero mean and variance equal to $\sigma^2/2$. Under these conditions the variance of the noise sample $N_{\kappa'}$ is given by

$$\sigma^2 = E\{|N_{\kappa'}|^2\}. \tag{2.40}$$

Note that the receive pulse-shaping filter is not taken into account in this thesis. In ideal case, the receive pulse-shaping function should be matched to the function which is a linear convolution of the transmit pulse-shaping function $g(t)$ and the CIR $h(\tilde{t}, t)$. The CIR $h(\tilde{t}, t)$ is not known at the OFDM receiver, and equalization is performed in frequency domain [NP02] by using the detectors described in Sec. 5.2.1. These detectors eliminate the negative impact of the channel in an optimum way.

The receive pulse-shaping filter suppresses noise in the out-of-band frequency range, and thus, makes it possible to increase SNR. However, noise becomes colored in the passband [Pro00]. For broadband systems, the SNR gain due to noise suppression in the out-of-band frequency range is of minor importance and this is not considered in this thesis.

2.2.5 Technical Assumptions

As already mentioned, OFDM provides higher spectral efficiency than single-carrier and FDM modulation schemes and has better immunity against multipath propagation. Another advantage of OFDM is that the OFDM receiver can be efficiently realized by using computationally efficient fast Fourier transform (FFT) [WE71]. However, the following effects, which are not further considered in this thesis, can have an impact on OFDM system performance:

- The effect of channel estimation: The basic principle of channel estimation in OFDM systems is to insert pilot symbols into the OFDM frame with the intention to estimate the channel fading coefficients $H_{2\kappa}, \kappa = 0, \ldots, N_\mathrm{c} - 1$. If the distance between pilot symbols in time direction is smaller than the coherence time of the channel and if the distance between pilot symbols in frequency direction is smaller than the coherence bandwidth of the channel then the estimates of the fading coefficients $H_{2\kappa}$ can be obtained by interpolation [BS99, CSM95, HSR97, CEPA02].

In these contributions is shown that the quality of channel estimation affects OFDM system performance. If not explicitly stated otherwise, it is assumed throughout this thesis that the channel fading coefficients $H_{2\kappa}$ are perfectly known at the receiver.

- The impact of multiple transmit and receive antennas: A key component of a multiple-input multiple-output (MIMO) system is the MIMO detector at the receiver, that has to recover the symbols transmitted simultaneously from multiple transmit antennas. A MIMO system provides antenna diversity techniques such as space-time coding [Ala98, THC99] and space-frequency coding [LXG02] or makes it possible to achieve spacial transmit diversity [Kai00a, Kai00b, DK01] which can be applied to already existing single-input single-output systems. In the sequel, the MIMO issue is not considered. However, most of the algorithms proposed in this thesis can be adopted to the MIMO case.

- The effect of the phase noise: The term phase noise is used to describe phase fluctuations due to random frequency deviations of a local oscillator at the receiver or transmitter. Phase noise can be caused by a number of factors, but is mostly caused by frequency instability of oscillators. The influence of phase noise on the performance on OFDM based systems is out of the scope of this thesis is investigated in [Arm01].

2.2.6 Mathematical Notation

In order to simplify the mathematical representation of OFDM a vector/matrix notation is utilized throughout this thesis. Bold variables designate matrices or vectors. The variables denoting signals in time domain are written in small letters, variables denoting signals in frequency domain are written in capital letters. The symbol $(.)^T$ denotes transposition of a vector or a matrix.

The source data sequence $S_\kappa, \kappa = 0, \ldots, N_\mathrm{c} - 1$, is represented by the frequency domain vector $\mathbf{S}$

$$\mathbf{S} = (S_0, S_1, \ldots, S_{N_\mathrm{c}-1})^T. \tag{2.41}$$

The sequence $x_\upsilon, \upsilon = 0, \ldots, N_\mathrm{c} + 2N_\mathrm{w} - 1$, obtained after IDFT and window operation is represented by the transmit vector

$$\mathbf{x} = (x_0, x_1, \ldots, x_{N_\mathrm{c}+2N_\mathrm{w}-1})^T. \tag{2.42}$$

The sequence $y_\upsilon, \upsilon = 0, \ldots, N_\mathrm{c} + 2N_\mathrm{w} - 1$, obtained after guard interval removal is represented by the received vector

$$\mathbf{y} = (y_0, y_1, \ldots, y_{N_\mathrm{c}+2N_\mathrm{w}-1})^T. \tag{2.43}$$

In order to closely describe the influence of a mobile radio channel on the received OFDM symbol, a CIR vector $\mathbf{h}$ of length M_ch is introduced as

$$\mathbf{h} = (h_0, h_1, \ldots, h_{M_\mathrm{ch}-1})^T. \tag{2.44}$$

The channel matrix

$$\underline{\mathbf{h}} = \begin{pmatrix} h_0 & \cdots & h_{M_\mathrm{ch}-1} & 0 & \cdots & 0 \\ 0 & h_0 & \cdots & h_{M_\mathrm{ch}-1} & \cdots & 0 \\ \cdots & 0 & h_0 & \cdots & h_{M_\mathrm{ch}-1} & 0 \\ 0 & \cdots & 0 & h_0 & \cdots & h_{M_\mathrm{ch}-1} \\ \vdots & \vdots & \ddots & \vdots & \vdots & \vdots \\ \ldots & h_{M_\mathrm{ch}-1} & 0 & 0 & \ldots & h_0 \end{pmatrix} \tag{2.45}$$

is the $(N_c + 2N_w) \times (N_c + 2N_w)$ right circular matrix which rows are cyclically shifted versions of the vector with the size $N_c + 2N_w$, which is obtained by appending $N_c + 2N_w - M_{ch}$ zeros to the CIR vector $\breve{\mathbf{h}}$.

The AWGN sequence $n_\upsilon, \upsilon = 0, \ldots, N_c + 2N_w - 1$, is represented by the AWGN vector

$$\mathbf{n} = (n_0, n_1, \ldots, n_{N_c+2N_w-1})^T \tag{2.46}$$

of size $N_c + 2N_w$. The window function elements $w_\upsilon, \upsilon = 0, \ldots, N_c + 2N_w - 1$, form a diagonal square matrix

$$\underline{\mathbf{w}} = \mathrm{diag}(w_0, w_1, \ldots, w_{N_c+2N_w-1}). \tag{2.47}$$

With this notation, the received vector $\mathbf{y}$ is expressed in time domain as

$$\mathbf{y} = \underline{\mathbf{h}}\mathbf{x} + \mathbf{n}. \tag{2.48}$$

The $N_c \times N_c$-dimensional channel matrix in the frequency domain is given as

$$\underline{\mathbf{H}} = \begin{pmatrix} H_0 & 0 & \ldots & 0 \\ 0 & H_2 & & 0 \\ \vdots & & \ddots & \vdots \\ 0 & 0 & \ldots & H_{2N_c-1} \end{pmatrix}. \tag{2.49}$$

The sequence of the received values $Y_{\kappa'}, \kappa' = 2\kappa, \kappa' = 2\kappa, \kappa = 0, \ldots, N_c - 1$, obtained after inverse OFDM is represented by the received vector $\mathbf{Y}$

$$\mathbf{Y} = (Y_0, Y_2, \ldots, Y_{2N_c-1})^T \tag{2.50}$$

of length N_c. With these notations, $\mathbf{Y}$ is given as

$$\mathbf{Y} = \underline{\mathbf{H}}\mathbf{S} + \mathbf{N}, \tag{2.51}$$

where $\mathbf{N}$ is the AWGN vector in the frequency domain

$$\mathbf{N} = (N_0, N_2, \ldots, N_{2N_c-1})^T. \tag{2.52}$$

2.3 Uplink OFDMA and Its Extensions

2.3.1 Uplink Communications

As already mentioned in Chapter 1, the focus of this thesis is on the uplink mobile radio communications, i.e., on the communication link between several MTs and one BS. The maximum K MTs and one BS form a mobile radio cell and share the same frequency band. The number of active MTs (or active users) is $N_u, N_u \leq K$. Therefore, we introduce index $i, i = 0, \ldots, N_u - 1$, in order to distinguish the signals of different users. The received signal $\mathbf{y}$ at the input of the BS antenna can be modeled as a superposition of the received signals from N_u users. The signal of the ith user is transmitted through the ith independent mobile radio channel which is completely described by its channel matrix $\underline{\mathbf{h}}^{(i)}$. Thus, the received signal $\mathbf{y}$ at the input of the BS antenna is given as

$$\mathbf{y} = \sum_{i=0}^{N_u-1} \underline{\mathbf{h}}^{(i)}\mathbf{x}^{(i)} + \mathbf{n}. \tag{2.53}$$

It is assumed that the received signals of different users have equal energy. This can be considered as a realistic condition because of the automatic power control at the MT which adjusts the transmit power according to the distance between MT and BS and signal propagation conditions.

2.3.2 OFDMA

OFDMA is a multiple-access technique, which is based on OFDM and where different users utilize unique set of subcarriers for data transmission. In doing so, users remain orthogonal and the received signals of different users might be separated in the receiver without interference. Which set of subcarriers is assigned to each particular user is denoted by the frequency allocation scheme that is implemented in the frequency mapper block as shown in Fig. 2.7.

The generation of an OFDMA signal, shown in Fig. 2.7, is applicable on the transmitter side in both the up- and downlink. Each OFDMA user $i, i = 0, \ldots, N_{\mathrm{u}} - 1$, performs a blocked transmission of L complex-valued symbols $d_q^{(i)}, q = 0, \ldots, L-1$, which form vector

$$\mathbf{d}^{(i)} = (d_0^{(i)}, d_1^{(i)}, \ldots, d_{L-1}^{(i)})^T. \tag{2.54}$$

of length L. The vector $\mathbf{d}^{(i)}$ is obtained after channel encoding and code bit interleaving.

The basic idea of channel code is to introduce controlled redundancy into the transmitted data that is exploited at the receiver to correct channel induced errors by means of forward error correction [Pro00]. There are many types of channel codes, but without loss of generality, only a commonly used convolutional codes are utilized in the rest of the thesis. At first, a transmit bit sequence with length L_{a} is coded. At the output of the channel encoder, a coded bit sequence has length L_{b}.

The code rate R_{c}, which defines the amount of the controlled redundancy and the protection capability of the channel code is equal to

$$R_{\mathrm{c}} = \frac{L_{\mathrm{a}}}{L_{\mathrm{b}}}. \tag{2.55}$$

Then, the obtained bit sequence is interleaved. Code bit interleaving is as an efficient technique to combat the BER degradation due to fading, noise, interference and other channel impairments. Signal fading due to time-variant multipath propagation often causes the received signal to fall below the noise level, thus, resulting in a large number of errors, called burst errors. An efficient method for dealing with burst error channel is to interleave the code bits in such a way that bursty channel is transformed into a channel having independent errors. Thus, a code designed for independent errors or short bursts can be used. Code bit interleaving has become an extremely useful technique in wireless communication systems and can be realized as block, diagonal, or random interleaver [Ste94]. At the output of the interleaver, the code bit sequence is given by

$$\mathbf{b}^{(i)} = (b_0^{(i)}, b_1^{(i)}, \ldots, b_{L_{\mathrm{b}}-1}^{(i)})^T \tag{2.56}$$

and is mapped to the vector $\mathbf{d}^{(i)}$. In doing so, $\mathbf{b}^{(i)}$ is separated into groups of $\log_2(M_{\mathrm{d}})$ data bits. Totally, M_{d} unique bit sequences are possible. Each bit sequence is mapped to one of the complex-valued functions $\Omega_0, \Omega_1, \ldots, \Omega_{M_{\mathrm{d}}}$, which form the modulation alphabet

$$\mathbf{\Omega} = \{\Omega_0, \Omega_1, \ldots, \Omega_{M_{\mathrm{d}}}\}. \tag{2.57}$$

The L data symbols $d_q^{(i)}, d_q^{(i)} \subseteq \mathbf{\Omega}$, are assumed to be equally probable with zero mean and are delivered to the OFDM with the rate $1/T_c$. The average energy of the data symbol $d_q^{(i)}$ is chosen to be

$$E\{|d_n^{(i)}|^2\} = 1. \tag{2.58}$$

The L transmitted symbols $d_q^{(i)}$ of the ith user are transmitted on $L < N_{\mathrm{c}}$ subcarriers. Normally, signal fading often causes the adjacent subcarriers to fall below the noise level, and if one user utilizes

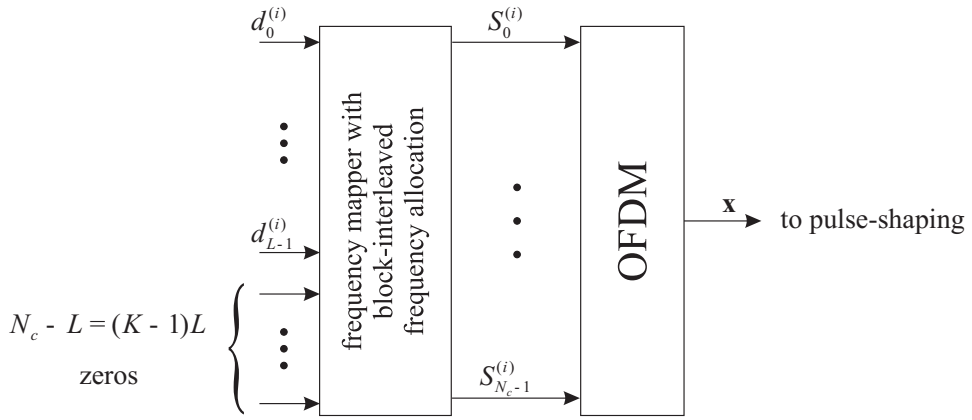

Figure 2.7: OFDMA transmitter of the ith user with L transmit data symbols and $N_\mathrm{c} = LK$ subcarriers.

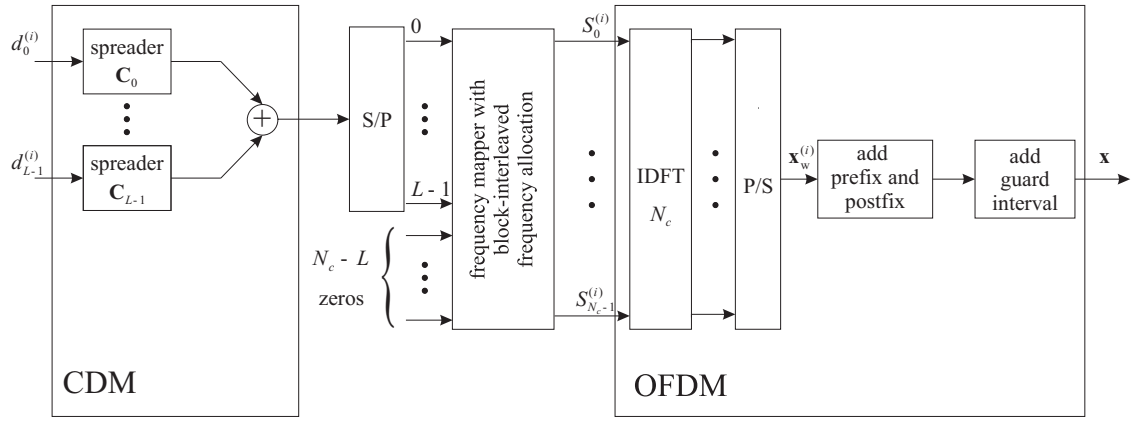

Figure 2.8: OFDMA-CDM transmitter of the ith user with L transmit data symbols and $N_\mathrm{c} = LK$ subcarriers.

adjacent subcarriers for data transmission, transmit data might be impossible to recover at the receiver. It is worth to separate these subcarriers in the frequency reducing probability that these two subcarriers are deep faded at the same time. In the following, a block- interleaved frequency allocation scheme is utilized, which provides maximum frequency separation. The block-interleaved frequency allocation scheme assigns the subcarriers $\kappa = 0, \ldots, N_\mathrm{c} - 1$, to the user i, such

$$S_\kappa^{(i)} = \begin{cases} d_q^{(i)} & \text{if } \kappa = qK + i, q = 0, \ldots, L-1 \\ 0 & \text{otherwise.} \end{cases} \tag{2.59}$$

Note that only L subcarriers are occupied by the data symbols of the ith user. The other $(K-1)L$ subcarriers remain empty and are used for the data transmission of other users.

2.3.3 OFDMA-CDM

As already mentioned in the previous section, separation of subcarriers in frequency increases a probability that these subcarriers are faded independently. If one achieves that bit errors appeared on one subcarrier are independent from the bit errors on another subcarrier and then the received bit stream

is less bursty. It can be achieved with block interleaved frequency allocation scheme which provides simple and robust method to improve the BER performance of OFDMA.

However, further improvement of OFDMA with block-interleaved allocation is possible. Consider the situation, where one subcarrier is deeply faded. In this case, data transmitted on this subcarrier has low SNR and the probability to receive data correctly reduces tremendously. The countermeasure is to transmit data on separated subcarriers simultaneously, but this approach is not spectrum efficient.

The logical solution is to apply code-division multiplexing (CDM) component, and transmit each data symbol $d_q^{(i)}$ on L subcarriers simultaneously. For keeping spectrum efficiency the same as in the conventional OFDMA, other $L-1$ data symbols are transmitted on the same subcarriers. The separation of data symbols in the receiver is possible if orthogonal spreading codes are used.

OFDMA-CDM transmitter, described in [Kai98, FK00] and illustrated in Fig. 2.8, combines serially concatenated CDM component, frequency mapper and OFDM. Before proceeding with the detailed description of OFDMA-CDM transmitter, we introduce Walsh-Hadamard spreading codes $\mathbf{C}_n, n = 0, \ldots, L-1$, of length $L = 2^\iota, \iota = 1, 2, \ldots$, which form a square WH matrix $\underline{\mathbf{C}}_L$ of size $L \times L$ so that

$$\underline{\mathbf{C}}_L = \{\mathbf{C}_0, \mathbf{C}_1, \ldots, \mathbf{C}_{L-1}\}. \tag{2.60}$$

The WH matrix $\underline{\mathbf{C}}_L$ is defined recursively by

$$\underline{\mathbf{C}}_L = \frac{1}{\sqrt{2}} \begin{pmatrix} \underline{\mathbf{C}}_{L/2} & \underline{\mathbf{C}}_{L/2} \\ \underline{\mathbf{C}}_{L/2} & -\underline{\mathbf{C}}_{L/2,} \end{pmatrix} \forall L = 2^\iota, \iota \geqslant 1, \underline{\mathbf{C}}_1 = 1. \tag{2.61}$$

The CDM component is introduced by multiplying each data symbol $d_q^{(i)}$ by the WH code $\mathbf{C}_n, n = 0, \ldots, L-1$, and the summation of the obtained products. In order to preserve the advantages of systems with separated transmit subcarriers, we apply a block-interleaved frequency allocation scheme by assigning symbol $S_\kappa^{(i)}$ to the subcarrier $\kappa, \kappa = 0, \ldots, N_\mathrm{c} - 1$,

$$S_\kappa^{(i)} = \begin{cases} \sum\limits_{q=0}^{L-1} C_{n,q} \cdot d_q^{(i)} & \text{if } \kappa = nK + i, \kappa = nK + i \\ 0 & \text{otherwise,} \end{cases} \tag{2.62}$$

where $C_{n,q}$ is the qth, $q = 0, \ldots, L-1$, element of the serial spreading WH code $\mathbf{C}_n$. As can be seen from (2.62), OFDMA-CDM exclusively assigns to each of the N_u users a set of L subcarriers out of the possible N_c subcarriers. The spectrum efficiency and the BER performance in AWGN channel[1] for OFDMA-CDM is the same as for OFDMA.

The detailed structure of OFDM block is shown in Fig. 2.8, since generation of the transmit signal $\mathbf{x}_\mathrm{w}^{(i)}$ for the systems with block-interleaved frequency allocation can be slightly simplified as shown in the following derivation. The elements $x_{\mathrm{w},l}^{(i)}, l = 0, \ldots N_\mathrm{c} - 1$ of the vector $\mathbf{x}_\mathrm{w}^{(i)}$, obtained after IDFT operation and parallel-to-serial conversion can be represented by

$$x_{\mathrm{w},l}^{(i)} = \frac{1}{\sqrt{N_\mathrm{c}}} \sum_{\kappa=0}^{N_\mathrm{c}-1} S_\kappa^{(i)} e^{j\frac{2\pi}{N_\mathrm{c}}\kappa l}, \tag{2.64}$$

[1] if $C_{n,q} \subseteq \left\{-1/\sqrt{L}, 1/\sqrt{L}\right\}$, where $1/\sqrt{L}$ is the power normalization coefficient, then average transmit power transmitted on the subcarrier $\kappa = nK + i, n = 0, \ldots, L-1$, is expressed as

$$E\{|S_{nK+i}^{(i)}|^2\} = \frac{1}{L} \sum_{q=0}^{L-1} E\{|d_q^{(i)}|^2\} = E\{|d_q^{(i)}|^2\} = 1. \tag{2.63}$$

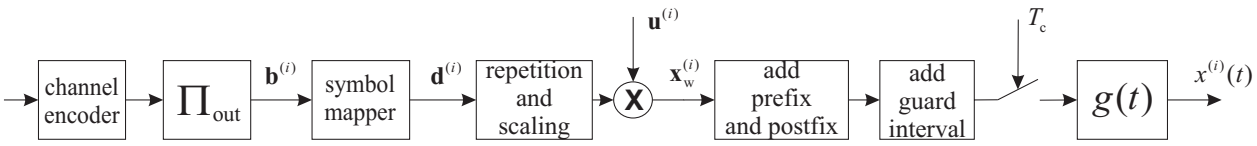

Figure 2.9: IFDMA transmitter of the ith user.

Substituting (2.62) into (2.64) and bearing in mind that $N_{\text{c}} = LK$, the signal $x_{\text{w},l}^{(i)}, l = 0, \dots N_{\text{c}} - 1$, obtained after the IDFT operation in the OFDMA-CDM transmitter can be represented by

$$x_{\text{w},l}^{(i)} = \frac{1}{\sqrt{N_{\text{c}}}} \sum_{n=0}^{L-1} S_{nK+i}^{(i)} e^{j\frac{2\pi}{N_{\text{c}}}(nK+i)l} = e^{j\frac{2\pi}{N_{\text{c}}}il} \frac{1}{\sqrt{K}} \sum_{n=0}^{L-1} S_{nK+i}^{(i)} e^{j\frac{2\pi}{L}nl}. \tag{2.65}$$

Since the exponent in (2.65) is periodic with the period L, the transmit signal $x_{\text{w},l}^{(i)}$ also have periodic structure. Hence, one can take only values $x_{\text{w},l}^{(i)}$ calculated for one period, and then repeat them K times. In doing so, (2.65) we can represent by

$$x_{\text{w},l}^{(i)} = e^{j\frac{2\pi}{N_{\text{c}}}il} \frac{1}{\sqrt{K}} \sum_{n=0}^{L-1} S_{nK+i}^{(i)} e^{j\frac{2\pi}{L}n(l \bmod L)}. \tag{2.66}$$

The derived expression shows that for multi-carrier systems with block-interleaved frequency allocation, the shorter DFT operation of length L instead of N_{c} can be applied that minimizes the transmitter complexity and might be essential for the systems with large number of transmit subcarriers.

2.3.4 IFDMA

The previous sections demonstrate that CDM and block-interleaved frequency allocation scheme might improve the robustness of OFDMA based systems against the negative influence of the mobile radio channel. However, CDM not only improves BER but can also be used for the reduction of the transmitter complexity and minimization of amplitude fluctuations of the transmit signal [AS04b]. It is well known that OFDM transmit signal has large amplitude fluctuations, known as high peak-to-average power ratio (PAPR) problem. The proposed modification of OFDMA-CDM with block-interleaved frequency allocation scheme, termed as interleaved frequency-division multiple-access (IFDMA), allows reducing PAPR and obtained IFDMA transmit signal has PAPR of single-carrier systems.

This modification can be achieved if Fourier codes are applied instead of WH codes, i.e., IFDMA can be understood as a special case of OFDMA-CDM. Before proceeding with the IFDMA transmitter, we introduce Fourier matrix

$$\underline{\mathbf{C}}_L = \{\mathbf{C}_0, \mathbf{C}_1, \dots, \mathbf{C}_{L-1}\}. \tag{2.67}$$

The rows of the matrix $\underline{\mathbf{C}}_L$ are Fourier codes $\mathbf{C}_n, n = 0, \dots, L-1$, of size L with elements

$$C_{n,q} = \frac{1}{\sqrt{L}} e^{-j\frac{2\pi}{L}nq}, q = 0, \dots, L-1, \tag{2.68}$$

Substituting (2.68) into (2.66) the elements of the Fourier codes $C_{n,q}$ and the rotation factors of the IDFT $e^{j\frac{2\pi}{L}nl}$ in (2.66) cancel out and the transmit signal $x^{(i)}_{\mathrm{w},l}, l = 0, \ldots N_\mathrm{c} - 1$, reduces to

$$x^{(i)}_{\mathrm{w},l} = \underbrace{e^{\frac{j2\pi}{N_\mathrm{c}}il}}_{\text{the } l\text{th element } u^{(i)}_l \text{ of vector } \mathbf{u}^{(i)}} \cdot \frac{1}{\sqrt{K}} d^{(i)}_{l \bmod L}. \tag{2.69}$$

The N_c elements

$$u^{(i)}_l = e^{j\frac{2\pi}{N_\mathrm{c}}il}, l = 0, \ldots, N_\mathrm{c} - 1, \tag{2.70}$$

form a user specific phase vector

$$\mathbf{u}^{(i)} = (u^{(i)}_0, u^{(i)}_1, \ldots, u^{(i)}_{N_\mathrm{c}-1})^T. \tag{2.71}$$

Note, the multiplication with the user specific vector $\mathbf{u}^{(i)}$ ensures the user separation by assigning to each user L subcarriers orthogonal to all other users' subcarrier sets. Each element $x^{(i)}_{\mathrm{w},l}$ represents the lth transmission chip in the following. The duration of the resulting chips coincides with the duration of the data symbol d_q and is equal to T_c. The N_c chips form a vector

$$\mathbf{x}_\mathrm{w} = (x_0, x_1, \ldots, x_{N_\mathrm{c}-1})^T. \tag{2.72}$$

Comparing (2.69) and the IFDMA signal generation as described in [SBS99] [SBS98] it follows that IFDMA transmit signal can be completely generated in the time domain without using IDFT. The IFDMA transmitter is shown in Fig. 2.9. Comparing it with OFDMA-CDM transmitter in Fig. 2.8, one can conclude that IFDMA transmitter has simplified structure. Instead of IDFT, the data symbols $d^{(i)}_q, q = 0, \ldots, L-1$, are repeated K times, scaled by the energy normalization factor $1/\sqrt{K}$ and multiplied by the user specific phase vector $\mathbf{u}^{(i)}$. The obtained chips $x^{(i)}_l$ are then filtered with the pulse-shaping filter which is described by the pulse-shaping function $g(t)$. In the case of IFDMA, complex-valued envelope $x^{(i)}(t)$ of an OFDM symbol can be represented as

$$\begin{aligned} x^{(i)}(t) &= \frac{1}{\sqrt{K}} \sum_{l=0}^{N_\mathrm{c}-1} d^{(i)}_{l \bmod L} g(t - T_\mathrm{c}l) e^{j\frac{2\pi}{T}it} = \\ &\frac{1}{\sqrt{K}} \sum_{l=0}^{N_\mathrm{c}-1} \left[\underbrace{\Re\{d^{(i)}_{l \bmod L}\} g(t - T_\mathrm{c}l)}_{\text{in-phase component}} + \underbrace{j\Im\{d^{(i)}_{l \bmod L}\} g\,(t - T_\mathrm{c}l)}_{\text{quadrature component}} \right] \cdot e^{j\frac{2\pi}{T}it}, \end{aligned} \tag{2.73}$$

where $\Re(.)$ and $\Im(.)$ denote real and imaginary parts of a complex number, respectively.

Note that the complex-valued envelope $x^{(i)}(t)$ of an OFDM symbol in (2.73) is represented without guard interval, postfix and prefix, which can be added as described in Sec 2.2.2. IFDMA was introduced as a special kind of a multi-carrier spread-spectrum scheme, where the property of a repeated data sequence has been used for multiple-access in [SBS98]

2.3.5 MSK-IFDMA and GOQPSK-IFDMA

In this section, we combine MSK and GOQPSK with IFDMA. MSK can be viewed as offset (or staggered) QPSK with sinusoidal pulse-shaping [Pro00]. The literature contains much research on MSK. Pasupathy [Pur87] provides a primer on MSK and can be referred to for an overview. Couch [Cou93] also discusses the basic principles of MSK modulation. MSK has continuous phase and constant

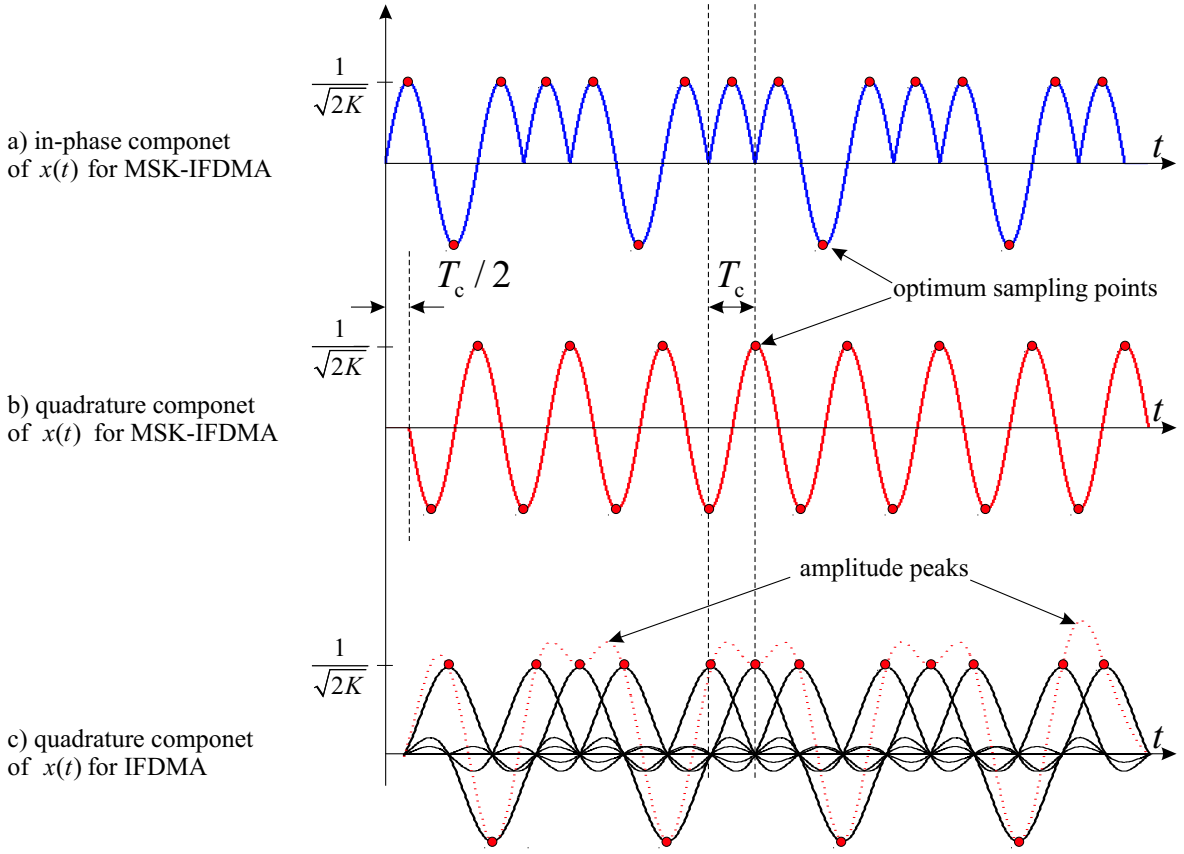

Figure 2.10: In-phase and quadrature components of IFDMA versus time a) in-phase component of MSK-IFDMA b) quadrature component of MSK-OFDMA c) quadrature component of IFDMA with Nyquist pulse-shaping; $i = 0$.

envelope which makes an application of cheap nonlinear power amplifies possible. Moreover, MSK is easy to implement. GOQPSK is a modification of MSK, where Gaussian pulse-shaping makes it possible to obtain a narrow bandwidth of the transmit signal and more efficiently suppress the emitted energy in the out-of-band frequency range.

The proposed combination of MSK and GOQPSK with IFDMA is novel and has not yet been described in literature. Due to this combination, a new FDMA technique is created which have better spectral characteristics than conventional IFDMA with Nyquist pulse-shaping. In the following, we refer to the combination of MSK and IFDMA as a MSK-IFDMA and to the combination of GOQPSK with IFDMA as a GOQPSK-IFDMA. The IFDMA with Nyquist pulse-shaping function, defined in (2.7) is referred to as a conventional IFDMA. Note that we use equivalent lowpass domain signal representation for the description of MSK-IFDMA and GOQPSK-IFDMA. At first, we start with MSK-IFDMA and, then, introduce the GOQPSK-IFDMA as a special case of MSK-IFDMA. The MSK-IFDMA complex-valued envelope $x(t)$ of the ith user can be represented as

$$x^{(i)}(t) = \frac{1}{\sqrt{2K}} \sum_{l=0}^{N_c-1} \left[\underbrace{b^{(i)}_{2l \bmod 2L} g(t - lT_c)}_{\text{in-phase component}} - \underbrace{j b^{(i)}_{2l+1 \bmod 2L} g\left(t - lT_c - \frac{T_c}{2}\right)}_{\text{quadrature component}} \right] \cdot e^{j\frac{2\pi}{T} it}. \quad (2.74)$$

The MSK-IFDMA can be viewed as quadrature modulation scheme where the pulse-shaping function

$$g(t) = \begin{cases} \sin\left(\frac{\pi t}{T_\mathrm{c}}\right) & \text{if } 0 \leq t \leq T_\mathrm{c} \\ 0 & \text{otherwise.} \end{cases} \tag{2.75}$$

is a one-half period of the sinusoid and the expression

$$g^2(t) + g^2\left(t + \frac{T_\mathrm{c}}{2}\right) = 1 \tag{2.76}$$

holds true. In (2.74), even numbered bits $b_{2l}, l = 0, \ldots, N_\mathrm{c}-1$, of the bit sequence $\mathbf{b}$ are transmitted on the in-phase component of $x(t)$, whereas odd numbered bits $b_{2l+1}, l = 0, \ldots, N_\mathrm{c} - 1$, are transmitted on the quadrature component of $x(t)$. The example of the lowpass MSK-GOQPSK signal is shown in the Fig. 2.10. In-phase component of the MSK envelope $x(t)$ is shown in Fig. 2.10a whereas the quadrature component $x(t)$ is shown in Fig. 2.10b. For illustration, the quadrature component of the IFDMA signal with the conventional Nyquist pulse is depicted in Fig. 2.10c as a dotted line. In all cases, only one user $i = 0$ is active.

For GOQPSK-IFDMA, the pulse-shaping function $g(t)$ is defined as

$$g(t) = \frac{1}{2T_\mathrm{c}}\left[\mathrm{Q}\left(2\pi BT_\mathrm{c}\frac{t - T_\mathrm{c}/2}{T_\mathrm{c}\sqrt{\ln(2)}}\right) - \mathrm{Q}\left(2\pi BT_\mathrm{c}\frac{t + T_\mathrm{c}/2}{T_\mathrm{c}\sqrt{\ln(2)}}\right)\right], \tag{2.77}$$

where $\mathrm{Q}(t)$ is a Q-function

$$\mathrm{Q}(t) = \frac{1}{\sqrt{2\pi}}\int_t^\infty e^{-\tilde{t}^2/2}d\tilde{t}. \tag{2.78}$$

and BT_c is a normalized bandwidth of the Gaussian pulse-shaping function, where B denotes 3 dB bandwidth of the filter. The following remarks are of interest:

- MSK/GOQPSK-IFDMA has the same data rate as the conventional IFDMA with the QPSK and Nyquist pulse-shaping. Thus, all considered systems have the same spectral efficiency [Pro00].

- The quadrature component of MSK/GOQPSK-IFDMA is staggered in time by $T_\mathrm{c}/2$ seconds with respect to the in-phase component.

- The optimum sampling points for the in-phase and quadrature components of the MSK/GOQPSK-IFDMA are offset by $T_\mathrm{c}/2$ seconds as shown in Fig. 2.10a and Fig. 2.10b. In contrast, both in-phase and quadrature components of the conventional IFDMA have a common optimum sampling points as depicted in Fig. 2.10c. Clearly, in-phase and quadrature components of the MSK/GOQPSK-IFDMA might be processed separately at the receiver, in contrast to the conventional IFDMA.

- MSK/GOQPSK-IFDMA has the same repetitive structure as the conventional IFDMA. This repetitive structure makes is possible to have null frequencies in the transmit spectrum. These frequencies are used for the data transmission of other users and, thus, allow FDMA. The user-specific exponent $e^{j\frac{2\pi}{T}it}, i = 0, \ldots, N_\mathrm{u} - 1$, in (2.74) provides cyclic frequency shift and secures the orthogonality of users.

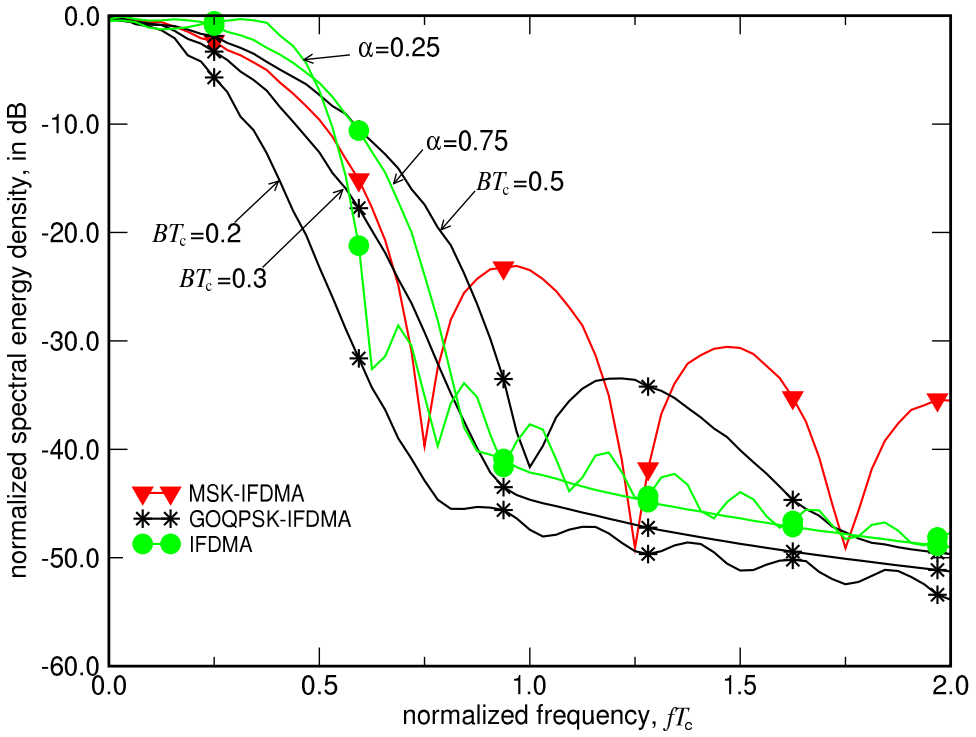

Figure 2.11: Normalized power density spectra of MSK-IFDMA, GOQPSK-IFDMA and conventional IFDMA versus normalized frequency fT_{c}; $M = 32$; $K = 32$; $L = 32$; $N_{\mathrm{u}} = 1$.

- The in-phase and quadrature components of MSK/GOQPSK-IFDMA do not have the amplitude peaks as the quadrature or in-phase components of the conventional IFDMA. This peaks increase PAPR of the transmit signal $x(t)$ and might have a negative impact on the quality of the transmit spectrum if non-linear power amplifier is applied.

- The type of pulse-shaping does not have any influence on the IFDMA system performance. If signals in Fig. 2.10a, Fig. 2.10b and Fig. 2.10c are sampled at the optimum time instances, then obtained samples have the same SNR and are free from SI and MAI. Therefore, the same BER performance is expected for IFDMA, MSK-IFDMA and GOQPSK-IFDMA.

2.3.6 Spectral Properties

The normalized power density spectra of MSK-IFDMA, GOQPSK-IFDMA and conventional IFDMA are shown in Fig. 2.11. For IFDMA, spectra are plotted for different values of the roll-off factor α, whereas for GOQPSK-IFDMA spectra are simulated for the different values of the normalized bandwidth BT_{c}. The considered IFDMA and MSK/GOQPSK-IFDMA systems have $N_{\mathrm{c}} = 1024$ subcarriers. The spreading length is $L = 32$ and only one IFDMA user $i = 0$ is active. The systems are fully loaded and all subcarriers are occupied.

For the sake of clarity, SEDs of individual subcarriers are not shown. Only values $|G(f)|^2$ are depicted in Fig. 2.11, where frequency response $G(f)$ is the Fourier transform of the pulse-shaping function $g(t)$. It is seen that MSK pulse-shaping has very large amount of the out-of-band radiation in comparison with the conventional Nyquist pulse and GOQPSK. With the GOQPSK pulse, out-of-band radiation can be further reduced by decreasing BT_{c}, however, at the cost of the energy reduction

in the passband, i.e., in the normalized frequency range $|fT_{\mathrm{c}}| \leq 0.5$. GOQPSK-IFDMA is the best candidate for the implementation, since the pulse-shaping function defined in (2.77) provides lower out-of-band radiation than Nyquist and MSK pulse-shaping functions. It's worth noting that IFDMA system with the Nyquist pulse-shaping can achieve the spectral efficiency of the GOQPSK pulse-shaping, but at the cost of large amplitude peaks in $x(t)$. The obtained results are important since OFDMA and OFDMA-CDM systems with Nyquist pulse-shaping have the same transmission spectra as IFDMA. Unfortunately, an application of MSK and GOQPSK pulse-shaping to conventional OFDMA and OFDMA-CDM systems is not possible since their time-domain samples have different amplitudes.

2.3.7 M-Modification

The data symbol spreading together with block interleaved frequency allocation improve the BER performance of an OFDMA-CDM/IFDMA system. In this section, we introduce so called M-modification which allows increasing the transmit data rate per user by decreasing the number of active users N_{u}. The M-modification can be applied to the both OFDMA or OFDMA-CDM/IFDMA systems and was introduced in [Kai98].

With the M-modification, each user transmits ML data symbols per OFDM symbol, where M is referred to as a coefficient of the M-modification. The vector of transmit data symbols $\mathbf{d}^{(i)}$ has a length ML and is given by

$$\mathbf{d}^{(i)} = (\underbrace{d_0^{(i)}, \ldots, d_{L-1}^{(i)}}_{\text{group } 0}, \ldots, \underbrace{d_{(M-1)L-1}^{(i)}, \ldots, d_{ML-1}^{(i)}}_{\text{group } M-1})^T. \tag{2.79}$$

The elements of the vector $\mathbf{d}^{(i)}$ are subdivided into M independent groups and each group consist of L data symbols. Within the m_{gr}th group, $m_{\mathrm{gr}} = 0, \ldots, M-1$, the data symbols $d_{q+Lm_{\mathrm{gr}}}^{(i)}, q = 0, \ldots, L-1$, are spread with the spreading codes $\mathbf{C}_n, n = 0, \ldots, L-1$, which are the same for each group. The frequency mapper with block-interleaved frequency allocation assigns the symbol S_κ to the subcarrier $\kappa, \kappa = 0, \ldots, N_{\mathrm{c}} - 1$, according to the rule

$$S_\kappa^{(i)} = \begin{cases} \sum\limits_{q=0}^{L-1} C_{n,q} \cdot d_{q+Lm_{\mathrm{gr}}}^{(i)} & \text{if } \kappa = nK + i + m_{\mathrm{gr}}, n = 0, \ldots, L-1 \\ 0 & \text{otherwise.} \end{cases} \tag{2.80}$$

As a result of M-modification, the ML data symbols of the ith user are transmitted on ML subcarriers. The subcarriers are subdivided into L groups and each group consists of M adjacent subcarriers as shown in Fig. 2.12b where an OFDM frame with block-interleaved frequency allocation scheme and M-modification is depicted for $K = 4$, $M = 2$, $L = 4$, $N_{\mathrm{c}} = 16$ and $N_{\mathrm{u}} = 1$. M-modification has following advantages:

- The M-modification allows to increase the robustness of the OFDMA/IFDMA uplink in presence of frequency offsets [AS03].
- The M-modification reduces the number of pilot symbols required for the channel estimation in IFDMA uplink [SFF+07].
- Link adaptation requires link quality estimation and M-modification makes it possible to reduce the amount of link quality information transmitted to the BS, since the link quality of a group

of adjacent subcarriers needs to be estimated and transmitted, instead of the link quality of each individual subcarrier [SFSA05]

As a main drawback, M-modification increases the PAPR of the transmit signal as demonstrated in Chapter 3.

In the following, the important relations between the maximum number of users K, the total number of available subcarriers N_{c}, the spreading length L, and the number of active users N_{u} are derived. The total number of available subcarriers N_{c} is a product of the maximum number of users K and the spreading length L, i.e.,

$$N_{\mathrm{c}} = LK. \tag{2.81}$$

The number of active users N_{u} is a parameter which may change dynamically, since some users enter the cell, whereas others leave it. With the M-modification, the maximum allowed number of users K, the coefficient M of the M-modification and number of users N_{u} are related as

$$MN_{\mathrm{u}} \leq K. \tag{2.82}$$

With M-modification, the number of occupied subcarriers per user is equal to ML and the total number of occupied subcarriers in the OFDMA-CDM/IFDMA uplink with N_{u} active users is equal to MLN_{u}. The relationship between the number of subcarriers N_{c}, spreading length L, the maximal number of users N_{u} and M can be expressed as

$$M \leq \frac{N_{\mathrm{c}}}{LN_{\mathrm{u}}}. \tag{2.83}$$

The multi-carrier uplink system is called fully loaded if $N_{\mathrm{u}} = K$ and the following expression is true

$$M = \frac{N_{\mathrm{c}}}{LK}. \tag{2.84}$$

If the spreading length L and maximum number of users K are fixed, then, from (2.82) and (2.81), it follows that increasing of the coefficient M is only possible by simultaneous reducing the number of active users N_{u}.

2.3.8 Remarks on IFDMA system design

The Sec. 2.3.4 states that IFDMA is able to achieve the PAPR of a single-carrier system, if no M-modification is applied. An OFDM frame of such IFDMA systems is shown in Fig. 2.12a. If one wants to increase the data rate per user, additional subcarriers in the OFDM frame need to be occupied as shown in Fig. 2.12b, where the OFDM frame with M-modification is depicted.

However, it is possible to increase the data throughput of one individual user, not applying the M-modification but just varying the parameters L and K as demonstrated in Fig. 2.12c. Both systems, considered in Fig. 2.12b and in Fig. 2.12c, have $N_{\mathrm{c}} = 16$ subcarriers and only eight subcarriers are utilized for data transmission. The depicted systems differ only in a subcarrier allocation scheme. In Fig. 2.12b, $K = 4$, $L = 4$ and $M = 2$ are set and in Fig. 2.12c, $L = 8$ and $K = 2$ are chosen.

The IFDMA system in Fig. 2.12c has the lowest possible PAPR (0 dB for GOQPSK-IFDMA), since condition of block-interleaved frequency allocation remains. In contrast, IFDMA system shown in Fig. 2.12b does not have constant amplitude of the transmit signal as it will be demonstrated in the next Chapter.

Therefore, it is possible to adjust parameters L and K in order to obtain the IFDMA system with any required data throughput while keeping the lowest possible PAPR. This modification shown in Fig. 2.12c is referred to as LK-modification in the following.

The IFDMA system with LK-modification demonstrated in Fig. 2.12c provides more channel diversity than IFDMA system shown in Fig. 2.12b and, thus, provides better BER performance. For IFDMA, the LK-modification is preferably to use than M-modification, since the obtained transmit signal has constant envelope.

It is expected that PAPR of OFDMA and OFDMA-CDM does not depend on used modification. The PAPR of these systems solely depends on the number of occupied subcarriers.

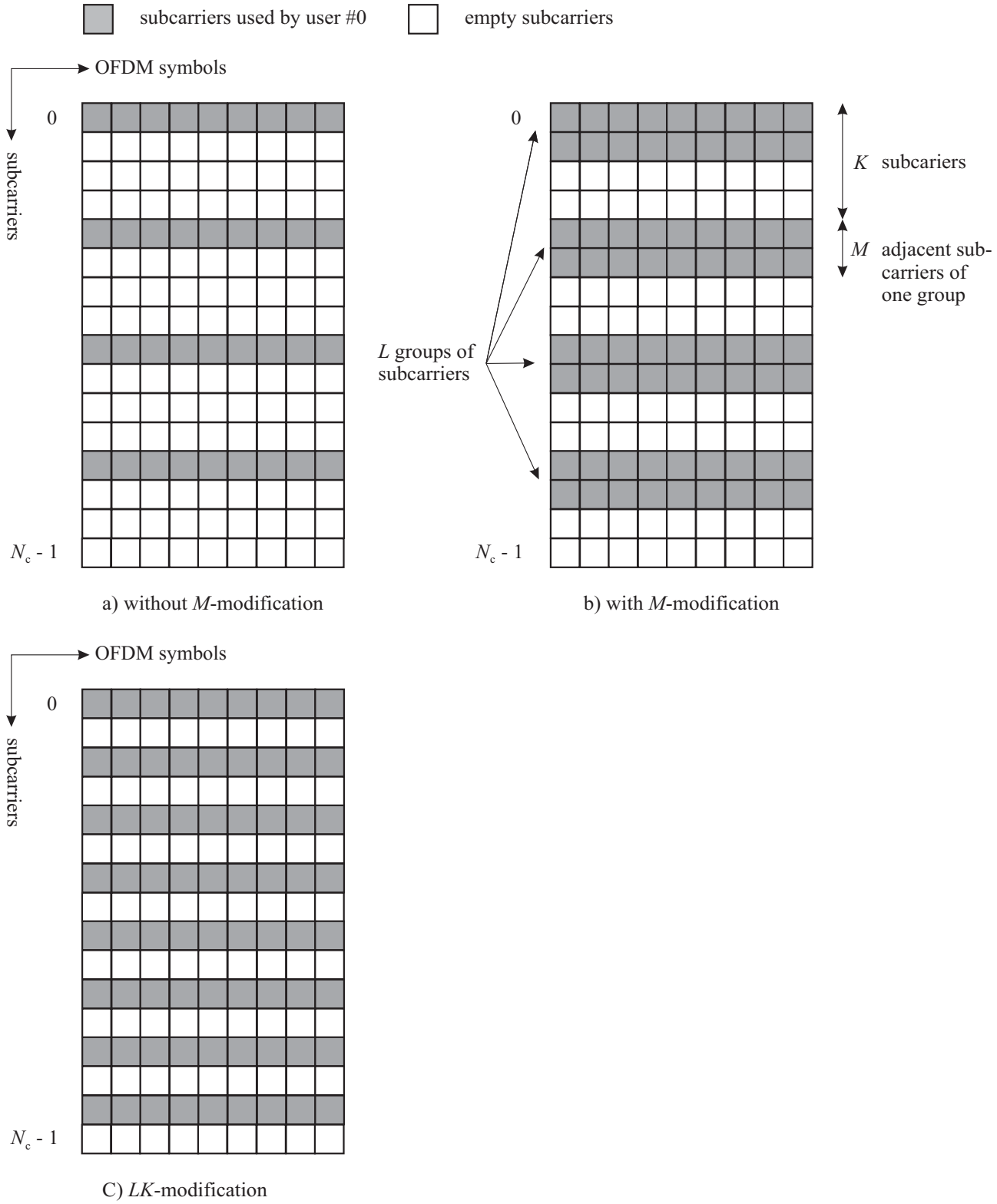

Figure 2.12: OFDM frames with $N_c = 16$ subcarriers and with block interleaved frequency allocation scheme: a) without M-modification $K = 4$; $L = 4$ b) with M-modification $K = 4$; $L = 4$; $M = 2$ c) with LK-modification; $K = 2$; $L = 8$; $N_u = 1$.

Chapter 3

Peak-to-Average Power Ratio

3.1 Introduction

Coincident with the first IFDMA publication, OFDMA-CDM, has been introduced in [Kai02] as a promising candidate for the next generation of mobile communications systems. In both systems, a user transmits its data on a fixed set of orthogonal subcarriers and MAI is avoided. IFDMA, the same as OFDMA-CDM, uses WH codes for spreading of data symbols, which improves the robustness of the received signal against the negative influence of the multipath channel with frequency selective fading. Moreover, IFDMA transmit signal can be generated without DFT operation, by performing the repetition of the transmit data sequence in the time domain.

In Chapter 2, an attempt to combine the IFDMA with continuous phase modulations has been done and, as a result, MSK-IFDMA together with GOQPSK-IFDMA are introduced. As will be shown in Chapter 6, such a combination allows further improving spectral properties of OFDMA based systems. The MSK/GOQPSK-IFDMA transmit signal is generated without phase transitions and has better spectral properties than OFDMA transmit signal. In this section, we compare PAPR of proposed MSK-IFDMA and GOQPSK-IFDMA systems and identify the circumstances under which PAPR distribution of GOQPSK-IFDMA outperforms the PAPR distribution of the conventional IFDMA.

The content and the most important contributions and results of the investigations which are performed in this chapter are shortly summarized as follows:

- The PAPR of multi-carrier systems is analyzed in Sec. 3.2. The upper bounds of the PAPR are derived in Sec. 3.2.1 for the OFDMA, IFDMA and MSK/GOQPSK-IFDMA. The cumulative distribution function (CDF) of PAPR is introduced in Sec. 3.2.2.

- Simulation results are presented in Sec. 3.3 and system parameters are given in Sec. 3.3.1. The CDF of PAPR distribution is analyzed for the GOQPSK- and MSK-IFDMA system for different values of the M-modification coefficient and different values of the spreading length. As a reference, the conventional OFDMA and OFDMA-CDM systems are used. Finally, the circumstances under which the GOQPSK-IFDMA transmit signal has smaller PAPR than the transmit signal of the conventional OFDMA and OFDMA-CDM systems with Nyquist pulse-shaping are identified. The PAPR simulation results are discussed in Sec. 3.3.2.

3.2 PAPR definition

In this section, we compare PAPR of IFDMA, GOQPSK-IFDMA, MSK-IFDMA, OFDMA-CDM and OFDMA. Only one user is considered in this section, thus, index i is omitted for simplicity. For PAPR calculation, we consider complex-valued envelope $x(t)$. The PAPR is defined as ration of the power of maximum peak of $x(t)$ to the average power of $x(t)$. The average power of $x(t)$ is calculated as the average power of samples obtained at the optimum time instances. For all considered systems, the PAPR can be defined as

$$PAPR = \frac{\max\limits_{0 \le t \le N_c T_c} \{|x(t)|^2\}}{\frac{1}{N_c} \sum\limits_{l=0}^{N_c-1} |x(lT_c)|^2}. \tag{3.1}$$

The denominator in (3.1) is the average power of $x(t)$ which is equal to a ration of the number of occupied subcarriers LM of one user to the total number of available subcarriers N_c multiplied by the average energy $E\{|S_n|^2\}$ of the source data symbol S_n

$$\frac{1}{N_c} \sum_{l=0}^{N_c-1} |x(lT_c)|^2 = \frac{LM}{N_c} E\{|S_n|^2\}. \tag{3.2}$$

Bearing in mind that $E\{|S_n|^2\} = 1$, as defined in (2.14), and $N_c = LK$, (3.2) can be simplified

$$\frac{1}{N_c} \sum_{l=0}^{N_c-1} |x(lT_c)|^2 = \frac{M}{K}. \tag{3.3}$$

3.2.1 PAPR Upper Bound for IFDMA and OFDMA

In this subsection, we calculate the PAPR upper bounds for OFDMA and IFDMA systems with the conventional Nyquist pulse-shaping. It is shown that the PAPR upper bound for the IFDMA depends on the pulse-shaping function $g(t)$ and is independent on the spreading length L. In contrast to IFDMA, the PAPR upper bound for OFDMA solely depends on the number of occupied subcarriers and is independent on $g(t)$.

At the beginning, the upper bound of the conventional IFDMA with the Nyquist pulse-shaping is calculated. The solid line in Fig. 2.10c represents the pulse-shapes corresponding to the different transmit chips and the dotted line represents the quadrature component of the IFDMA complex-valued envelope $x(t)$. It is seen that the amplitude peaks occur as a superposition of the pulse-shaping functions of several adjacent chips. These peaks are always in the middle between two successive transmitted chips, and are shifted by $T_c/2$ with respect to the optimum sampling points. The maximum amplitude peak

$$x_{\max} = \max_{0 \le t \le N_c T_c} \{|x(t)|\} \tag{3.4}$$

depends on the transmitted data sequence $\mathbf{d}$ and the modulation alphabet $\mathbf{\Omega}$. With this notation, PAPR in (3.1) is given by[1]

$$PAPR = x_{\max}^2 \frac{K}{M}. \tag{3.5}$$

It is possible to determine the value of the maximum amplitude peak $x_{\max}$ analytically. For this purpose, we choose the sequence $\mathbf{d}$ in such a way that pulse-shaping functions of different chips

[1]Note that PAPR is independent from K, since $x(t)$ is normalized by the coefficient $1/\sqrt{K}$ as shown in Fig 3.1.

add up constructively. The IFDMA envelope $x(t)$ is shown in Fig. 3.1 and represents the worst case scenario with maximum $x_{\max}$. In order to obtain such a maximum, the BPSK modulation alphabet is chosen and data sequence $\mathbf{d} = (1,-1,1,-1,1,1,-1,1,-1,1)^T$ is utilized. For simplicity, we assume that the pulse-shaping function $g(t)$ is infinite and influence of N_c chips is taken into account. The M-modification coefficient is $M = 1$. In the case of an arbitrary modulation alphabet $\mathbf{\Omega}$, the

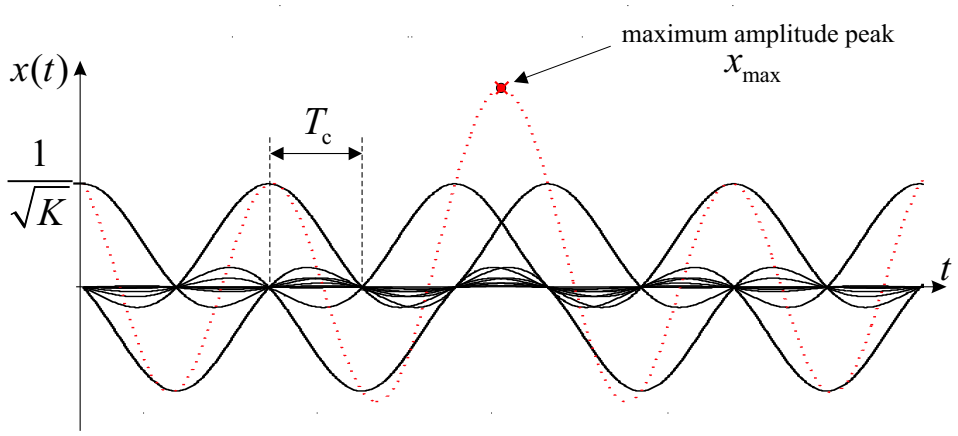

Figure 3.1: A part of an IFDMA complex-valued envelope $x(t)$ versus time. The sequence $\mathbf{d} = (1,-1,1,-1,1,1,-1,1,-1,1)^T$ results in the maximum possible PAPR; BPSK; $L = 10$; $M = 1$.

maximum amplitude $x_{\max}$ of an IFDMA complex-valued envelope is calculated and upper bounded as

$$\begin{aligned} x_{\max} &= \left| \frac{2}{\sqrt{K}} \max_{\mathbf{\Omega}}\{|d_q|\} \sum_{l=0}^{N_c-1} (-1)^l g\left(lT_c + \frac{T_c}{2}\right) \sum_{i=0}^{M-1} e^{j\frac{2\pi}{N_c} il} \right| \\ &\leq \left| \frac{2}{\sqrt{K}} \max_{\mathbf{\Omega}}\{|d_q|\} \sum_{l=0}^{N_c-1} (-1)^l g\left(lT_c + \frac{T_c}{2}\right) \right| \left| \sum_{i=0}^{M-1} e^{j\frac{2\pi}{N_c} il} \right| \\ &\leq \left| \frac{2M}{\sqrt{K}} \max_{\mathbf{\Omega}}\{|d_q|\} \sum_{l=0}^{N_c-1} (-1)^l g\left(lT_c + \frac{T_c}{2}\right) \right|, \end{aligned} \tag{3.6}$$

where $\max_{\mathbf{\Omega}}\{.\}$ denotes the maximum value over the whole modulation alphabet $\mathbf{\Omega}$. The maximum PAPR of the IFDMA reduces to

$$PAPR_{\max} = x_{\max}^2 K/M \leq M \left[2 \max_{\mathbf{\Omega}}\{|d_q|\} \sum_{l=0}^{N_c-1} (-1)^l g\left(lT_c + \frac{T_c}{2}\right) \right]^2. \tag{3.7}$$

Note that $x(t)$ is multiplied by $1/\sqrt{K}$, which is the energy normalization coefficient in IFDMA systems as shown in (2.69) and depicted in Fig. (3.1).

For the case of MSK/GOQPSK-IFDMA, the maximum amplitude value is given as

$$x_{\max} = \frac{M}{\sqrt{K}} \tag{3.8}$$

and $PAPR_{\max}$ is given by

$$PAPR_{\max} = x_{\max}^2 K/M = M. \tag{3.9}$$

Note that the maximum PAPR, $PAPR_{\text{max}}$, is independent of the maximum number of users K because the amplitude of $x(t)$ and its average power depend on K, refer to Fig. (3.1) and (3.5).

For comparison, we obtain the PAPR upper bound for OFDMA system with block-interleaved frequency allocation scheme. In the case of OFDMA, the maximum possible amplitude value occurs when the same data symbol S is transmitted on each subcarrier $\kappa = nL + i$ of the ith user. Note, that we omitted index κ in S_κ, for simplicity. Then, the maximum amplitude value for the case of OFDM with L subcarriers can be represented by

$$x_{\text{max}} = \left| \frac{MS}{\sqrt{K}} \sum_{n=0}^{L-1} e^{\frac{2\pi}{L} nl} \right|. \tag{3.10}$$

Bearing in mind that

$$\sum_{n=0}^{L-1} e^{\frac{2\pi}{L} nl} = \begin{cases} L & \text{if } l = \imath L, \text{ where } \imath \text{ any integer number} \\ 0 & \text{otherwise} \end{cases} \tag{3.11}$$

the PAPR upper bound for the OFDMA simplifies to

$$PAPR_{\text{max}} = ML^2 |S|^2. \tag{3.12}$$

Note that the PAPR upper bound obtained for the OFDMA depends on the number of occupied subcarriers L whereas $PAPR_{\text{max}}$, obtained in (3.7) for IFDMA, is independent of L. $PAPR_{\text{max}}$ of an OFDMA system depends on the number of occupied subcarrier ML, whereas for the IFDMA system, $PAPR_{\text{max}}$ depends only on the coefficient M of the M-modification. In OFDMA, maximum amplitude value occurs only when the same data symbol is transmitted on all subcarriers. In this case, only one sample in the time domain signal has maximum amplitude, whereas other samples are equal to zero. Therefore, obtained PAPR upper bound for OFDMA is independent of the pulse-shaping function $g(t)$. In contrast to OFDMA, in conventional IFDMA systems the amplitude peak occurs as a superposition of the pulse-shaping functions of several chips, therefore, $PAPR_{\text{max}}$ depends on $g(t)$.

3.2.2 PAPR Distribution

The PAPR of a multi-carrier system takes on different values and PAPR depends on the transmit data sequence, modulation alphabet, spreading length and spreading type [FK00]. Thus, PAPR values of OFDM symbols form a distribution which can be characterized by its cumulative distribution function (CDF) [Pap02].

Thus, if $PAPR$ is the PAPR of an OFDM symbol, the CDF function $CDF(x)$ is given by

$$CDF(x) = \Pr\{PAPR \leq x\}, \tag{3.13}$$

where $\Pr\{.\}$ denotes probability. Thus, $CDF(x)$ shows the percentage of OFDM symbols which have PAPR less than x.

3.3 Simulation Results

3.3.1 Simulation Parameters

The simulated IFDMA, MSK-IFDMA, GOQPSK-IFDMA, OFDMA-CDM and OFDMA systems have

$$N_{\mathrm{c}} = 1024 \tag{3.14}$$

subcarriers. The carrier frequency is

$$f_{\mathrm{c}} = 5 \text{ GHz} \tag{3.15}$$

and the transmission bandwidth is

$$BW = 20 \text{ MHz}. \tag{3.16}$$

The maximum number of users is K. For OFDMA-CDM and IFDMA, the spreading length is L. For OFDMA, no spreading is applied. The parameters L and K are variable and an expression

$$N_{\mathrm{c}} = LK \tag{3.17}$$

always holds true. In order to variate the data rate per user the M-modification is applied. The total number of subcarriers occupied by each user is given as the product LM. Four different scenarios are considered: $M = 1$, $M = 4$, $M = 16$ and $M = 32$. Only one user is active, i.e.,

$$N_{\mathrm{u}} = 1. \tag{3.18}$$

With $M = L = K = 32$, the considered systems are fully loaded and all N_{c} subcarriers are occupied. An oversampling rate is

$$N_{\mathrm{ov}} = 16 \tag{3.19}$$

and perfect time and frequency synchronization at the BS receiver is assumed. The roll-off factor α of the RC pulse-shaping function is chosen as

$$\alpha = 0.25 \tag{3.20}$$

and the normalized bandwidth of the Gaussian pulse-shaping function defined in (2.77) is given by

$$BT_{\mathrm{c}} = 0.3. \tag{3.21}$$

The length of the RC pulse-shaping function is

$$N_{\mathrm{f}} = 3, \tag{3.22}$$

which results in a filter with 96 taps. The Gaussian and MSK pulse-shaping functions $g(t)$ in (2.75) and (2.77), respectively, are truncated symmetrically around zero and the length of these function is $N_{\mathrm{f}} = 2$ for both cases. As are result, MSK and Gaussian pulse-shaping filters have 64 taps each. All filters are modeled as finite impulse response (FIR) filters.

In OFDMA, OFDMA-CDM and IFDMA systems, QPSK is used as a modulation alphabet. For the MSK-IFDMA and GOQPSK-IFDMA, the modulation is chosen as described in Sec. 2.3.5. Therefore, all transmission systems have the same bandwidth efficiency and data rate. Table 3.1 briefly summarizes the parameters of the IFDMA/OFDMA/OFDMA-CDM/GOQPSK-IFDMA/MSK-IFDMA systems used in simulations. For simplicity, OFDM symbols of IFDMA, OFDMA and OFDMA-CDM systems are referred to as IFDMA, OFDMA and OFDMA-CDM symbols in the following.

Table 3.1: Parameters of the uplink IFDMA/OFDMA/OFDMA-CDM/GOQPSK-IFDMA/MSK-IFDMA systems.

Carrier frequency	$f_c = 5$ GHz
Number of subcarriers	$N_c = 1024$
Transmission bandwidth	$BW = 20$ MHz
Subcarrier spacing	$\Delta f = 19.53$ kHz
Chip duration	$T_c = 50$ ns
Number of OFDM symbols in an OFDM frame	$N_{\text{frame}} = 24$
Window type	rectangular
Modulation alphabet for IFDMA, OFDMA-CDM and OFDMA	QPSK with Gray coding
Spreading length (except OFDMA)	L, variable
Maximum allowed number of users	K, variable
Useful OFDM symbol duration	$T = 51.2$ μs
Guard interval duration	$T_\Delta = 1$ μs
LE technique	MMSE
Roll-off factor of the RC pulse-shaping function	$\alpha = 0.25$
Length of the RC pulse-shaping function	$N_f = 3$
Length of MSK and Gaussian pulse-shaping functions	$N_f = 2$
Oversampling coefficient	$N_{ov} = 16$
Filter type	FIR
Number of taps of the RC filter	96
Number of taps of Gaussian and MSK filters	64

3.3.2 Results and Discussions

In this section, we compare PAPR upper bounds and PAPR distributions of IFDMA, OFDMA, OFDMA-CDM, GOQPSK-IFDMA and MSK-IFDMA transmission systems.

The PAPR upper bounds are derived in (3.7), (3.9) and (3.12) for IFDMA, MSK-IFDMA and OFDMA respectively. The derived upper bounds are plotted in Fig. 3.2 as functions of the coefficient M of the M-modification, cf. Sec. 2.3.7. The spreading length is $L = 32$ and the maximum number of users is $K = 32$. Note that the product LM denotes the number of occupied subcarriers. Clearly, MSK-IFDMA and GOQPSK-IFDMA outperform conventional IFDMA and OFDMA, and have the lowest possible $PAPR_{\text{max}}$, since MSK-IFDMA and GOQPSK-IFDMA have a constant value $|x(t)|$ which is independent on the data sequence. The gap between the OFDMA and IFDMA curves is more than 20 dB and the gap between OFDMA and MSK/GOQPSK-IFDMA curves exceeds 30 dB. The $PAPR_{\text{max}}$ of the conventional IFDMA can be decreased by increasing the roll-off factor α of the pulse-shaping function $g(t)$. With increasing α, $PAPR_{\text{max}}$ of the conventional IFDMA approaches $PAPR_{\text{max}}$ of MSK/GOQPSK-IFDMA. The maximum value of α is one, but even if $\alpha = 1$, $PAPR_{\text{max}}$ of IFDMA does not reach the PAPR upper bound of MSK/GOQPSK-IFDMA. It is worth noting that the increasing of α increases an excess bandwidth of IFDMA, which is not desirable.

The CDF of PAPR is an important parameter and should be taken into account by the design of multi-carrier systems. For convenience, we put the PAPR values on the abscissa, whereas the corresponding CDF values, CDF, are plotted on the vertical axis. The CDFs of PAPR are shown in Fig. 3.3 for $M = 1$. Clearly, IFDMA outperforms OFDMA and OFDMA-CDM. Nearly 80% of OFDMA symbols and, approximately, a 90% of OFDMA-CDM symbols have PAPR less than 6 dB, whereas the maximum

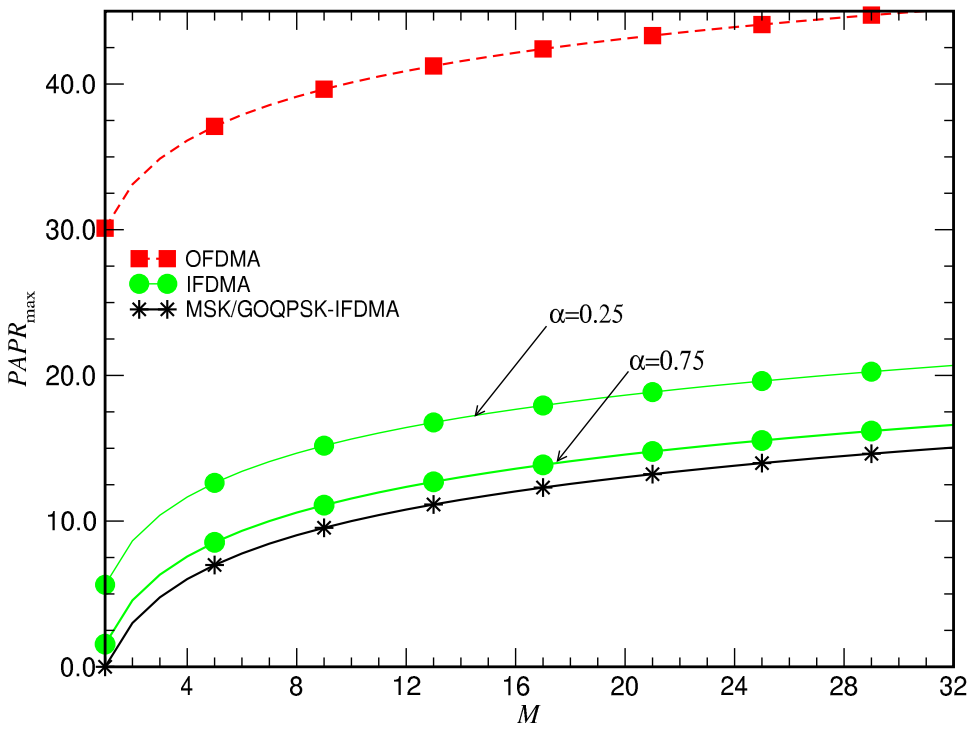

Figure 3.2: PAPR upper bound versus coefficient M of M-modification for IFDMA, MSK/GOQPSK-IFDMA and OFDMA; $L = 32$; $K = 32$.

PAPR of IFDMA is only 5.1 dB as calculated in (3.7). At the same time, only a 60% of OFDMA symbols and a 75% of OFDMA-CDM symbols have PAPR less than 5.1 dB. The PAPR performance of MSK-IFDMA and GOQPSK-IFDMA is the best among all other considered techniques. The PAPR of MSK-IFDMA is 0 dB, and GOQPSK-IFDMA has constant PAPR equal to 0.2 dB. The close analysis of Gaussian pulse-shaping function $g(t)$ in (2.77) reveals that it has ripples which are about 0.2 dB. These ripples does not provide the constant value of $|x(t)|$ and, in contrast to the sinusoid, the equation (2.76) is violated for GOQPSK. However, the amplitudes of ripples are small and have only minor influence on the results in Fig. 3.3. Generally, MSK/GOQPSK-IFDMA performs nearly 4 dB better than the conventional IFDMA and more than 6 dB better than OFDMA and OFDMA-CDM.

In Fig. 3.4, the CDFs of the PAPR are shown for the case of $M = 4$. Again, IFDMA outperforms OFDMA and OFDMA-CDM. The PAPR gap between the OFDMA and IFDMA curves is approximately 1.5 dB. The PAPR gap between the OFDMA-CDM and OFDMA curves is about 0.3 dB. Nearly a 60% of the MSK-IFDMA and GOQPSK-IFDMA symbols have PAPR larger than OFDMA and OFDMA-CDM symbols, however, the maximum PAPR for MSK-IFDMA and GOQPSK-IFDMA is less than the PAPR of the conventional IFDMA.

In Fig. 3.5, the CDFs of the PAPR are shown for the case of $M = 16$. Again, IFDMA outperforms OFDMA and OFDMA-CDM and the performance gain is approximately 0.3 dB. Note that the gain decreases with an increase of M if one compares Fig. 3.3, Fig. 3.4 and Fig. 3.5. In Fig. 3.6, M is equal to 32 and all subcarriers are occupied. The PAPR distributions are the same for IFDMA, OFDMA and OFDMA-CDM. The MSK/GOQPSK-IFDMA performs worse than IFDMA, OFDMA and OFDMA-CDM and the gap is approximately 2 dB.

In Fig. 3.7, PAPR values $PAPR$ versus M are shown. These values are taken so that a 90% of the transmit symbols of the considered multi-carrier system have PAPR less than $PAPR$.

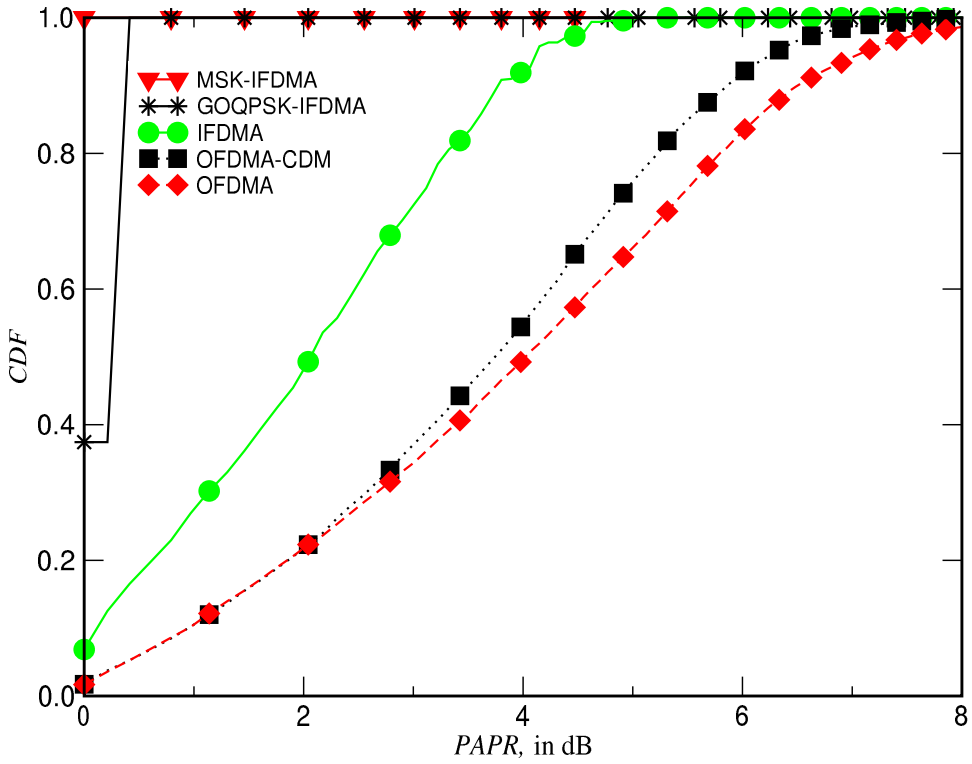

Figure 3.3: The CDF of the PAPR for IFDMA, OFDMA, OFDMA-CDM, GOQPSK-IFDMA and MSK-IFDMA; $M = 1$; $L = 32$; $K = 32$.

It can be concluded from Fig. 3.7 that the application of MSK-IFDMA and GOQPSK-IFDMA makes sense only for small values of M when MSK/GOQPSK-IFDMA results in the reduced PAPR comparing to OFDMA and OFDMA-CDM.

In the following, we investigate PAPR of fully loaded IFDMA, OFDMA, OFDMA-CDM, GOQPSK-IFDMA and MSK-IFDMA systems, when all subcarriers are occupied. We fix $M = 1$ and vary L and K bearing in mind that

$$N_c = LK = 1024. \tag{3.23}$$

The simulation parameters are summarized in Table 3.2. The PAPR for IFDMA, OFDMA and

Table 3.2: System parameters for fully loaded systems

Spreading length, L	Max. number of users, K	$\log_2(L)$
2	512	1
8	128	3
64	16	6
512	2	9
1024	1	10

OFDMA-CDM fully loaded systems versus $\log_2(L)$ are shown in Figure 3.8. As expected, IFDMA, GOQPSK-IFDMA and MSK-IFDMA outperform OFDMA and OFDMA-CDM for large values of L. If all subcarriers are occupied, PAPR of OFDMA and OFDMA-CDM is constant and is independent from L and K.

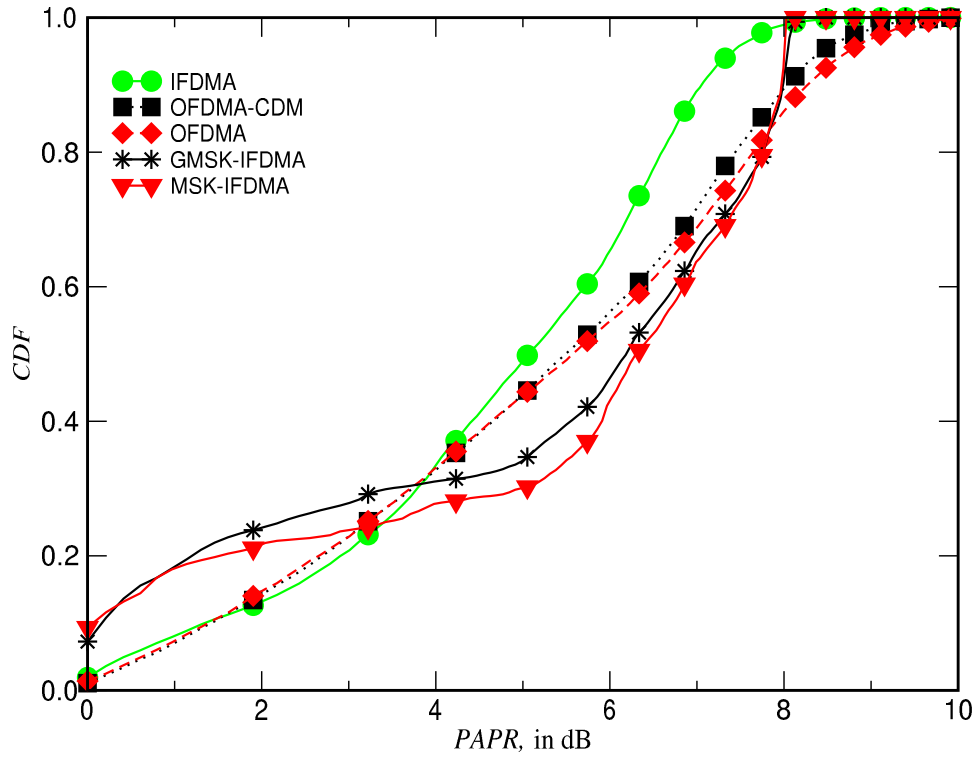

Figure 3.4: The CDF of the PAPR for IFDMA, OFDMA, OFDMA-CDM, GOQPSK-IFDMA and MSK-IFDMA; $M = 4$; $L = 32$; $K = 32$.

The IFDMA special case $L = 1024$ results in a single-carrier system with frequency domain equalization (SC-FDE) described in [FA02]. One of the advantages of SC-FDE is that it achieves the PAPR of single-carrier systems. With MSK/GOQPSK-IFDMA, the PARP of SC-FDE is minimized and equal to 0 dB. The SC-FDE has the same BER performance, spectral efficiency, complexity, immunity to the multi-path propagation as conventional OFDM [FA02].

Two cases $L = 1024$, $K = 1$ and $L = 512$, $K = 2$ are very promising for the downlink since they result in the lowest PAPR. If data from more than K users is required to be transmitted at the same time, one might simply mix the data streams of different users as in a conventional OFDM and do not assign to each user a separated set of subcarriers.

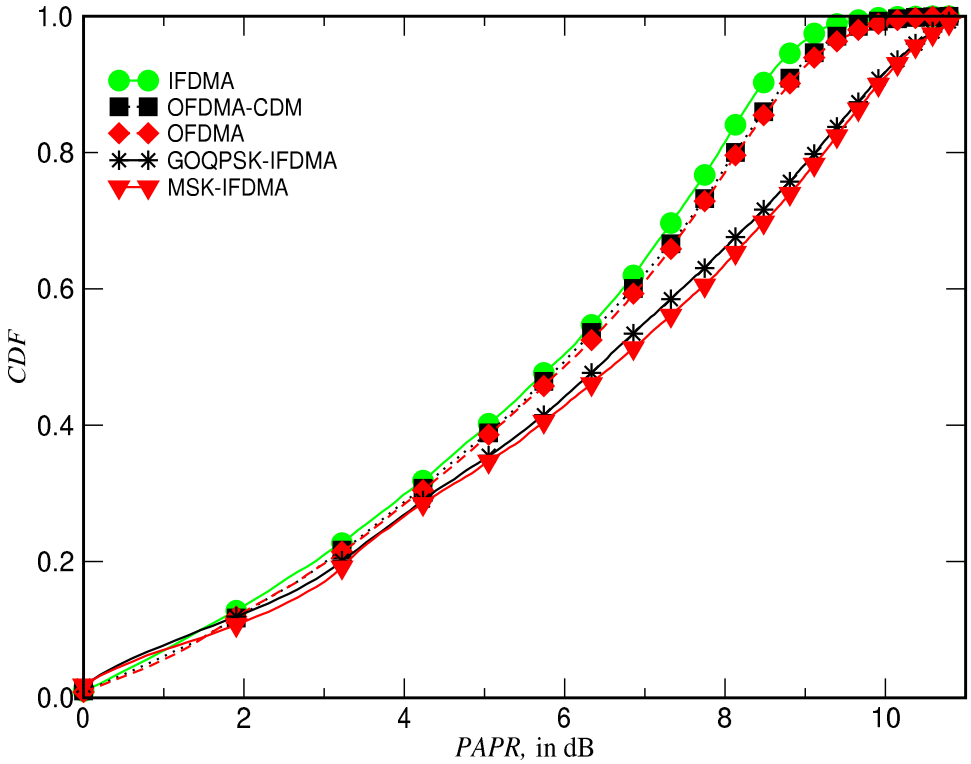

Figure 3.5: The CDF of the PAPR for IFDMA, OFDMA, OFDMA-CDM, GOQPSK-IFDMA and MSK-IFDMA; $M = 16$; $L = 32$; $K = 32$.

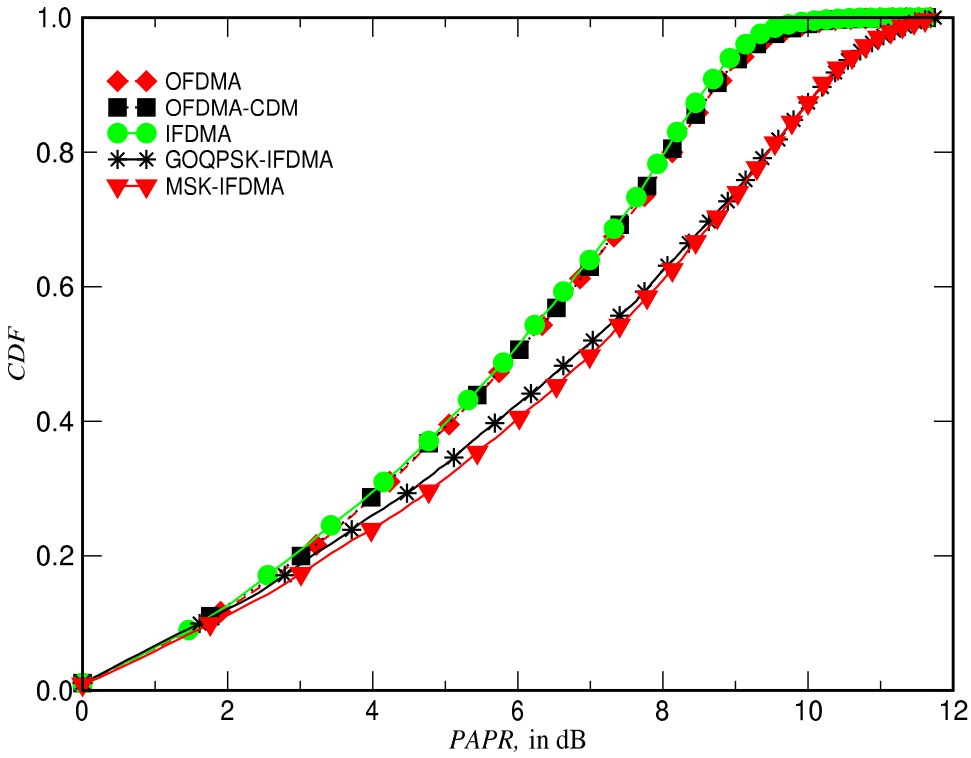

Figure 3.6: The CDF of the PAPR for IFDMA, OFDMA, OFDMA-CDM, GOQPSK-IFDMA and MSK-IFDMA; $M = 32$; $L = 32$; $K = 32$.

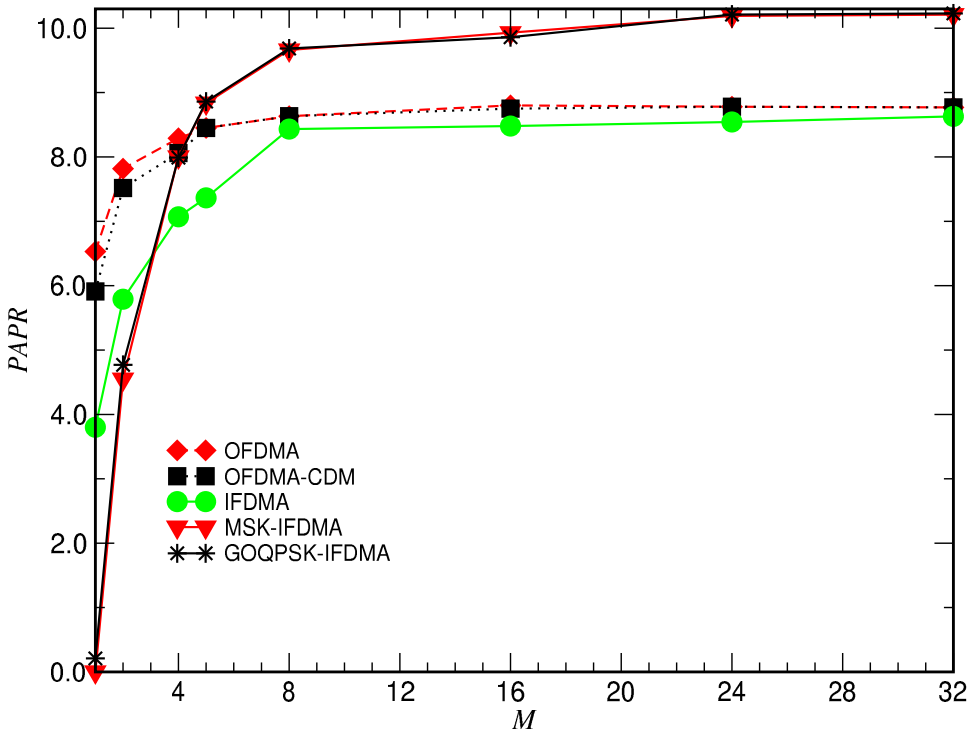

Figure 3.7: The PAPR values $PAPR$ versus coefficient M of the M-modification; $CDF(PAPR) = 0.9$; $L = 32$; $K = 32$.

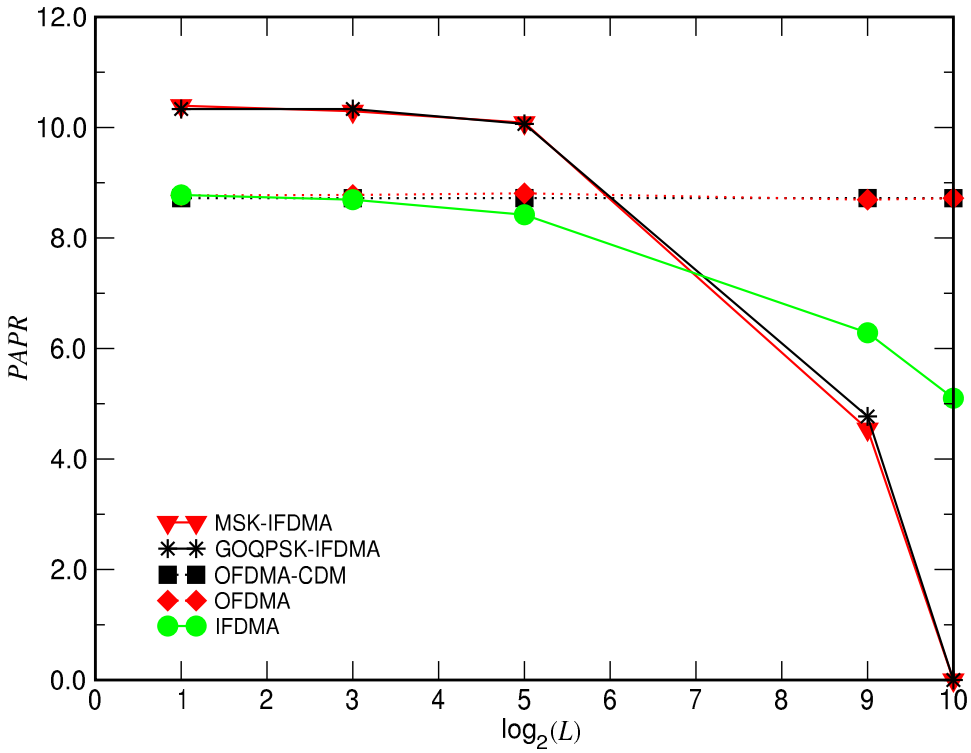

Figure 3.8: The PAPR values versus $\log_2(L)$ for fully loaded system; $CDF(PAPR) = 0.9$; $K = 32$; $M = 1$.

Chapter 4

Frequency Offset

4.1 Introduction

The system design of a multi-carrier uplink assumes that the distance between subcarriers of one user is larger than the coherent bandwidth of the transmission channel so that these subcarriers experience non-correlated fading [Kai98]. One of the advantages of IFDMA systems is that the subcarriers of one user are interleaved equidistantly, providing maximum frequency diversity for the received signal. Moreover, the orthogonality of subcarriers enables the BS to avoid MAI, since data symbols of different users are modulated on different subcarriers. However, these advantages come at the cost of sensitivity to frequency offsets. Multi-carrier systems with a block interleaved frequency allocation scheme especially suffer from the performance degradation due to frequency offsets [AS03].

In IFDMA uplink systems, frequency offsets are different for different users. These offsets occur because of a non-zero relative speed between the BS and MT or because of slightly disparate oscillator's frequencies at the receiver and transmitter [Haa03, PSM94]. Since IFDMA is a special case of OFDMA, IFDMA inherits the sensitivity of OFDMA to frequency offsets. The performance of an OFDMA uplink in the presence of frequency offsets is studied in [TLP00, Ste00]. The frequency offsets cause MAI, which leads to the performance degradation. Different methods to combat MAI in an OFDMA uplink can be divided into two groups. The first group requires the knowledge of the frequency offsets for each user at the receiver. If the frequency offsets of each user are perfectly known at the BS, interference cancelation schemes can be applied [HL05]. Another possibility is to estimate the frequency offset of each user at the BS. These estimates can be used to correct the sampling time instances at the BS receiver or can be sent back to the MTs where they are used to pre-compensate for the frequency offsets before transmission.

A second group of techniques to combat MAI assumes special construction of the OFDMA transmit signal such that the frequency offsets cause a reduced amount of MAI. One promising technique is windowing at the receiver or transmitter, which, however, has been investigated only for the case of an OFDM downlink [Mus96, MW01, SL05, YH03]. Another technique employs a subband frequency allocation scheme, where data of a particular user is transmitted on a specific subset of adjacent subcarriers as described in [AS03, LH05].

Unfortunately, the techniques of the second group suffer from a number of drawbacks such as low frequency diversity – as in the case of an adjacent subcarrier allocation scheme – or low bandwidth efficiency – as in the case of windowing at the transmitter or receiver.

Thus, the techniques which require frequency offset estimation at the BS seem to be only an alternative for a future IFDMA uplink. Generally, frequency offset estimation in the uplink of multi-carrier systems is a complicated task, since the signal received at the BS comprises the received signals from many users each of which can have its own frequency offset. Moreover, received signals from different users are distorted by different transmission channels, which complicates the issue. Several interesting research results for frequency offset estimation in OFDMA uplink have been presented in the literature. In [PTK04] and [PMK05], Pun proposed an algorithm to estimate and correct frequency synchronization errors with an arbitrary subcarrier allocation scheme. The performance of the proposed algorithm was studied in [RE05], under realistic conditions. In [CTY03], it is pointed out that the repetitive structure can be exploited for frequency offset estimation. Recently, Morelli presented a joint timing and frequency offset estimator for OFDMA uplink systems, which uses a block-interleaved subcarrier allocation scheme [Mor04].

In this chapter, we propose frequency domain (FD) and time domain (TD) algorithms for frequency offset estimation in the IFDMA uplink system. The algorithms use pilot symbols and exploit the signal structure of IFDMA for ML frequency offset estimation. As in [Mor04], we assume that other users have no time delay and are perfectly aligned to the BS reference. The obtained frequency estimate is returned to the MT via the downlink control channel and is used to adjust the MT carrier frequency.

The content and most important contributions and results of the investigations performed in this chapter are shortly summarized as follows:

- Simulation model for the IFDMA uplink with frequency offsets is presented in Sec. 4.2.
- The effect of frequency offsets on the performance of the IFDMA uplink system is studied in Sec. 4.3. It is shown that MAI can be reduced if the RC window is applied and that this reduction is achieved at the cost of bandwidth efficiency.
- A special construction of pilot symbols with additional spreading in the time domain is proposed in Sec. 4.4 which allows reduction of the frequency offset estimation error.
- A frequency domain algorithm for frequency offset estimation is proposed in Sec. 4.5. This algorithm utilizes pilot symbols and, together with frequency offset estimation, uses the ML principle for channel estimation.
- A practical time domain algorithm is proposed in Sec. 4.6, which uses the repetitive structure of the IFDMA transmit signal in the time domain. The TD algorithm is independent of the transmission channel and modulation alphabet.
- Statistical properties of the estimate provided by the time domain algorithm are analyzed analytically Sec. 4.6. As a result, the obtained estimate is unbiased and is able to provide a reliable result at an SNR of practical interest.
- The simulation parameters and Monte-Carlo simulation results are presented in Sec. 4.7. The performance of the proposed TD and FD algorithms is studied for different mobility scenarios. Additionally, the performance of the TD algorithm is compared with the technique presented in [Mor04]. The simulation results illustrate the TD algorithm's superior performance over existing techniques.

  Note that the investigations carried out in this chapter are partly presented in [AS, AS03, AS04a].

4.2 Simulation Model

The IFDMA uplink system inherits the main drawback of OFDMA - sensitivity to frequency offsets. In this subsection, a mathematical model of the IFDMA uplink system with frequency offsets is introduced and it is shown that frequency offset cause MAI which has a strong impact on the system performance. In what follows, an IFDMA uplink system with N_{u} active users is considered ($N_{\mathrm{u}} \leq K$) and each user transmits on its own set of L independent subcarriers as described in Chapter 2. The total number of subcarriers in the IFDMA uplink system is N_{c}. For simplicity, but without loss of generality, the M-modification coefficient M is equal to one.

We define $\epsilon^{(i)}$ as the frequency offset of user i normalized to the subcarrier spacing, i.e.,

$$\epsilon^{(i)} = \frac{\varepsilon^{(i)}}{\Delta f}, \tag{4.1}$$

where Δf denotes the subcarrier spacing defined in (2.3) and $\varepsilon^{(i)}$ is a frequency offset value measured in Hz.

In this chapter, we consider the case $|\epsilon^{(i)}| \leq 1$. This requirement must be kept in mind by the system designer. Therefore, the subcarrier spacing Δf should be larger than a given maximum Doppler frequency offset, which depends on the maximum speed of the MT and on the carrier frequency f_{c} [Pro00].

Moreover, we assume that each user i has its own frequency offset $\epsilon^{(i)}, i = 0, \ldots, N_{\mathrm{u}} - 1$, which is independent of the frequency offsets of other users. The received vector $\mathbf{y}$ after the guard interval removal can be represented by

$$\mathbf{y} = \sum_{i=0}^{N_{\mathrm{u}}-1} \underline{\mathbf{f}}^{(i)} \underline{\mathbf{h}}^{(i)} \mathbf{x}^{(i)} + \mathbf{n}, \tag{4.2}$$

where $\mathbf{n}$ is the AWGN vector, $\underline{\mathbf{h}}^{(i)}$ is a channel matrix of the ith user and $\mathbf{x}^{(i)}$ is a vector representing the transmit signal of the ith user. The diagonal matrix $\underline{\mathbf{f}}^{(i)}$ of a user frequency offset with dimensions $(N_{\mathrm{c}} + 2N_{\mathrm{w}}) \times (N_{\mathrm{c}} + 2N_{\mathrm{w}})$ can be represented as

$$\underline{\mathbf{f}}^{(i)} = \mathrm{diag}\{f_0^{(i)}, f_1^{(i)}, \ldots, f_{N_{\mathrm{c}}+2N_{\mathrm{w}}-1}^{(i)}\}, \tag{4.3}$$

where the lth diagonal element $f_l^{(i)}, l = 0, \ldots, N_{\mathrm{c}} + 2N_{\mathrm{w}} - 1$, is given by

$$f_l^{(i)} = e^{-j\frac{2\pi}{N_{\mathrm{c}}} i l \epsilon^{(i)}}. \tag{4.4}$$

The equation (4.2) mathematically describes the extended linear transmission model of IFDMA uplink. In contrast to model (2.3), the effects of N_{c} independent carrier frequency offsets are taken into account. With these offsets, the different subcarriers of the different users are no longer orthogonal.

At first, the received vector $\mathbf{y}$ is converted into the frequency domain by performing a DFT operation as described in Chapter 2. As a result, vector $\mathbf{Y}$ is obtained. Due to the frequency offsets, different subcarriers of different users are not orthogonal and have crosstalks.

When frequency offset is presented, the received SED of each individual subcarrier is shifted in frequency, and therefore, two independent effects appear. The first one is the signal-to-noise ratio degradation because each subcarrier is "sampled" not on its optimum point with the highest transmit power. The second one is MAI since subcarriers are not orthogonal to each other. If uplink is considered where each user has it own frequency offset as in considered IFDMA uplink, the MAI is a dominating negative factor which influences BER performance.

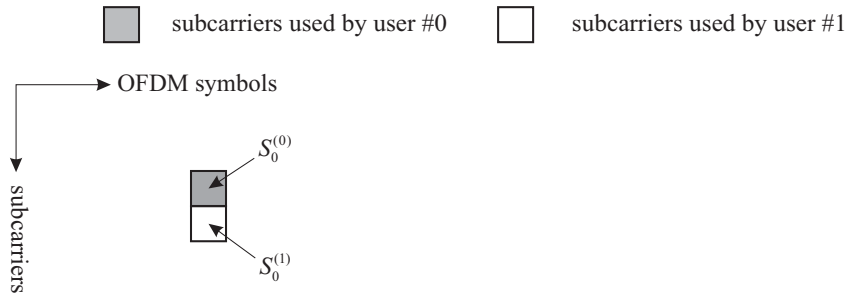

Figure 4.1: Example of OFDM frame with two active users. Each user utilizes only one subcarrier for data transmission.

In order to closely analyze MAI, we consider simplified IFDMA system with $N_c = 2$ subcarriers and only two active users. Each users utilizes only one subcarriers for data transmission and transmits only one data symbol per OFDM symbol. The source data vector for user #0 is

$$\mathbf{S}^{(0)} = \begin{pmatrix} S_0^{(0)} \\ 0 \end{pmatrix} \tag{4.5}$$

and the source data vector for user #1 is given by

$$\mathbf{S}^{(1)} = \begin{pmatrix} 0 \\ S_0^{(1)} \end{pmatrix}. \tag{4.6}$$

The matrix of fading coefficients $\underline{\mathbf{H}}^{(0)}$ of user #0 is given by

$$\underline{\mathbf{H}}^{(0)} = \begin{pmatrix} H_0^{(0)} & 0 \\ 0 & H_1^{(0)} \end{pmatrix}. \tag{4.7}$$

For the user #1, the matrix of fading coefficients $\underline{\mathbf{H}}^{(1)}$ is given by

$$\underline{\mathbf{H}}^{(1)} = \begin{pmatrix} H_0^{(1)} & 0 \\ 0 & H_1^{(1)} \end{pmatrix}. \tag{4.8}$$

The received vector $\mathbf{Y}$ obtained after DFT operation is given by

$$\mathbf{Y} = \begin{pmatrix} Y_0^{(0)} \\ Y_1^{(0)} \end{pmatrix}. \tag{4.9}$$

The element $Y_0^{(0)}$ can be represented by

$$Y_0^{(0)} = \underbrace{I_0(\epsilon^{(0)}) S_0^{(0)} H_0^{(0)}}_{\text{useful part}} + \underbrace{I_1(\epsilon^{(1)}) S_1^{(1)} H_0^{(1)}}_{\text{MAI}} + N_0^{(0)} \tag{4.10}$$

and the element $Y_0^{(0)}$ is represented by

$$Y_0^{(0)} = \underbrace{I_0(\epsilon^{(1)}) S_0^{(1)} H_0^{(1)}}_{\text{useful part}} + \underbrace{I_{-1}(\epsilon^{(0)}) S_1^{(0)} H_0^{(0)}}_{\text{MAI}} + N_1^{(0)}, \tag{4.11}$$

where $I_{\kappa-\kappa'}(\epsilon^{(i)})$ is a carrier frequency offset (CFO) coefficient. The CFO coefficients $I^{(i)}_{\kappa-\kappa'}$ shows the crosstalk, which subcarrier κ has on the subcarrier κ'. The CFO coefficient is defined in (A.2) as

$$I_{\kappa-\kappa'}(\epsilon^{(i)}) = \frac{1}{N_{\mathrm{c}}\sqrt{2}} \sum_{\upsilon=0}^{N_{\mathrm{c}}+2N_{\mathrm{w}}-1} w_\upsilon e^{j\frac{2\pi\upsilon(2\kappa+2\epsilon^{(i)}-\kappa')}{2N_{\mathrm{c}}}}. \tag{4.12}$$

The CFO coefficient $I_{\kappa-\kappa'}(\epsilon^{(i)})$ depends on the frequency offset $\epsilon^{(i)}$ and represents the DFT of the window function, as shown in (A.2). In our simplified case with two users, the received element in (4.10) and (4.10) is composed of three addends. The last one is an AWGN sample, the first one represents the useful part of the data received on this subcarrier and the second one is the MAI, which represents the crosstalk which subcarrier has on the adjacent one. Note that the subscripts 0 in $I_0(\epsilon^{(0)})$ and $I_0(\epsilon^{(1)})$ represents the energy degradation on the considered subcarrier due to the frequency offset. The CFO coefficients build the CFO matrix $\underline{\mathbf{I}}$ as

$$\underline{\mathbf{I}} = \begin{pmatrix} I_0(\epsilon^{(0)}) & I_1(\epsilon^{(1)}) \\ I_{-1}(\epsilon^{(0)}) & I_0(\epsilon^{(1)}) \end{pmatrix}, \tag{4.13}$$

where main diagonal represents the useful part of the received signal $\mathbf{Y}^{(i)}$, whereas other elements represent MAI. In the common case, when N_{u} users transmit simultaneously $\mathbf{Y}$ is given by

$$\mathbf{Y} = \underline{\mathbf{I}} \sum_{i=0}^{N_{\mathrm{u}}-1} \underline{\mathbf{H}}^{(i)}\mathbf{S}^{(i)} + \mathbf{N}, \tag{4.14}$$

where $\underline{\mathbf{H}}^{(i)}$ and $\mathbf{S}^{(i)}$ represent the matrix of fading coefficient and the vector of transmit data symbols of the ith user, respectively, and $\mathbf{N}$ designates the vector of AWGN samples in the frequency domain.

The square matrix $\underline{\mathbf{I}}$ of CFO coefficients has dimensions of $N_{\mathrm{c}} \times N_{\mathrm{c}}$ and is composed of the CFO coefficients. Note if all frequency offset are equal to zero then $\underline{\mathbf{I}}$ is a unity matrix and no MAI is presented. Otherwise, if only one user has frequency offset, all N_{c} subcarriers are affected. The CFO coefficients in each row can be arbitrarily subdivided into two groups: CFO coefficients representing the useful part of the signal and CFO coefficients representing the MAI.

4.3 Performance Degradation due to Frequency Offset

In this section, we consider IFDMA uplink performance degradation due to frequency offsets $\epsilon^{(i)}, i = 0, \ldots, N_{\mathrm{u}} - 1$. In doing so, we vary the frequency offsets and calculate the signal-to-interference ratio (SIR) for different β. For this consideration, we assume that frequency offsets of different users are constant and equal to one another.

In order to demonstrate the effect of different window function on each individual subcarrier, we consider Fig. 4.2 where only one subcarrier is depicted for different values of the roll-off factor β. By varying the window function $w(t)$, SED of each individual subcarrier can be changed. If we take β large, which simultaneously means large prefix and postfix, the sidelobes of subcarriers can be significantly reduced. Reduced sidelobes simultaneously means reduced amount of MAI induced on neighboring subcarriers.

In our analysis of the performance degradation, we utilize CFO coefficients introduced in the previous section. The SIR is calculated as the ratio between the variance of the useful part, which is represented by the coefficient I_0 and the variance of MAI, which comes from other N_{u} users, each

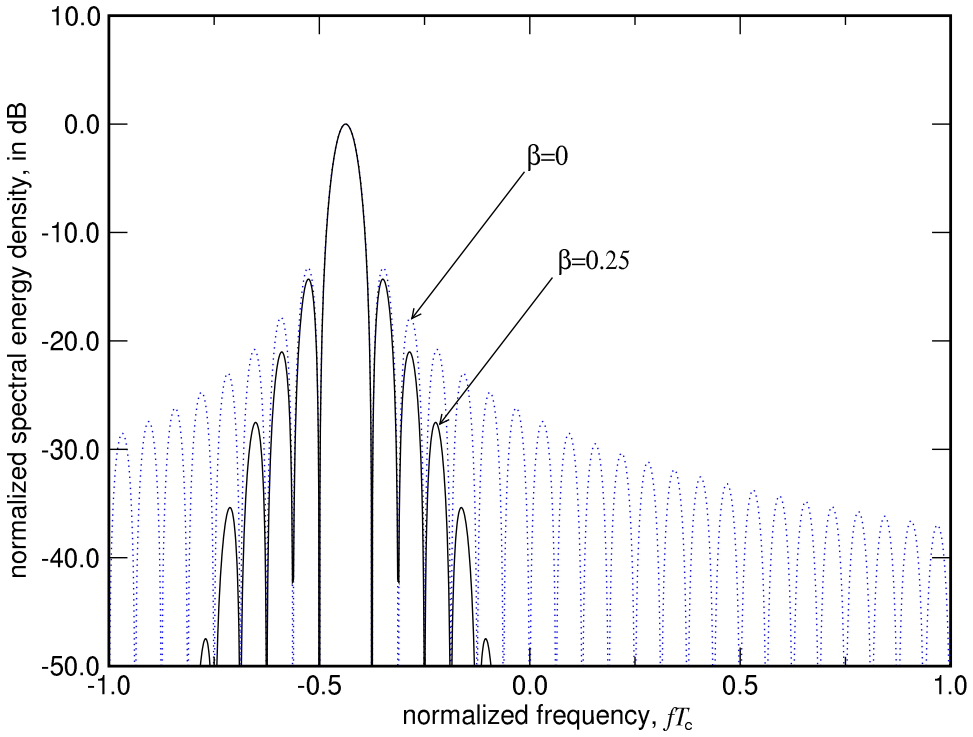

Figure 4.2: The normalized received SEDs of the modulated subcarrier $\kappa = 1$ versus normalized frequency fT_{c} for $\beta = 0$ and $\beta = 0.25$; $N_{\mathrm{c}} = 16$.

with L subcarriers. Since all users are equivalent and all subcarriers of one user suffer from the same amount of MAI, the SIR curves are plotted for subcarrier $n = 0$ of user $i = 0$. The SIR is calculated as ration of the square of the useful part to the sum of square values of the MAI

$$SIR = \frac{|I_0(\epsilon^{(i)})|^2}{\sum\limits_{\substack{v=0 \\ v\neq i}}^{N_{\mathrm{u}}-1} \sum\limits_{u=0}^{L-1} |I_{uK+v}(\epsilon^{(v)})|^2}. \tag{4.15}$$

In Fig. 4.3, the SIR versus the normalized frequency offset $\epsilon^{(i)}$ is depicted, which is calculated via (4.15) for different roll-off factors β. The considered IFDMA system has $N_{\mathrm{c}} = 1024$ subcarriers and $N_{\mathrm{u}} = 32$ active users. The spreading length is $L = 32$.

Obviously, the SIR curves tend to plus infinity if $\epsilon^{(i)}$ approaches zero since the denominator in (4.15) tends to zero. The SIR decreases with increasing $\epsilon^{(i)}$, and reaches nearly 0 dB, if $\epsilon^{(i)}$ approaches one half of the subcarrier spacing. If $\epsilon^{(i)} = 0.5$ then it is not possible to distinguish between two adjacent subcarriers at the receiver, since at $\epsilon^{(i)} = 0.5$ the influences coming from the two neighboring subcarriers are equal.

As can be seen, windowing is an efficient countermeasure against MAI, albeit with a sacrifice in spectral efficiency. At $\epsilon^{(i)} = 0.1$, SIR can be improved by 7 dB if a window with $\beta = 0.75$ is used instead of the conventional rectangular window with $\beta = 0$. However, such a performance gain is at the cost of a 75% loss in the spectral efficiency. The SIR gain decreases rapidly with decreasing β. If $\beta = 0.25$, which is a 25% loss in spectral efficiency, the SIR gain is only about 2 dB. With an increase in the normalized frequency offset $\epsilon^{(i)}$, the positive effect of windowing decreases. If $\epsilon^{(i)} = 0.4$ then

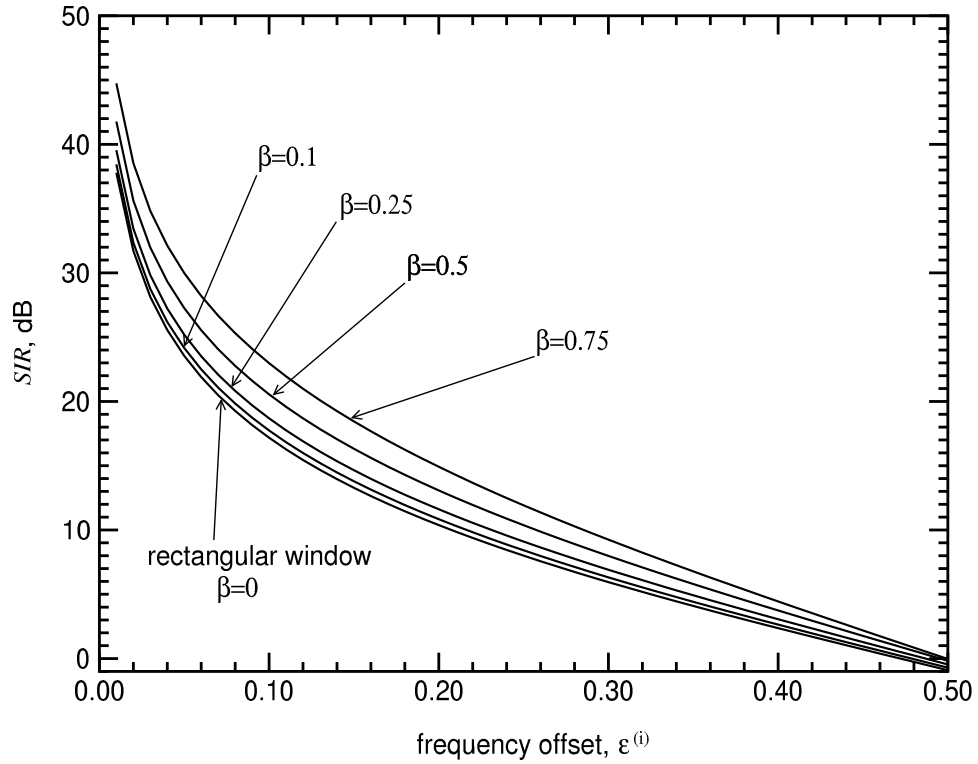

Figure 4.3: SIR versus frequency offset $\epsilon^{(i)}$.

the SIR gain between the curve with $\beta = 0.75$ and the rectangular window is only 3 dB. Therefore, it makes sense to apply a window with $\beta > 0$ for low values of $\epsilon^{(i)}$.

4.4 MAI Reduction

The main objective of this chapter is to evaluate practical and simple algorithms for frequency offset estimation in uplink IFDMA. All algorithms proposed in this chapter are pilot-aided, and thus, we introduce pilot symbols in an OFDM frame of IFDMA system. Before processing with frequency offset estimation algorithms, a special construction of pilot symbols is described in this subsection, which makes it possible to suppress MAI in the receiver.

The MAI reduction can be easily understood by considering a simple example in Fig. 4.4. For the purpose of clarity we consider simplified IFDMA system with $N_{\mathrm{c}} = 2$ subcarriers where each user transmits only one data symbols within one OFDM symbol. Two users are active: user #0 and user #1 and two successive OFDM symbols are considered for the MAI reduction. It is assumed that user #0 utilizes pilot symbol $\bar{S}_0^{(0)}$ and user #1 transmits pilot symbol $\bar{S}_0^{(1)}$. User #0 transmits pilot symbols which have opposite signs: $\bar{S}_0^{(0)}$ in the first OFDM symbol and $-\bar{S}_0^{(0)}$ in the second one. The user #1 transmit $\bar{S}_0^{(1)}$ twice in both OFDM symbols.

In this example, user #0 utilizes the WH spreading sequence of length $P_{\mathrm{p}} = 2$

$$\bar{\mathbf{C}}^{(0)} = (\bar{C}_0^{(0)}, \bar{C}_1^{(0)})^T = (1, -1)^T, \tag{4.16}$$

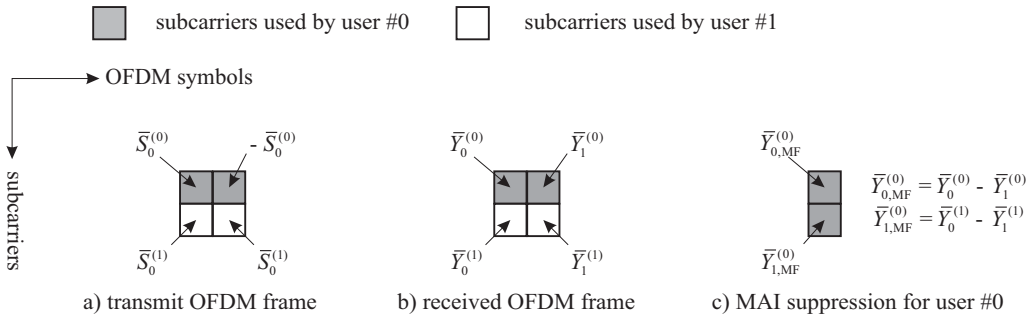

Figure 4.4: Example of OFDM frame with two active users. Each user utilizes only one subcarrier for data transmission. For the MAI reduction, two OFDM symbols are shown.

whereas user #1 uses the WH sequence

$$\bar{\mathbf{C}}^{(1)} = (\bar{C}_0^{(1)}, \bar{C}_1^{(1)}) = (1,1)^T. \tag{4.17}$$

Vector $\bar{\mathbf{S}}^{(0)}$ represents pilot symbols transmitted in one OFDM frame for user #0

$$\bar{\mathbf{S}}^{(0)} = \bar{\mathbf{C}}^{(0)}\bar{S}_0^{(0)} = (\bar{S}_0^{(0)}, -\bar{S}_0^{(0)})^T \tag{4.18}$$

and the vector $\bar{\mathbf{S}}^{(1)}$ represents pilot symbols for user #1

$$\bar{\mathbf{S}}^{(1)} = \bar{\mathbf{C}}^{(1)}\bar{S}_0^{(1)} = (\bar{S}_0^{(1)}, \bar{S}_0^{(1)})^T. \tag{4.19}$$

Such a construction of pilot symbols demonstrates additional spreading in the time direction, and can be performed for the WH spreading code with length more than two. For the MAI reduction, we consider received data symbols $\bar{Y}_0^{(0)}$, $\bar{Y}_1^{(0)}$, $\bar{Y}_0^{(1)}$, $\bar{Y}_1^{(1)}$ as shown in Fig. 4.4b. $\bar{Y}_0^{(0)}$ is given by

$$\bar{Y}_0^{(0)} = \underbrace{I_0(\epsilon^{(0)})S_0^{(0)}H_0^{(0)}}_{\text{useful part}} + \underbrace{I_1(\epsilon^{(1)})S_0^{(1)}H_0^{(1)}}_{\text{MAI}} + N_0^{(0)}, \tag{4.20}$$

where $\bar{Y}_0^{(1)}$ is given by

$$\bar{Y}_1^{(0)} = \underbrace{-I_0(\epsilon^{(0)})S_0^{(0)}H_0^{(0)}}_{\text{useful part}} + \underbrace{I_1(\epsilon^{(1)})S_0^{(1)}H_0^{(1)}}_{\text{MAI}} + N_1^{(0)}. \tag{4.21}$$

$\bar{Y}_0^{(1)}$ is represented by

$$\bar{Y}_0^{(1)} = \underbrace{I_0(\epsilon^{(1)})S_0^{(1)}H_0^{(1)}}_{\text{useful part}} + \underbrace{I_{-1}(\epsilon^{(0)})S_0^{(0)}H_0^{(0)}}_{\text{MAI}} + N_0^{(1)}, \tag{4.22}$$

and $\bar{Y}_1^{(1)}$ is given by

$$\bar{Y}_1^{(1)} = \underbrace{I_0(\epsilon^{(1)})S_1^{(1)}H_0^{(1)}}_{\text{useful part}} - \underbrace{I_{-1}(\epsilon^{(0)})S_0^{(0)}H_0^{(0)}}_{\text{MAI}} + N_1^{(1)}. \tag{4.23}$$

The received symbols $\bar{Y}_0^{(0)}$, $\bar{Y}_1^{(0)}$ $\bar{Y}_0^{(1)}$ and $\bar{Y}_1^{(1)}$ are comprised of the received signals of users #0 and #1. Note that considered users have different frequency offsets and received signals $\bar{Y}_0^{(0)}$, $\bar{Y}_1^{(0)}$ $\bar{Y}_0^{(1)}$ and $\bar{Y}_1^{(1)}$ are influenced by different mobile radio channels. Fading coefficients are not known.

Our main goal is to eliminated MAI so that the result contains only data of user #0, and information about frequency offset remains. Note that useful parts in (4.20) and (4.21) have opposite signs, whereas MAI addends are equal in both equation. In contrast, in (4.22) and (4.23) useful parts are the same and the signs of MAI parts are different.

We eliminate MAI for the user #0 as shown in Fig. 4.4c. In doing so, we simply subtract (4.21) from (4.20)

$$\bar{Y}_{0,\mathrm{MF}}^{(0)} = (\bar{Y}_0^{(0)} - \bar{Y}_1^{(0)})/2 = I_0(\epsilon^{(0)}) S_0^{(0)} H_0^{(0)} + (N_0^{(0)} - N_1^{(0)})/2, \tag{4.24}$$

where division by two is performed for the energy normalization. This division is not necessary, since it does not have any impact on the SNR of the $\bar{Y}_{0,\mathrm{MF}}^{(0)}$ and might be omitted.

The subtraction of $\bar{Y}_1^{(1)}$ from $\bar{Y}_0^{(1)}$ gives

$$\bar{Y}_{1,\mathrm{MF}}^{(0)} = (\bar{Y}_0^{(1)} - \bar{Y}_1^{(1)})/2 = I_{-1}(\epsilon^{(0)}) S_0^{(0)} H_0^{(0)} + (N_0^{(1)} - N_1^{(1)})/2. \tag{4.25}$$

The MAI, induced by user #1 is removed ideally. MAI-free received values $\bar{Y}_{0,\mathrm{MF}}^{(0)}$ and $\bar{Y}_{1,\mathrm{MF}}^{(0)}$ are comprised only of the received signal of user #0 and bear information about frequency offset $\epsilon^{(0)}$. Elements $\bar{Y}_{0,\mathrm{MF}}^{(0)}$ and $\bar{Y}_{1,\mathrm{MF}}^{(0)}$ form vector

$$\bar{\mathbf{Y}}^{(0)} = \{\bar{Y}_{0,\mathrm{MF}}^{(0)}, \bar{Y}_{1,\mathrm{MF}}^{(0)}\}^T, \tag{4.26}$$

which is used for frequency offset estimation $\epsilon^{(0)}$. Note that we omitted subscript MF for simplicity. After despreading, the CFO matrix $\underline{\mathbf{I}}^{(i)}$ for the received vector $\bar{\mathbf{Y}}^{(0)}$ is given by

$$\underline{\mathbf{I}}^{(i)} = \begin{pmatrix} I_0(\epsilon^{(0)}) & 0 \\ I_{-1}(\epsilon^{(0)}) & 0 \end{pmatrix}. \tag{4.27}$$

For the user #1, the decomposition is performed in the same way, only addition is required instead of substraction. The considered example with two users MAI is suppressed ideally if mobile channels remain constant for two consecutive OFDM symbols. If total number of active users N_u is more than two, odd users can use WH sequence $\bar{\mathbf{C}}^{(0)}$, whereas even users might utilize sequence $\bar{\mathbf{C}}^{(1)}$. In this case, the MAI induced by odd users can be eliminated, but the even users will experience residual MAI, since interference between even users cannot be suppressed with the proposed method. MAI can be further suppressed if WH codes with a length more than two are applied, which means that more than two successive pilot OFDM symbols are required. For the successful MAI elimination, channels should remain constant for the time duration of all pilot OFDM symbols, which is realistic only for the small number of such pilots.

Pilot symbols can be allocated anywhere in the OFDM frame, and without loss of generality, they can be allocated at the beginning of the OFDM frame, as shown in Fig. 4.5. MAI reduction can also be performed in the time domain without the DFT operation. The time domain signal $\bar{\mathbf{y}}^{(i)}$ obtained for the user i can also be used for frequency offset estimation

4.5 Frequency Offset Estimation in the Frequency Domain

In the following, the frequency offset estimation algorithm for user i is presented, which operates in the frequency domain and uses pilot symbols. For frequency offset estimation, we consider the received vector $\bar{\mathbf{Y}}^{(i)}$ which represents pilot symbols after MAI suppression. The L received elements

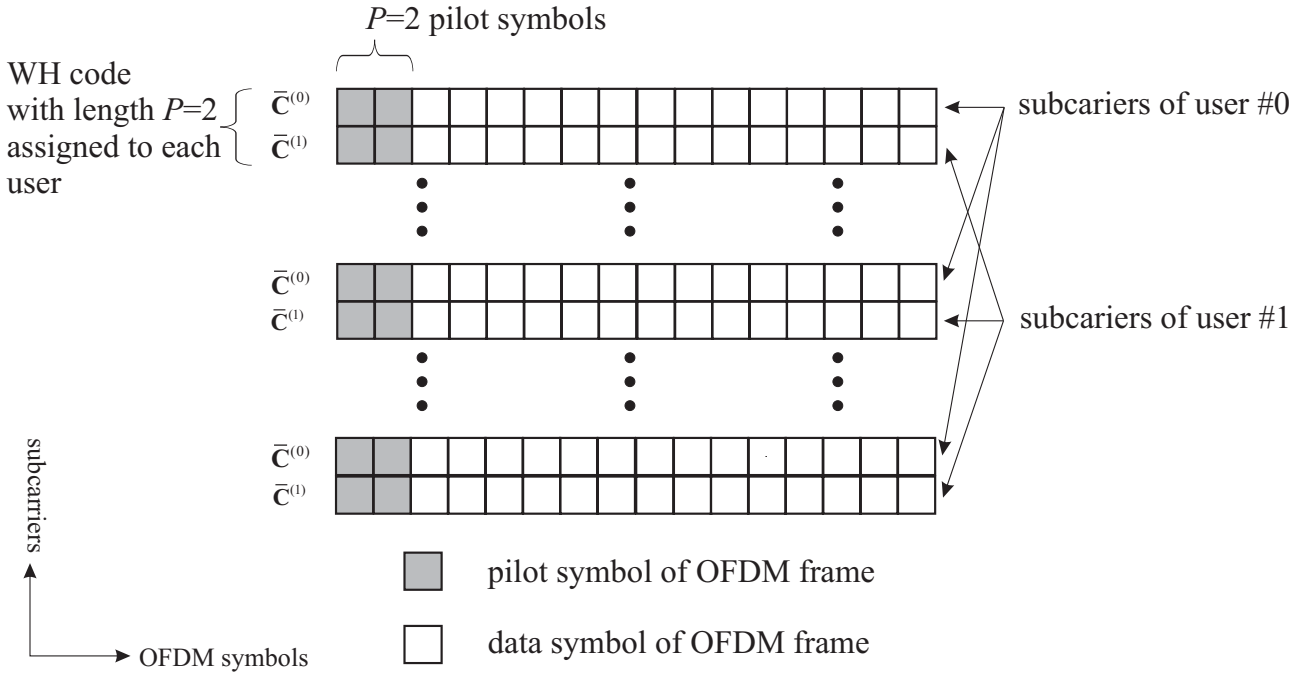

Figure 4.5: Received OFDM frame of IFDMA system in the frequency domain with $P_{\mathrm{p}} = 2$ pilot symbols.

$\bar{Y}^{(i)}_{\kappa'}, \kappa' = 2\kappa, \kappa = nK + i, n = 0, \ldots, L-1$, represent data of user i. Each element $\bar{Y}^{(i)}_{\kappa'}, \kappa' = 2\kappa$, represent data received on the κth subcarrier. For frequency offset estimation, we additionally consider elements $\bar{Y}^{(i)}_{\kappa'+2}$, of the the vector $\bar{\mathbf{Y}}^{(i)}$. The element $\bar{Y}^{(i)}_{\kappa'+2}$ represents the received data on the subcarrier $\kappa + 1$.

In the proposed algorithm, $2L$ subcarriers are utilized for frequency offset estimation. For each subcarrier $\kappa, \kappa = nL + i, n = 0, \ldots, L-1$, one additional subcarrier $\kappa + 1$ is used. We introduce a new vector $\bar{\mathbf{Y}}_{\mathrm{r}}$, of length $2L$ composed of received values $\bar{Y}^{(i)}_{\kappa'}$ and $\bar{Y}^{(i)}_{\kappa'+2}$, given by

$$\bar{\mathbf{Y}}_{\mathrm{r}} = (\bar{Y}^{(i)}_{2i}, \bar{Y}^{(i)}_{2i+2}, \bar{Y}^{(i)}_{2K+2i}, \bar{Y}^{(i)}_{2K+2i+2}, \bar{Y}^{(i)}_{4K+2i}, \bar{Y}^{(i)}_{4K+2i+2}, \ldots, \bar{Y}^{(i)}_{2(L-1)K+2i}, \bar{Y}^{(i)}_{2(L-1)K+2i+2})^T. \quad (4.28)$$

Moreover, we introduce the vector of fading coefficients $\mathbf{H}_{\mathrm{r}}$ which is composed of L elements $H_{\mathrm{r},n}, n = 0, \ldots, L-1$, and can be represented as

$$H_{\mathrm{r},n} = H^{(i)}_{2nK+2i}, \quad (4.29)$$

where $H^{(i)}_{nK+i}$ are the diagonal elements of the channel matrix $\underline{\mathbf{H}}^{(i)}$ defined in (2.49). Thus, vector $\mathbf{H}_{\mathrm{r}}$ represents the fading coefficients of the L subcarriers where user i transmits its pilot symbols $\bar{S}^{(i)}_{\kappa}, \kappa = nK + i, n = 0, \ldots, L-1$.

Note that the vector $\mathbf{H}_{\mathrm{r}}$ is unknown at the receiver and needs to be estimated together with the frequency offset $\epsilon^{(i)}$. As a result, the proposed algorithm is considered as a joint estimation of the frequency offset $\epsilon^{(i)}$ and the vector $\mathbf{H}_{\mathrm{r}}$, i.e., the fading coefficients of the ith user. For simplicity, we omit index (i) in the reminder of this section.

The relation between vector $\mathbf{H}_{\mathrm{r}}$ and $\bar{\mathbf{Y}}_{\mathrm{r}}$ can be written as

$$\bar{\mathbf{Y}}_{\mathrm{r}} = \underline{\mathbf{\Theta}}(\epsilon)\mathbf{H}_{\mathrm{r}} + \bar{\mathbf{N}}, \quad (4.30)$$

where $\underline{\mathbf{\Theta}}(\epsilon)$ is a $2L \times L$-dimensional matrix, which is determined by the frequency offset coefficients given in (4.12)

$$\underline{\mathbf{\Theta}}(\epsilon) = \begin{pmatrix} I_0(\epsilon) & I_K(\epsilon) & I_{2K}(\epsilon) & \dots & I_{(L-1)K}(\epsilon) \\ I_{-1}(\epsilon) & I_{K-1}(\epsilon) & I_{2K-1}(\epsilon) & \dots & I_{(L-1)K-1}(\epsilon) \\ I_{-K}(\epsilon) & I_0(\epsilon) & I_K(\epsilon) & \dots & I_{(L-2)K}(\epsilon) \\ \vdots & \vdots & \vdots & \vdots & \\ I_{(1-L)K}(\epsilon) & I_{(2-L)K}(\epsilon) & \dots & I_{-K}(\epsilon) & I_0(\epsilon) \\ I_{(1-L)K-1}(\epsilon) & I_{(2-L)K-1}(\epsilon) & \dots & I_{-K-1}(\epsilon) & I_{-1}(\epsilon) \end{pmatrix} \begin{pmatrix} \bar{S}_0 \\ \bar{S}_{K+i} \\ \bar{S}_{2K+i} \\ \vdots \\ \vdots \\ \bar{S}_{K(L-1)+i} \end{pmatrix} \tag{4.31}$$

and $\bar{\mathbf{N}}$ is a vector of AWGN samples of length $2L$.

Our task is to estimate the frequency offset $\hat{\epsilon}$ by exploiting the vector $\bar{\mathbf{Y}}_{\mathrm{r}}$ and equation (4.30). A ML approach can be utilized for this purpose. Initially, we keep $\tilde{\epsilon}$ constant and try to find the estimate $\hat{\mathbf{H}}$ for the unknown vector $\mathbf{H}_{\mathrm{r}}$, and, then, we build a trial function and vary $\tilde{\epsilon}$. The ML estimation $\hat{\mathbf{H}}$ of the vector $\mathbf{H}_{\mathrm{r}}$ is given by [Sch02]

$$\hat{\mathbf{H}} = [\underline{\mathbf{\Theta}}^H(\tilde{\epsilon})\underline{\mathbf{\Theta}}(\tilde{\epsilon})]^{-1}\underline{\mathbf{\Theta}}^H(\tilde{\epsilon})\bar{\mathbf{Y}}_{\mathrm{r}}. \tag{4.32}$$

Substituting (4.32) into (4.30) and maximizing with respect to $\tilde{\epsilon}$ produces the trial function of the ML estimate $\hat{\epsilon}$ of the frequency offset ϵ

$$\hat{\epsilon} = \arg\max_{\tilde{\epsilon}} \bar{\mathbf{Y}}_{\mathrm{r}}^H \underline{\mathbf{\Theta}}(\tilde{\epsilon}) \left[\underline{\mathbf{\Theta}}^H(\tilde{\epsilon})\underline{\mathbf{\Theta}}(\tilde{\epsilon})\right]^{-1} \underline{\mathbf{\Theta}}^H(\tilde{\epsilon})\bar{\mathbf{Y}}_{\mathrm{r}}. \tag{4.33}$$

This algorithm is referred to as the frequency domain frequency offset estimation algorithm (FD) in the following.

The following remarks are of interest:

- The FD algorithm requires one-dimensional search for ϵ over the interval $[-\epsilon_{\text{max}}, \epsilon_{\text{max}}], \epsilon_{\text{max}} < 0.5$, where ϵ_{max} is the maximum possible frequency offset.
- Inversion of an $L \times L$-dimensional matrix $\left[\underline{\mathbf{\Theta}}^H(\tilde{\epsilon})\underline{\mathbf{\Theta}}(\tilde{\epsilon})\right]$ is required in (4.33).
- The FD algorithm is performed in the frequency domain. Thus, user separation is performed by choosing an appropriate subcarrier set in (4.28).
- The FD algorithm cannot be applied when only the elements $\bar{Y}^{(i)}_{2nK+2i}$ are utilized for frequency offset estimation. In this case, matrix $\underline{\mathbf{\Theta}}(\epsilon)$ is square and the matrix $\underline{\mathbf{\Theta}}(\tilde{\epsilon})\left[\underline{\mathbf{\Theta}}^H(\tilde{\epsilon})\underline{\mathbf{\Theta}}(\tilde{\epsilon})\right]^{-1}\underline{\mathbf{\Theta}}^H(\tilde{\epsilon})$ is an identity matrix. Also, the trial function (4.33) is constant and independent of $\tilde{\epsilon}$.
- Only one neighboring subcarrier $\kappa + 1$ is utilized for each subcarrier κ in (4.28). The best result is achieved if K available subcarriers are utilized. In this case, estimate improvement can be achieved at the cost of complexity.
- The FD algorithm makes it possible to estimate the fading coefficients together with the frequency offset ϵ. The correct estimates of the fading coefficients are obtained by (4.32) when function (4.33) achieves its maximum. Thus, the proposed FD algorithm can be considered as a joint frequency offset and channel estimation algorithm.

- The trial function in (4.33) does not have a clearly defined maximum, and thus, the obtained estimate $\hat{\epsilon}$ is sensitive to noise, which leads to the low precision of the estimate.
- In order to build a trial function in (4.33), the transmit vector $(\bar{S}_0, \bar{S}_{K+i}, \bar{S}_{2K+i}, \ldots, \bar{S}_{K(L-1)+i})^T$ in (4.31) must be known at the receiver. This explains why the FD algorithm requires pilots for joint channel and frequency offset estimation.

The next step is to develop a practical and simple algorithm for estimation of of the frequency offset, ϵ, in the time domain without any exhaustive brute-force search.

4.6 Frequency Offset Estimation in the Time Domain

In this section, an algorithm is described which uses time domain signal $\bar{\mathbf{y}}^{(i)}$ for frequency offset estimation. For simplicity, the rectangular windowing in the transmitter is applied, i.e the length of the prefix and postfix N_{w} is set to zero.

After successful reduction of the MAI, the received signal $\bar{\mathbf{y}}^{(i)}$, is used for frequency offset estimation. We form two vectors $\boldsymbol{\zeta}_1$ and $\boldsymbol{\zeta}_2$ of length $N_{\mathrm{c}}/2$ using the received signal $\bar{\mathbf{y}}^{(i)}$. The elements $\zeta_{1,k}, k = 0, \ldots, \frac{N_{\mathrm{c}}}{2} - 1$, of the vector $\boldsymbol{\zeta}_1$ are defined as

$$\zeta_{1,k} = \bar{y}_k^{(i)} e^{-j\frac{2\pi}{N_{\mathrm{c}}}ki}, \tag{4.34}$$

where $\bar{y}_k^{(i)}$ are the elements of the vector $\bar{\mathbf{y}}^{(i)}$. Thus, the vector $\boldsymbol{\zeta}_{1,k}$ is a copy of the first half of the vector $\bar{\mathbf{y}}^{(i)}$ where each element $\bar{y}_k^{(i)}$ is multiplied by the rotating phase $e^{-j\frac{2\pi}{N_{\mathrm{c}}}ki}$. This rotating phase is added in order to eliminate the influence of the user-specific phase vector $\mathbf{u}$ which is defined in (2.71).

The elements $\zeta_{2,k}, k = 0, \ldots, \frac{N_{\mathrm{c}}}{2} - 1$, of the vector $\boldsymbol{\zeta}_2$ are given by

$$\zeta_{1,k} = \bar{y}_{k+\frac{N_{\mathrm{c}}}{2}}^{(i)} e^{-j\frac{2\pi}{N_{\mathrm{c}}}ki}. \tag{4.35}$$

A closer analysis reveals that due to the repetitive structure of the IFDMA time domain signal in (2.69) and the property of the right-circular matrix in (2.45), the obtained vectors $\boldsymbol{\zeta}_1$ and $\boldsymbol{\zeta}_2$ experience exactly the same influence from the transmission channel.

Vectors $\boldsymbol{\zeta}_1$ and $\boldsymbol{\zeta}_2$ differ only by a constant value, which is determined by the frequency offset. The following expression holds

$$\boldsymbol{\zeta}_2 = e^{j\pi\epsilon}\boldsymbol{\zeta}_2. \tag{4.36}$$

Therefore, if ϵ is determined using the observation in (4.36), it is possible to obtain an accurate estimate even if the normalized frequency offset ϵ is too large for successful data demodulation.

As shown in [Moo94], the maximum likelihood estimate $\hat{\epsilon}$ of ϵ can be written as

$$\hat{\epsilon} = \frac{1}{\pi}\tan^{-1}\left\{\frac{\Im\{\boldsymbol{\zeta}_2^H\boldsymbol{\zeta}_1\}}{\Re\{\boldsymbol{\zeta}_2^H\boldsymbol{\zeta}_1\}}\right\}, \tag{4.37}$$

where $\Re(.)$ and $\Im(.)$ denote the real and imaginary parts of a complex number, respectively.

The conditional variance of the estimate $\hat{\epsilon}$ can be addressed as follows, cf. A.3

$$\sigma_\epsilon^2 = \left(\frac{1}{\pi}\right)^2 \frac{1}{\mu L P_{\mathrm{p}}}, \tag{4.38}$$

where μ represents the SNR per data symbol defined in (5.15).

The following remarks are of interest:

- Function $\tan^{-1}$ can be approximated by its argument if ϵ is small enough. This assumption is easily met, since system design assumes that the 'worst case' frequency offset does not exceed 4% of the subcarrier spacing [TLP00], i.e., $|\epsilon| < 0.04$.
- The solution presented in (4.37) does not require knowledge of the channel state information and frequency offset estimation can be performed before the linear equalization block.
- The limits of the estimation given by (4.37) are $|\epsilon| \leq 0.5$ which is half of the subcarrier spacing. If $\epsilon > 0.5$, the expression (4.36) is no longer valid. When this happens, the estimate given by (4.37) becomes useless.
- The variance of the estimate (4.38) is conditionally unbiased and is independent of the transmission channel, cf. A.3.
- The length of the prefix and postfix N_{w} is set to zero in (4.37). However, the performance of the algorithm can be improved if the prefix and postfix are taken into account for frequency offset estimation.

The algorithm proposed in this section is referred to as the frequency offset estimation algorithm in the time domain (TD), in the following text.

4.7 Performance of the IFDMA Uplink System

4.7.1 Simulation Parameters

The considered IFDMA transmission system is used for the simulation of the FD and TD frequency offset estimation algorithms. The transmission system has a bandwidth of

$$BW = 2 \text{ MHz} \tag{4.39}$$

and the carrier frequency is located at

$$f_{\text{c}} = 5 \text{ GHz}. \tag{4.40}$$

The number of subcarriers is

$$N_{\text{c}} = 256, \tag{4.41}$$

which results in a subcarrier spacing equal to

$$\Delta f = 7.81 \text{ kHz}. \tag{4.42}$$

The IFDMA transmit signal is generated in the time domain without the IDFT operation. For spreading, Fourier codes of length

$$L = 32 \tag{4.43}$$

are applied. The maximum allowed number of users in the IFDMA uplink system is chosen to be

$$K = 8. \tag{4.44}$$

The IFDMA chip duration T_{c} is equal to, cf. (2.5),

$$T_{\mathrm{c}} = 0.5\ \mu\mathrm{s}. \tag{4.45}$$

The length of the guard interval is chosen such that the interference with the preceding IFDMA transmit symbol and inter-carrier interference are completely eliminated. The loss of SNR due to the guard interval, cf. (2.21), is not taken into account. The MMSE detector is used as described in Chapter 2. The transmission frame consists of 24 consecutive IFDMA symbols. A QPSK modulation alphabet is used.

The users do not have any time offsets and are perfectly aligned to the BS reference. This can be considered as a realistic scenario, since for each user, the start of the transmission is determined by the instructions transmitted from the BS via the control channel.

Table 4.1 briefly summarizes the parameters of the IFDMA reference system used for the simulation of the FD and TD frequency time offset estimation algorithms. A multipath channel model is consid-

Table 4.1: Parameters of the uplink IFDMA system used for the TD and FD frequency offset estimation algorithms.

Carrier frequency	$f_{\mathrm{c}} = 5$ GHz
Number of subcarriers	$N_{\mathrm{c}} = 256$
Transmission bandwidth	$BW = 2$ MHz
Subcarrier spacing	$\Delta f = 7.81$ kHz
Chip duration	$T_{\mathrm{c}} = 0.5\ \mu$s
Number of OFDM symbols in an OFDM frame	$N_{\mathrm{frame}} = 24$
Modulation alphabet	QPSK with Gray coding
Spreading length	$L = 32$
Window type	rectangular, $\beta = 0$
Maximum allowed number of users	K=8
Useful IFDMA symbol duration	$T = 128\ \mu$s
Guard interval duration	$T_{\Delta} = 6.5\ \mu$s
Number of pilot symbols	$P_{\mathrm{p}} = 2$ and $P_{\mathrm{p}} = 4$
Channel coding type	Convolutional
Channel code rate	$R_{\mathrm{c}} = 1/2$
Channel code memory length	6
Channel decoder	Viterbi
Linear detection	MMSE
Mobile speed	variable

ered, which consists of a tapped delay line with M_{ch} statistically independent Rayleigh fading taps. The average power for each channel component $h_m, m = 1, \ldots, M_{\mathrm{ch}} - 1$, is modeled as described in Chapter 2. The average channel attenuation is normalized to unity in our simulations. The speed of the MT takes on values 0 km/h, 60 km/h and 250 km/h, which allows realization of three different mobility scenarios.

4.7.2 System Performance

We evaluate the performance of both the TD and the FD algorithms in terms of the mean square error (MSE) of the frequency estimates and conditional variance of such estimates. The MSE and conditional variance are plotted versus SNR per data symbol μ, which is defined in (5.15). At first,

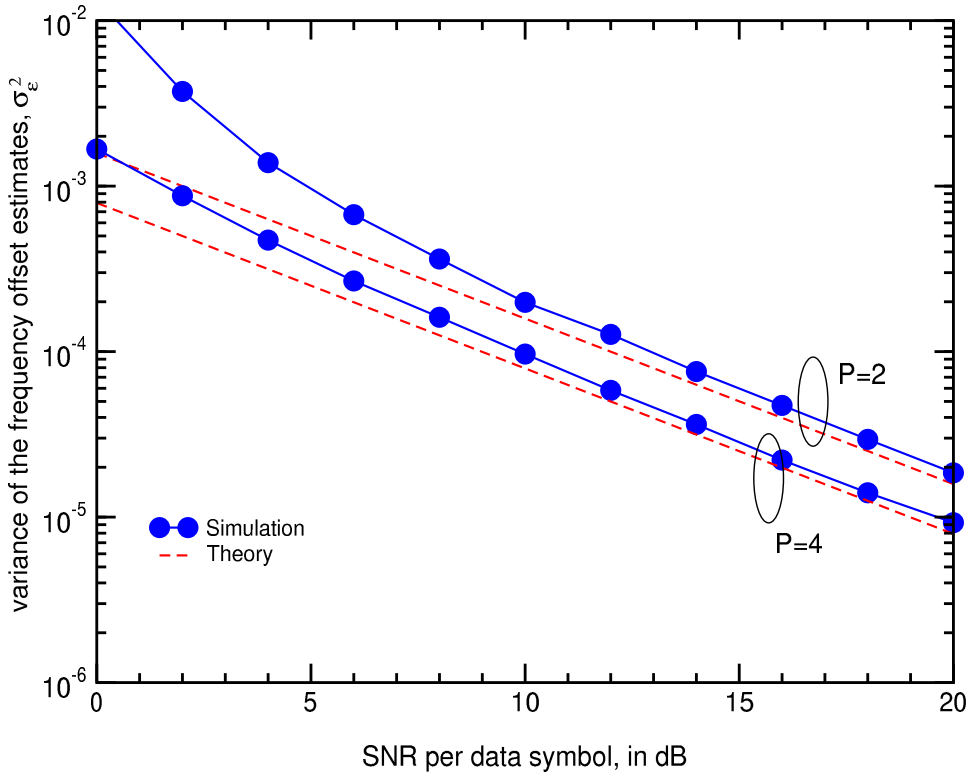

Figure 4.6: Variance σ_ϵ^2 of the frequency offset estimates versus SNR per data symbol; $N_\mathrm{u} = 1$; AWGN.

the TD algorithm for frequency offset estimation is considered. In Fig. 4.6, the conditional variance of the estimate is simulated for different values of P_p. Two cases are considered which differ in the number of pilot symbols at the beginning of the transmit OFDM frame of IFDMA system. The first case corresponds to a situation with two pilot symbols, i.e., $P_\mathrm{p} = 2$, whereas the second assumes that four pilot symbols are utilized for frequency offset estimation, i.e., $P_\mathrm{p} = 4$. Only one user $i = 0$ is active, thus, $N_\mathrm{u} = 1$. In doing so, MAI is completely avoided and Fig. 4.6 represents the theoretical bound of the conditional variance σ_ϵ^2.

For simplicity, an AWGN channel is chosen for the simulations in Fig. 4.6, however the same results can be obtained if a mobile radio channel with several taps is utilized. The theoretical curves are calculated and plotted according to (4.38) and simulations are performed by the Monte-Carlo method. At high SNR values, simulation results perfectly match the theoretical curves, validating our approach in (4.38).

It is shown in (4.38) that σ_ϵ^2 varies as the reciprocal of the number of IFDMA pilot symbols P_p and spreading length L. The product of P_p and L forms the power which is invested into frequency offset estimation. Thus, by increasing this power, one can decrease the conditional variance σ_ϵ^2, that is, the precision of the obtained estimate can be increased. Therefore, according to (4.38), the conditional

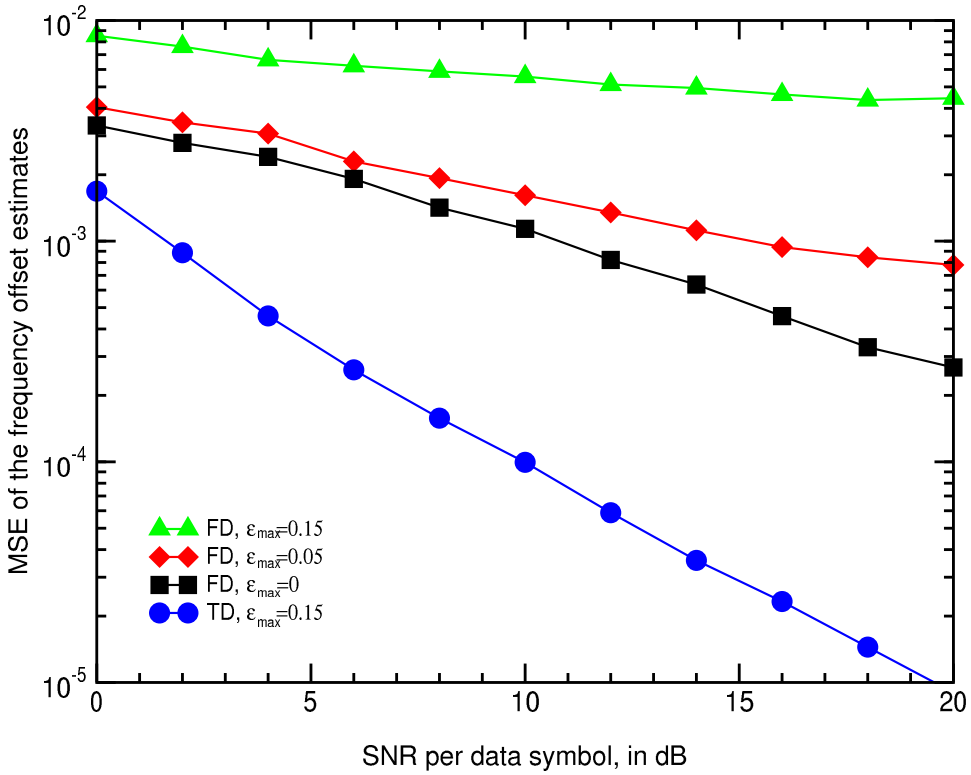

Figure 4.7: MSE of the frequency offset estimates versus SNR per data symbol; $P_{\text{p}} = 4$; $N_{\text{u}} = 1$.

variance (or precision of the estimate) can be improved by 3 dB if we increase the number of pilot symbols by two.

In Fig. 4.7, the MSE performance comparison between the TD and FD frequency estimation algorithms is presented versus SNR for one active user, i.e., $N_{\text{u}} = 1$. The number of pilot symbols is $P_{\text{p}} = 4$. The MT speed is $v = 0$ km/h. A multipath channel model is used with a tapped delay line of length $M_{\text{ch}} = 11$. The frequency offset ϵ is normally distributed and is taken from the interval $[-\epsilon_{\max}, \epsilon_{\max}]$.

The performance of the FD algorithm depends on $\epsilon_{\max}$. The reason for that is that in the FD algorithm the trial function (4.33) has a flat dependence on $\tilde{\epsilon}$ and is easily affected by noise. The performance of the FD estimation algorithm degrades rapidly since flatness in (4.33) increases with decreasing $\epsilon_{\max}$.

It can be seen that the TD algorithm outperforms the FD algorithm. If $\epsilon_{\max} = 0.15$, the TD algorithm outperforms FD by more than 20 dB at MSE equal to 10^{-3}. The performance gain between the TD and FD algorithms increases with increasing SNR.

From this point onwards we focus on the MSE performance of the TD frequency offset estimation algorithm, since TD provides the best MSE performance. It is interesting to observe the performance degradation of the TD algorithm in the channel where the speed of MT is different from zero. In this case, channel fading coefficients $H_{\kappa'}^{(i)}$ change slightly from one IFDMA pilot symbol to another. Thus, the ideal MAI suppression shown in Sec. 4.4 is not possible anymore. As a result, some amount of the residual MAI remains, which leads to the MSE performance degradation.

The next interesting point is the behavior of the MSE performance of the TD algorithm as the function of the number of active users N_{u}. The simulation results are shown in Fig. 4.8. The frequency offset ϵ is variable and taken from the uniform distribution in the range $[-\epsilon_{\max}, \epsilon_{\max}]$. The maximum frequency

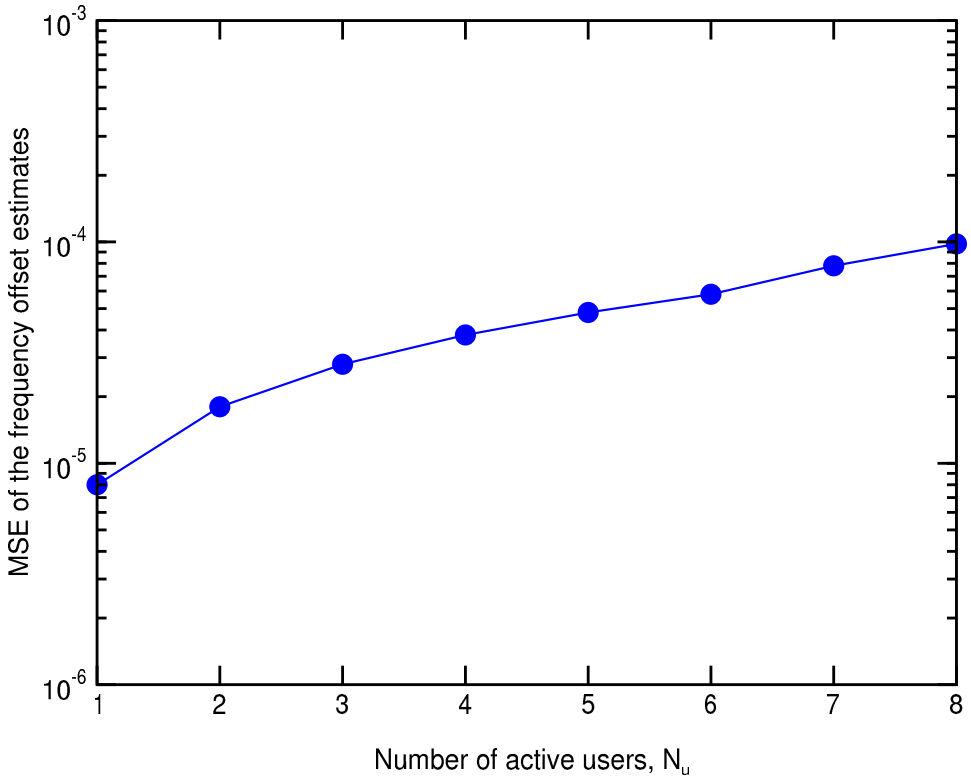

Figure 4.8: MSE of the frequency offset estimates versus number of active users N_{u}; TD algorithm; $\epsilon_{\max} = 0.15$; $P_{\mathrm{p}} = 2$; $N_{\mathrm{u}} = 1$; $v = 0$ km/h; SNR=20 dB.

offset is $\epsilon_{\max} = 0.15$. The SNR per data symbol is fixed, i.e., $\mu = 20$ dB and the speed of MT is chosen to be $v = 0$ km/h. The number of pilot symbols is $P_{\mathrm{p}} = 2$.

As a result, the MSE performance of the TD algorithm is impaired if N_{u} increases. With increasing N_{u}, the amount of MAI grows. However, more than half of the MAI is eliminated by the additional spreading in the time domain. In general, the MAI from $N_{\mathrm{u}}/2$ users is suppressed if $P_{\mathrm{p}} = 2$. Thus, the MSE performance degradation can be kept at a tolerable level.

4.7.3 Comparison with Existing Techniques

An attempt to solve the problem of frequency offset estimation for OFDMA/IFDMA uplinks in the presence of other frequency misaligned users has been made in this chapter. The TD and FD algorithms utilize additional spreading in the time domain and make it possible to eliminate the main part of MAI, which stems from neighboring users. In order to compare the proposed algorithms with the techniques published in the literature, we consider the TD algorithm which provides the best MSE performance.

In Fig. 4.9, the MSE of the TD frequency estimation algorithm is compared to the reduced complexity frequency estimator (RCFE) proposed in [Mor04]. The RCFE is an adaptation of the algorithm described in [MM99], which is developed for the OFDM downlink. The result in [MM99] is based on the work of [SC97]. In [SC97], the pilot symbol is constructed in such a way that it has two identical halves in the time domain. The correlation of these two halves in the time domain makes it possible to estimate the frequency offset in the OFDM downlink. In turn, the authors in [SC97] refer

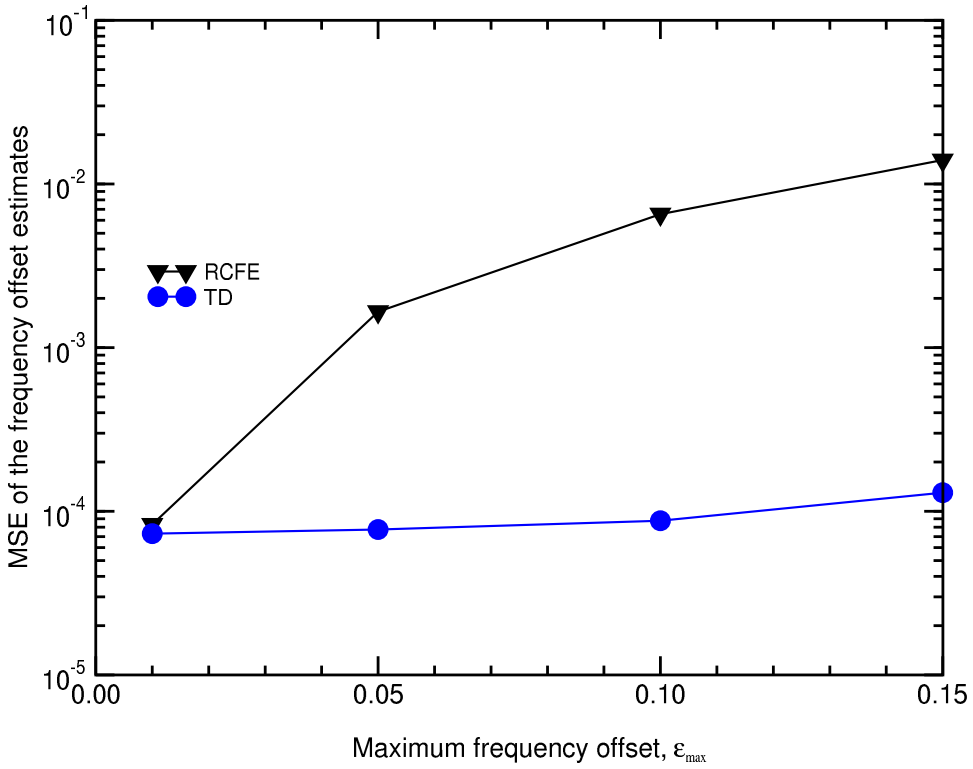

Figure 4.9: MSE of the frequency offset estimates versus maximum frequency offset ϵ_{max}; SNR=14 dB; TD algorithm; $P_{\text{p}} = 2$; $N_{\text{u}} = 8$; $v = 0$.

to the pioneering work of P.H. Moose [Moo94], who has proposed the frequency offset estimator for the OFDM downlink. Further improvements are achieved in [MM99], where the pilot symbol is composed of more than two identical parts. This makes it possible to achieve a better accuracy than in [SC97] at the cost of some increase in computational load. A similar idea was later realized for the time offset estimation algorithm [MZB00].

The algorithms for frequency offset estimation proposed in [MM99, SC97, Moo94] are suitable only for the OFDM downlink. The uplink scenario radically differs from the downlink scenario, since different users are simultaneously active and might have different frequency offsets, which affects the performance of the frequency offset estimator. In what follows, the TD and RCFE algorithms which are suitable for the frequency offset estimation in uplink are compared in terms of MSE. It is worth noting that RCFE is equal to the frequency estimator proposed in [Moo94] for the case of $P_{\text{p}} = 2$.

We have compared the performance of RCFE and the TD frequency estimation algorithm for the realistic scenario where all users are active i.e., $N_{\text{u}} = 8$. The MSE is simulated as a function of ϵ_{max}, where frequency offsets are normally distributed within the interval $[-\epsilon_{\text{max}}, \epsilon_{\text{max}}]$. The SNR per per data symbol is chosen to be 14 dB.

As a result, the proposed TD algorithm outperforms RCFE. The TD algorithm performs equivalently to RCFE, if ϵ_{max} is low. With increasing ϵ_{max}, MAI also increases and the performance of RCFE degrades rapidly. In contrast, the performance of the TD frequency estimation algorithm remains nearly constant.

If $\epsilon_{\text{max}} = 0.05$ then MSE of the RCFE algorithm is equal to $1.1 \cdot 10^{-3}$, whereas the MSE of the TD algorithm is $6 \cdot 10^{-5}$. Thus, the performance gain of the TD algorithm over RCFE is approximately

20-fold. With increasing ϵ_{max}, the MSE performance gain is further increased. For $\epsilon_{\text{max}} = 0.1$, the MSE of TD is 60 times better than the MSE of RCFE and for $\epsilon_{\text{max}} = 0.1$ it is over 100 times better.

Chapter 5

IFDMA Receiver and Optimum MMSE Equalization

5.1 Introduction

As shown in the previous chapters, IFDMA provides the lowest PAPR among all known multi-carrier systems and can potentially achieve the PAPR of single-carrier systems. Additional advantage of IFDMA is that IFDMA transmit signal can be generated without DFT operation, by performing the repetition of the transmit data sequence in the time domain.

This chapter describes IFDMA receiver, which is introduced in Sec 5.2. Linear equalization techniques are presented in Sec. 5.2.1 and the despreading operation is described in Sec. 5.2.2.

Self-interference (SI) is studied for IFDMA and OFDMA-CDM in Sec. 5.3 for the independent Rayleigh channel. A closed form solution for the BER performance is derived for the uncoded IFDMA and OFDMA-CDM systems. The theoretical analysis and simulation results show that the variance of the SI for IFDMA is two times smaller than the SI of OFDMA-CDM

In this thesis, the prefix and postfix are added as a cyclic extension of the complex-valued envelope $x(t)$ of an OFDM signal, and the generalized algorithm for the equalization is proposed as described in detail in Chapter 2. The application of the window in the receiver changes the received spectrum of each individual subcarrier. Varying the roll-off factor β of the window function and, therefore, changing the length of the prefix and postfix, MAI caused by the frequency offset can be reduced. Method that allows demodulating the information transmitted on individual subcarriers without interference and by using the DFT of double size was proposed in [BT07] and has been recapitulated in Chapter 2.

The results of such DFT operation is the frequency domain sequence which length is two times larger than the number of transmit subcarriers. The conventional MMSE equalizer [FK00] utilizes only even elements of this frequency domain sequence, which correspond to the data symbols transmitted on these OFDM subcarriers. At the same time, odd elements are discarded [BT07].

In Sec. 5.4 the optimal minimum-mean square equalizer is proposed which utilizes the whole sequence for data equalization. As the result, the proposed equalizer makes it possible to improve the BER performance of OFDM systems and utilizes the part of energy invested into prefix and postfix. It is shown that the performance of the obtained equalizer depends on the applied window type. Two window types are compared and, if window with better frequency characteristics is used, the performance of the proposed MMSE equalizer can be improved.

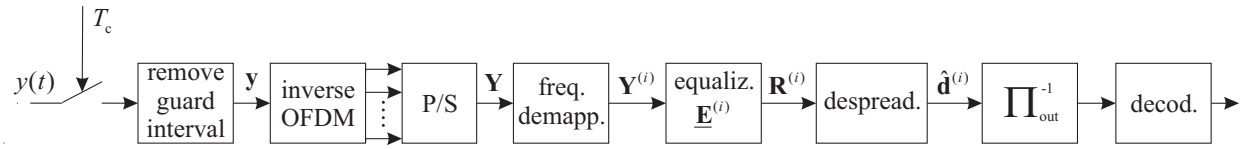

Figure 5.1: IFDMA receiver of the ith user

For the sake of simplicity, we describe the proposed MMSE equalizer for OFDM transmit systems only. Since IFDMA system is based on OFDM, the proposed equalizer can be applied for IFDMA with minor modifications.

Note that investigations carried out in this chapter are partly presented in [AS04b].

5.2 IFDMA/OFDMA-CDM Receiver

In this section, we describe the IFDMA receiver which utilizes inverse OFDM as described in Chapter 2, which allows utilizing different windowing functions in the OFDM receiver and minimize MAI.

The IFDMA receiver is shown in Fig. 5.1. The received waveform $y(t)$ is sampled at the time instances $t = \frac{lT}{Nc}, l = 0, \ldots, N_c + 2N_w - 1$. After guard interval removal, IFDMA time domain samples $y_l, l = 0, \ldots, N_c + 2N_w - 1$, are obtained and form vector $\mathbf{y}$. The vector $\mathbf{y}$ represents the received signal which is a superposition of signals of N_u users

$$\mathbf{y} = \sum_{i=0}^{N_u-1} \underline{\mathbf{h}}^{(i)} \mathbf{x}^{(i)} + \mathbf{n}. \tag{5.1}$$

The received signal $\mathbf{y}$ is transferred into the frequency domain by using inverse OFDM as described in Chapter 2. In doing so, $N_c - 2N_w$ zeros are added to the end of the vector $\mathbf{y}$ and after windowing operation and DFT, vector $\mathbf{Y}$ is obtained. At the output of the inverse OFDM and after parallel-to-serial conversion, the frequency domain vector $\mathbf{Y}$ represents the received data on N_c subcarriers and is composed of the received vectors of N_u active users

$$\mathbf{Y} = \sum_{i=0}^{N_u-1} \underline{\mathbf{H}}^{(i)} \mathbf{S}^{(i)} + \mathbf{N}, \tag{5.2}$$

where $\underline{\mathbf{H}}^{(i)}$ and $\mathbf{S}^{(i)}$ are the matrix of fading coefficients and the vector of data symbols of the ith user, respectively, and $\mathbf{N}$ denotes the vector of AWGN. Note that received data symbols of different users remain orthogonal, since users utilize different subcarriers for data transmission. Therefore, in the matrix $\underline{\mathbf{H}}^{(i)}$ and in the vector $\mathbf{S}^{(i)}$ only the elements $H_\kappa^{(i)}$ and $S_\kappa^{(i)}, \kappa = nK + i, n = 0, \ldots, L-1$, are non-zero.

In order to separate the received data of different users, frequency demapping is applied. The output of the frequency demapping block is a vector $\mathbf{Y}^{(i)}$ which has length L and is composed of elements $Y_n^{(i)}, n = 0, \ldots, L-1$. $\mathbf{Y}^{(i)}$ represents the received data of the ith user. Since each ith user transmit L data symbol S_κ on its own set of subcarriers $\kappa = nK + i, n = 0, \ldots, L-1$, the user separation is achieved by assigning

$$Y_n^{(i)} = Y_{nK+i}. \tag{5.3}$$

The vector $\mathbf{Y}^{(i)}$ is given by

$$\mathbf{Y}^{(i)} = \underline{\mathbf{H}}^{(i)}\mathbf{S}^{(i)} + \mathbf{N}^{(i)} \tag{5.4}$$

where vector $\mathbf{N}^{(i)}$ denotes AWGN samples on the subcarriers $\kappa = nK + i, n = 0, \ldots, L-1$ and has length L

5.2.1 Linear Equalizers

In Fig. 2.4, the multi-carrier receiver which utilizes inverse OFDM for data detection is depicted. In the inverse OFDM block, only even elements of the sequence $Y_{\kappa'}, \kappa' = 0, \ldots, 2N_{\mathrm{c}}-1$ are used for the purpose of equalization. In Sec. (5.4), the optimum linear equalizer is presented which utilizes both even and odd elements of the sequence $Y_{\kappa'}, \kappa' = 0, \ldots, 2N_{\mathrm{c}}-1$. The proposed equalizer is optimal is a sense that it utilizes power invested into prefix and postfix. It was developed for OFDM but can be easily applied to IFDMA system. In this subsection, however, we describe only commonly known suboptimal equalizers which uses vector $\mathbf{Y}^{(i)}$ for data detection.

The received signal $\mathbf{Y}$ is equalized by employing one-tap linear equalizer to combat phase and amplitude distortions caused by the mobile radio channel. This equalizers require only one complex valued multiplication per received data symbol.

The received sequence at the output of the linear equalization block is represented by a vector of equalized values of the ith user

$$\mathbf{R}^{(i)} = \underline{\mathbf{E}}^{(i)}\mathbf{Y} = (R_0, R_1, \ldots, R_{L-1})^T, \tag{5.5}$$

where $\underline{\mathbf{E}}^{(i)}$ is a diagonal equalization matrix of size $L \times L$, which is calculated for each user

$$\underline{\mathbf{E}}^{(i)} = \begin{pmatrix} E_0^{(i)} & 0 & \cdots & 0 \\ 0 & E_1^{(i)} & \cdots & 0 \\ \vdots & & \ddots & \vdots \\ 0 & 0 & \cdots & E_{L-1}^{(i)} \end{pmatrix}. \tag{5.6}$$

The matrix $\mathbf{R}^{(i)}$ is given by

$$\mathbf{R}^{(i)} = \underline{\mathbf{E}}^{(i)}\underline{\mathbf{H}}^{(i)}\mathbf{S}^{(i)} + \underline{\mathbf{E}}^{(i)}\mathbf{N}^{(i)}. \tag{5.7}$$

There are several LE techniques in the literature [Kai98, FK00] which make it possible to calculate coefficients $E_n^{(i)}, n = 0, \ldots, L-1$, from the known fading coefficients $H_n^{(i)}, n = 0, \ldots, L-1$. However, only a few of them represent a practical interest for the IFDMA.

Equal gain combining (EGC). The EGC equalization coefficient $E_n^{(i)}$ is calculated from fading coefficient $H_n^{(i)}$ as

$$E_n^{(i)} = \frac{H_n^{(i)*}}{|H_n^{(i)}|}, \tag{5.8}$$

where $(.)^*$ denotes complex conjugation. EGC compensates only the phase rotation caused by the channel fading coefficient $H_n^{(i)}$. EGC is the simplest LE technique, since only the phase of the $H_n^{(i)}$ is required.

Zero forcing (ZF). The ZF equalization coefficient is given by

$$E_n^{(i)} = \frac{1}{H_n^{(i)}}. \tag{5.9}$$

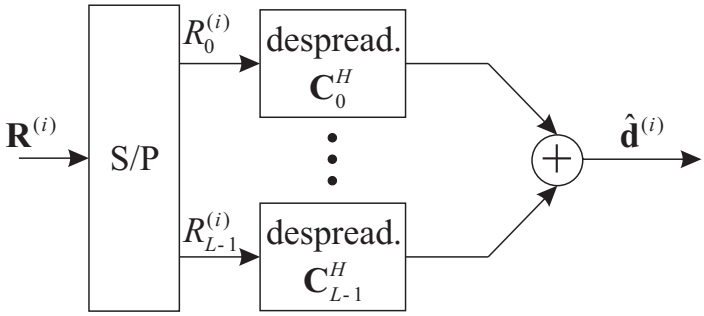

Figure 5.2: Despreading operation for IFDMA and OFDMA-CDM.

ZF is the simplest LE technique where the equalization coefficient $E_n^{(i)}$ is a reciprocal of $H_n^{(i)}$. With ZF, self-interference can be eliminated by restoring the orthogonally of Fourier spreading codes. The main drawback of ZF equalization technique is that it enhances a noise which leads to the poor BER performance in the mobile radio channel.

Minimum Mean Square Error (MMSE). The MMSE equalization coefficient is given by

$$E_n^{(i)} = \frac{H_n^{(i)*}}{|H_n^{(i)}|^2 + \sigma^2}. \tag{5.10}$$

MMSE is the optimal LE technique which minimizes the mean square error value between the transmitted signal $S_\kappa^{(i)}, \kappa = nK + i$ and the output of the linear detection block R_n. The main drawback of the MMSE technique is that the estimation of the noise variance σ^2 is required at the receiver.

Maximum Ratio Combining (MRC). The MRC equalization coefficient is calculated by

$$E_n^{(i)} = H_n^{(i)*}. \tag{5.11}$$

The drawback of the MRC is that it destroys the orthogonally between spreading codes and thus, additionally enhances SI.

The performance of EGC, ZF, MMSE, MRC techniques is studied in [Kai95] for uncoded and coded OFDMA-CDM system, whereas the performance of LE techniques for OFDMA is studied in [NP02]. For the multi-carrier systems with spreading such as OFDMA-CDM or IFDMA, the best BER performance results can be achieved with MMSE detector [AS04a, AS04b].

5.2.2 Despreading

After equalization, the vector $\mathbf{R}^{(i)}$ is transferred to the despreading block presented in Fig. 5.2. At the output of the despreading block, the vector of data symbol estimates

$$\hat{\mathbf{d}}^{(i)} = (\hat{d}_0^{(i)}, \hat{d}_1^{(i)}, \ldots, \hat{d}_{L-1}^{(i)})^T, \tag{5.12}$$

is calculated as a multiplication of the Fourier spreading matrix $\underline{\mathbf{C}}_L$ and the vector $\mathbf{R}^{(i)}$ of equalized values of ith user

$$\hat{\mathbf{d}}^{(i)} = \underline{\mathbf{C}}_L \mathbf{R}^{(i)}. \tag{5.13}$$

The data symbol estimate $\hat{d}_q^{(i)}, q = 0, \ldots, L-1$, is calculated by multiplying $\mathbf{R}^{(i)}$ by the Hermitian transpose $\mathbf{C}_q^H$ of the qth spreading code, i.e.,

$$\hat{d}_q^{(i)} = \mathbf{C}_q^H \mathbf{R}^{(i)} = \sum_{n=0}^{L-1} C_{q,n}^* R_n^{(i)}. \tag{5.14}$$

The considered receiver is equivalent to the conventional OFDMA-CDM receiver described in [Kai02], but in the IFDMA case, Fourier codes are used instead of WH codes. For IFDMA, the despreading operation is the IDFT operation of the size L, which can be implemented at the receiver as computationally efficient IFFT operation. After despreading, the vector of estimates $\hat{\mathbf{d}}^{(i)}$ is demapped, deinterleaved and decoded as shown in Fig 5.1.

Throughout this thesis two different SNR values are used which are introduced in the rest of this subsection. When assuming that channel power in normalized, i.e., $E\{|H_n|^2\} = 1$, the received SNR per data symbol is given by

$$\mu = \frac{E\{|H_n^{(i)} S_n^{(i)}|^2\}}{\sigma^2}\Big|_{E\{|H_n^{(i)}|^2\}=1} = \frac{E\{|S_n^{(i)}|^2\}}{\sigma^2} = \frac{E\{|d_q^{(i)}|^2\}}{\sigma^2}. \tag{5.15}$$

The received SNR per bit μ_b is given by

$$\mu_\mathrm{b} = \frac{\mu}{R_\mathrm{c} \log_2 M_\mathrm{d}}, \tag{5.16}$$

where M_d is a maximum number of different realizations of data symbol $d_q^{(i)}$ and R_c denotes the code rate. If not explicitly stated otherwise, the abbreviation SNR denotes SNR per bit μ_b, in the rest of the thesis.

5.3 Self-Interference in Independent Rayleigh Channel

In this section, SI in IFDMA is studied. The SI can be observed in the receiver if the IFDMA signal is transmitted through the mobile radio channel with a frequency selective fading. Despite equalization, the orthogonality between spreading codes cannot be fully restored and SI appears. The SI of two systems is considered: IFDMA and OFDMA-CDM, and both systems differ only in the type of spreading. Only one user is taken into account and, thus, index i is omitted, in the following text.

The estimates of data symbols $\hat{d}_q, q = 0, \ldots, L-1$, obtained after the despreading (IDFT operation) can be written as

$$\hat{d}_q = \underbrace{d_q \sum_{n=0}^{L-1} |C_{q,n}| H_n E_n}_{\text{useful part}} + \underbrace{\sum_{\substack{g=0 \\ g \neq q}}^{L-1} d_g \sum_{n=0}^{L-1} C_{g,n}^* C_{n,q} H_n E_n}_{SI} + \underbrace{\sum_{n=0}^{L-1} E_n N_n}_{\text{noise part}}. \tag{5.17}$$

The equation (5.17) is composed of the useful part, SI and noise part. The multiplication by the constant E_n does not change the statistical properties of the AWGN, thus, the noise term has Gaussian distribution. Product $H_n E_n$ is a real-valued variable, but its statistical properties depend on the used LE technique. Two assumptions have been made in the following: the MMSE technique introduced in (5.10) is utilized in this section, as a most promising technique for the IFDMA and independent

Rayleigh channel is used. Independent Rayleigh channel means that each fading coeffcients $|H_n|$ is a random variable with Rayleigh statistics.

Bearing in mind that $C_{g,n} \subseteq \left\{-1/\sqrt{L}, 1/\sqrt{L}\right\}$, energy of the useful signal part E_{rx} can be calculated as [Kai98]

$$E_{\text{rx}} = \frac{1}{L}|E\{H_n E_n\}|^2. \tag{5.17}$$

The integral $E\{H_n E_n\}$ has been calculated in [Kai98] for MMSE

$$\begin{aligned} E\{H_n E_n\} &= E\left\{\frac{|H_n|^2}{|H_n|^2+\sigma^2}\right\}\Bigg|_{|H_n| \text{is Rayleigh distributed}} \\ &= 1 + \frac{e^{\frac{1}{\mu_{\text{b}}}}}{\mu_{\text{b}}}\,\Gamma\left(-\frac{1}{\mu_{\text{b}}}\right), \end{aligned} \tag{5.18}$$

where μ_{b} is the SNR per bit as defined in (5.16) and exponential integral $\Gamma(x)$ is given by

$$\Gamma(x) = \int_x^{\infty} \frac{e^{-x}}{x} dx. \tag{5.19}$$

.

If BPSK is considered, i.e., d_q is a real number, the real part of the SI is given by

$$\begin{aligned} \Re\{SI\} = \Re\left\{\sum_{\substack{g=0\\g\neq q}}^{L-1} d_g \sum_{n=0}^{L-1} C^*_{g,n} C_{n,q} H_n E_n\right\} &= \sum_{\substack{g=0\\g\neq q}}^{L-1} d_g \sum_{n=0}^{L-1} \Re\left\{C^*_{q,n} C_{n,q} H_n E_n\right\} \\ &= \frac{1}{L}\sum_{\substack{g=0\\g\neq q}}^{L-1} d_g \sum_{n=0}^{L-1} \cos\left(2\pi n\left(\frac{g-q}{L}\right)\right) H_n E_n. \end{aligned} \tag{5.20}$$

The mean value of the SI is given by

$$E\{\Re\{SI\}\} = \frac{1}{L}\sum_{\substack{g=0\\g\neq q}}^{L-1} E\{d_g\} E\left\{\sum_{n=0}^{L-1} \cos\left(2\pi n\left(\frac{g-q}{L}\right)\right) H_n E_n\right\} = 0, \tag{5.21}$$

since the data symbols $d_q, q = 0, \ldots, L-1$, are equally probable., i.e.,

$$E\{d_q\} = 0. \tag{5.22}$$

Since $E\{|d_q|^2\} = 1$, the variance σ^2_{SI} of the SI is given by

$$\sigma^2_{\text{SI}} = E\{|\Re\{SI\}|^2\} = \frac{1}{L^2}\sum_{\substack{g=0\\g\neq q}}^{L-1} E\left\{\left|\sum_{n=0}^{L-1} \cos\left(2\pi n\left(\frac{g-q}{L}\right)\right) H_n E_n\right|^2\right\}. \tag{5.23}$$

In order to simplify (5.23), we consider properties of the the last sum in (5.23). Before preceding, it worth to note that $g-q$ is integer and that

$$-L+1 \leq g-q \leq L-1, \tag{5.24}$$

since $q = 0, \ldots, L-1$, $g = 0, \ldots, L-1$ and

$$g - g \neq 0. \tag{5.25}$$

The sum in (5.23) is represented as

$$\sum_{n=0}^{L-1} \cos\left(2\pi n \left(\frac{g-q}{L}\right)\right) H_n E_n =$$

$$= \begin{cases} \sum\limits_{n=0}^{L/4-1} \left[H_{2n}E_{2n} + H_{2n+\frac{L}{2}}E_{2n+\frac{L}{2}}\right] & \text{if } (g-q) = \frac{L}{4} \\ \sum\limits_{n=0}^{L/2-1} \left[H_n E_n + H_{n+\frac{L}{2}}E_{n+\frac{L}{2}}\right] & \text{if } (g-q) = \frac{L}{2} \\ \sum\limits_{n=0}^{L/2-1} \left[H_n E_n - H_{n+\frac{L}{2}}E_{n+\frac{L}{2}}\right] \cos\left(2\pi n \left(\frac{g-q}{L}\right)\right) & \text{otherwise.} \end{cases} \tag{5.26}$$

Two cases, $g - q = L/2$ and $g - q = L/4$, do not play an important role and do not have much influence on a result of the summation in (5.23). Therefore, (5.26) is approximated by

$$\sum_{n=0}^{L-1} \cos\left(2\pi n \left(\frac{g-q}{L}\right)\right) H_n E_n = \sum_{n=0}^{L/2-1} \left[H_n E_n - H_{n+\frac{L}{2}}E_{n+\frac{L}{2}}\right] \cos\left(2\pi n \left(\frac{g-q}{L}\right)\right). \tag{5.27}$$

Under assumptions that fading coefficients $H_n, n = 0, \ldots, L-1$, are uncorrelated, σ^2_{SI} can be represented

$$\sigma^2_{\text{SI}} = \frac{1}{L^2} \sum_{\substack{g=0 \\ g\neq q}}^{L-1} \sum_{n=0}^{L/2-1} E\left\{\left[H_n E_n - H_{n+\frac{L}{2}}E_{n+\frac{L}{2}}\right]^2\right\} \cos^2\left(2\pi n \left(\frac{g-q}{L}\right)\right) \tag{5.28}$$

Using the central limit theorem [Pap02], the SI variance σ^2_{SI} can be considered as additive white Gaussian noise with zero mean, if L is large enough. Both products $H_n E_n$ and $H_{n+\frac{L}{2}}E_{n+\frac{L}{2}}$ have the same statistics, its variances and mean values are equal. Moreover, their statistics is independent from the index n, which is omitted in the rest of the section. For simplicity, we introduce real-valued random variable HE. Using

$$E\left\{(H_n E_n)^2\right\} = E\left\{\left(H_{n+\frac{L}{2}}E_{n+\frac{L}{2}}\right)^2\right\} = E\left\{(HE)^2\right\} \tag{5.29}$$

and

$$E\left\{(H_n E_n)\right\} = E\left\{\left(H_{n+\frac{L}{2}}E_{n+\frac{L}{2}}\right)\right\} = E\left\{(HE)^2\right\} \tag{5.30}$$

(5.28) can be developed

$$\sigma^2_{\text{SI}} = \left[E\{H^2E^2\} - E^2\{HE\}\right] \frac{2}{L^2} \sum_{\substack{g=0 \\ g\neq q}}^{L-1} \sum_{n=0}^{L/2-1} \cos^2\left(2\pi n \left(\frac{g-q}{L}\right)\right) \tag{5.31}$$

The two sums in (5.31) converge for every L, $L = 2^\imath, \imath = 1, 2, 3 \ldots$, so that

$$\frac{2}{L^2} \sum_{\substack{g=0 \\ g \neq q}}^{L-1} \sum_{n=0}^{L/2-1} \cos^2 \left(2\pi n \left(\frac{g-q}{L} \right) \right) = \frac{1}{2}. \tag{5.32}$$

Finally, using (5.31) and (5.32), the variance σ^2_{SI} of SI can be written as

$$\sigma^2_{\text{SI}} = \frac{1}{2} \left(E\left\{ H^2 E^2 \right\} - E^2 \left\{ HE \right\} \right). \tag{5.33}$$

The first expectation is obtained in [Kai98]

$$\begin{aligned} E\left\{ H^2 E^2 \right\} &= E\left\{ \left| \frac{|H_n|^2}{|H_n|^2 + \sigma^2} \right|^2 \right\} \Bigg|_{|H_n| \text{is Rayleigh distributed}} \\ &= 1 + \frac{1}{\mu_\text{b}} + \left(\frac{1}{\mu_\text{b}^2} + \frac{2}{\mu_\text{b}} e^{1/\mu_\text{b}} \right) \Gamma\left(-\frac{1}{\mu_\text{b}} \right). \end{aligned} \tag{5.34}$$

and the integral $E\left\{ HE \right\}$ is calculated in (5.18). Therefore, σ^2_{SI} is further developed as

$$\sigma^2_{\text{SI}} \approx \frac{1}{2} \left(\frac{1}{\mu_\text{b}} + \frac{e^{\frac{1}{\mu_\text{b}}}}{\mu_\text{b}^2} \Gamma\left(-\frac{1}{\mu_\text{b}} \right) - \frac{e^{\frac{2}{\mu_\text{b}}}}{\mu_\text{b}^2} \Gamma^2 \left(-\frac{1}{\mu_\text{b}} \right) \right). \tag{5.35}$$

The variance σ^2_{noise} of the additive white Gaussian noise after equalization with the MMSE LE technique can be approximated

$$\begin{aligned} \sigma^2_{\text{noise}} = E\{|E|^2\} \frac{\sigma^2}{2} &= E\left\{ \left| \frac{E^*}{|H_n|^2 + \sigma^2} \right|^2 \right\} \Bigg|_{|H| \text{is Rayleigh distributed}} \\ &= \left[-1 - \left(1 + \frac{1}{\mu_\text{b}} \right) e^{\frac{1}{\mu_\text{b}}} \Gamma\left(-\frac{1}{\mu_\text{b}} \right) \right] \frac{\sigma^2}{2}. \end{aligned} \tag{5.36}$$

As σ^2_{noise} and σ^2_{SI} are statistically independent, zero mean Gaussian variables, the sum of the both has a zero-mean Gaussian distribution. Thus, the BER of the uncoded system P_b is calculated as

$$P_\text{b} = \frac{1}{2} \operatorname{erfc} \left(\sqrt{\frac{E_{\text{rx}}}{2(\sigma^2_{\text{noise}} + \sigma^2_{\text{SI}})}} \right). \tag{5.37}$$

The variance of the SI for WH spreading (OFDMA-CDM case) $\sigma^2_{\text{SI,OFDMA-CDM}}$ is obtained in [Kai95] and is given by [1]

[1] When applying WH codes as orthogonal spreading codes, the property can be exploited that product $C^*_{g,n} C_{n,q}, n = 0, \ldots, L-1$, in half of the cases equal $-1/L$ and in the other half equals $1/L$, when $g \neq q$ and $C_{g,n} \subseteq \left\{ -1/\sqrt{L}, 1/\sqrt{L} \right\}$. Therefore, for OFDMA-CDM, (5.31) is given by

$$\frac{2}{L^2} \sum_{\substack{g=0 \\ g \neq q}}^{L-1} \sum_{n=0}^{L/2-1} \left[E\{H^2 E^2\} - E^2\{HE\} \right] = \frac{L-1}{L} \left[E\{H^2 E^2\} - E^2\{HE\} \right]. \tag{5.38}$$

$$\sigma^2_{\text{SI,OFDMA-CDM}} \approx \frac{L-1}{L}\left(E\left\{H^2E^2\right\} - E^2\left\{HE\right\}\right). \tag{5.39}$$

Compare (5.39) and (5.33) one can see that the ratio between σ^2_{SI} and $\sigma^2_{\text{SI,OFDMA-CDM}}$ approaches 0.5 if the spreading length L tends to infinity, i.e.,

$$\lim_{L\to\infty}\left(\frac{\sigma^2_{\text{SI}}}{\sigma^2_{\text{SI,OFDMA-CDM}}}\right) = \frac{1}{2}. \tag{5.40}$$

For the validation of Gaussian approximation in (5.37), the simulation and theoretical curves are plotted in Fig. 5.3. Additionally, the BER performance of IFDMA and OFDMA-CDM are compared in terms of BER versus SNR using Monte-Carlo simulations. Uncoded, fully-loaded IFDMA and OFDMA-CDM systems are considered. The maximum number of active users is $K = 64$. Two different values of the spreading length are utilized: $L = 64$ and $L = 256$. The length of the prefix and postfix N_{w} is set to zero. For simplicity, the energy loss due to the guard interval in (2.21) is not taken into account. It is clearly seen, that the simulation results fit well with the proposed Gaussian

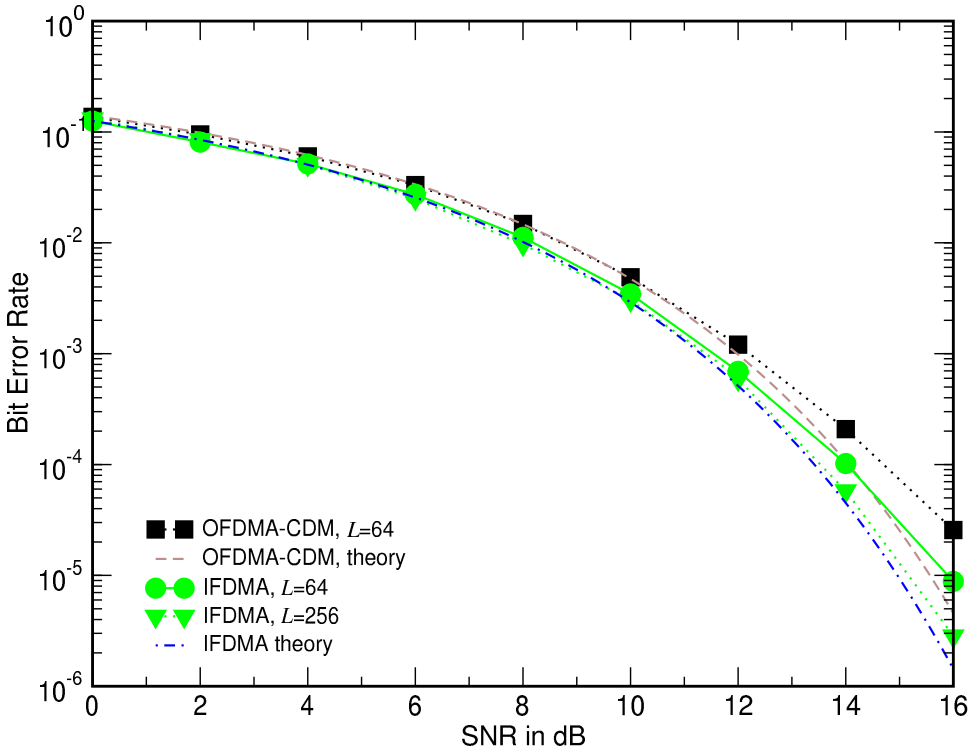

Figure 5.3: BER versus SNR for the IFDMA and OFDMA-CDM.

approximation. Both analytical performance evaluation and simulation results show that IFDMA clearly outperforms OFDMA-CDM, especially for large values of the spreading length L.

5.4 MMSE Equalizer for OFDM System with Windowing

In this section we propose algorithm which improves spectral efficiency of the OFDM systems with prefix and postfix. For the sake of simplicity, the algorithm is described for the OFDM system but can

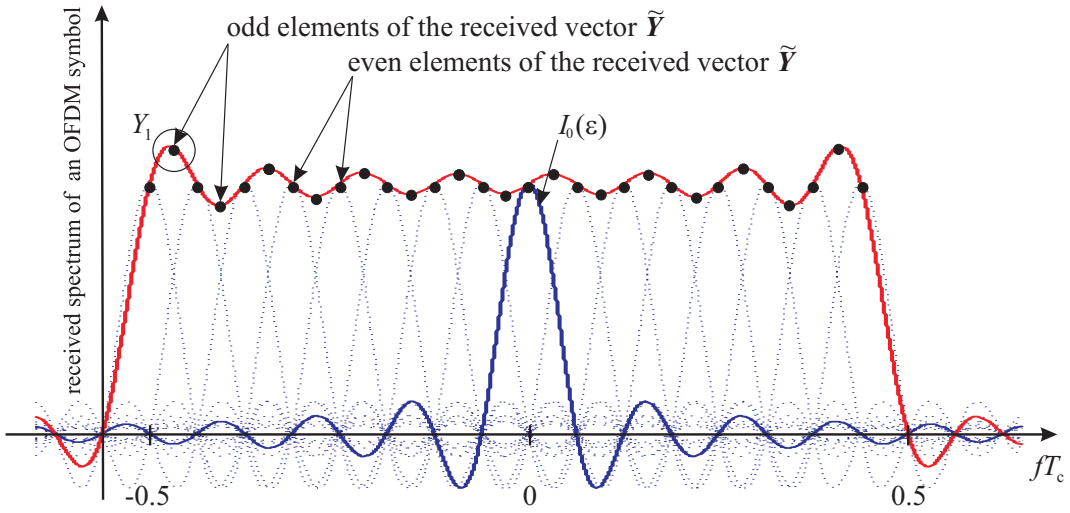

Figure 5.4: Received spectrum of an OFDM symbol versus normalized frequency fT_c; $N_c = 16$. The AWGN channel with negligible noise power.

also be applied to IFDMA with minor modifications. For the algorithm derivation, we use an OFDM system with N_c subcarriers and with the prefix and postfix of length N_w. In this thesis, the prefix and postfix are added as a cyclic extension of the complex-valued envelope $x(t)$ of an OFDM signal. As shown in Chapter 2, the application of the window in the receiver changes the received spectrum of each individual subcarrier. Varying the roll-off factor β of the window function and, therefore, changing the length of the prefix and postfix, MAI caused by the frequency offset can be reduced. Method that allows demodulating the information transmitted on individual subcarriers without interference and by using the DFT of double size was proposed in [BT07] and has been recapitulated in Chapter 2. After such a DFT operation, only even elements $Y_{\kappa'}, \kappa' = 2\kappa, \kappa = 0, \ldots, 2N_c - 1$, form vector $\mathbf{Y}$ and are further processed, whereas odd elements $Y_{\kappa'}, \kappa' = 2\kappa + 1, \kappa = 0, \ldots, 2N_c - 1$, are discarded.

The received spectrum of an OFDM symbol with $N_c = 16$ subcarriers is shown in Fig. 5.4, where AWGN channel with a negligible noise power is utilized. The filled circles in Fig. 5.4 denote the values of the frequency domain sequence $Y_{\kappa'}, \kappa' = 0, \ldots, 2N_c - 1$, obtained after the DFT operation as described in Chapter 2. In this section, we describe the MMSE algorithm which utilizes odd and even elements of the obtained frequency domain sequence $Y_{\kappa'}, \kappa' = 0, \ldots, 2N_c - 1$, for the equalization. For simplicity, we introduce vector $\tilde{\mathbf{Y}}$ of length $2N_c$,

$$\tilde{\mathbf{Y}} = \{Y_0, Y_1, \ldots, Y_{2N_c-1}\}^T. \tag{5.41}$$

Note that only even elements of $\tilde{\mathbf{Y}}$, represent the received data on subcarriers $\kappa = 0, \ldots, N_c - 1$ as depicted in (5.5). Odd elements of $\tilde{\mathbf{Y}}$ represent the received values which are located between two adjacent subcarriers.

The influence of the individual subcarrier κ on the received element κ' of the vector $\tilde{\mathbf{Y}}$ is defined by the CFO coefficient (A.2)

$$I_{\kappa-\kappa'}(\epsilon) = \frac{1}{N_c\sqrt{2}} \sum_{\upsilon=0}^{N_c+2N_w-1} w_\upsilon e^{j\frac{\pi\upsilon(2\kappa-\kappa'+2\epsilon)}{N_c}}, \tag{5.42}$$

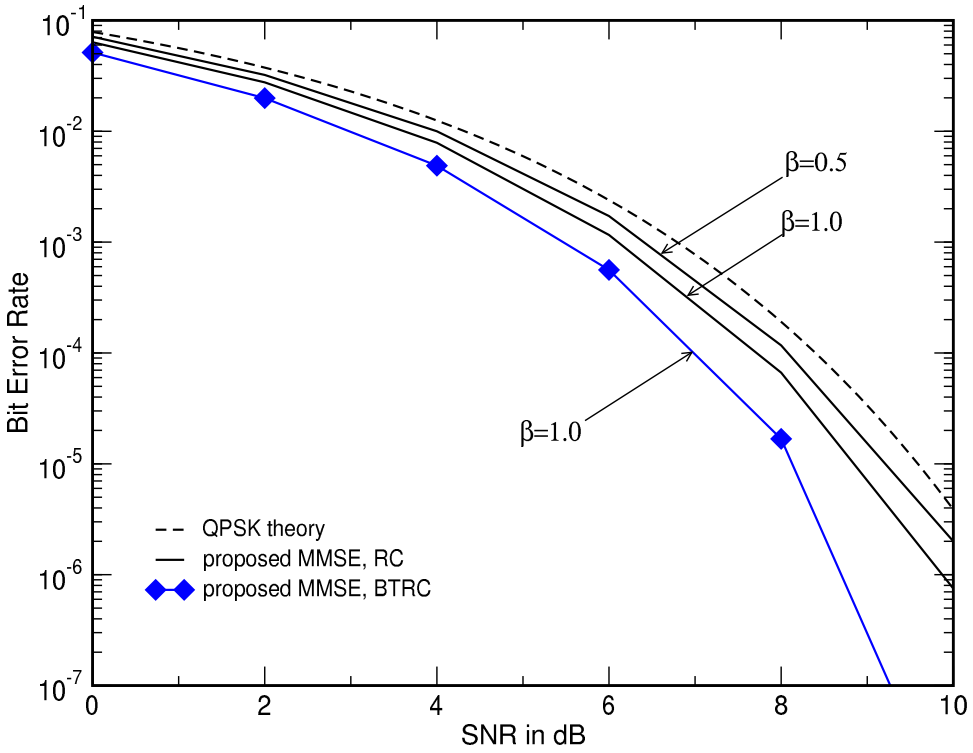

Figure 5.5: BER versus SNR for the proposed MMSE equalizer for different values of the roll-off factors β and for the RC and BTRC windows; QPSK performance is given as a reference.

where $w_\upsilon, \upsilon = 0, \ldots, N_\mathrm{c} + 2N_\mathrm{w} - 1$, denotes samples of the window function $w(t)$ as described in Chapter 2. It is seen that coefficient $I_{\kappa-\kappa'}(\epsilon)$ depends on the applied window function. The received subcarriers are orthogonal to each other, i.e., if frequency offset ϵ is equal to zero, for every subcarrier κ and every even κ'th element of $\mathbf{Y}$ the following expression

$$I_{\kappa-\kappa'}(\epsilon) = \begin{cases} \frac{1}{\sqrt{2}} & \text{if } \kappa' = 2\kappa \text{ and } \kappa' \text{ is even} \\ 0 & \text{if } \kappa' \neq 2\kappa \text{ and } \kappa' \text{ is even.} \end{cases} \tag{5.43}$$

holds true. The CFO coefficient denotes the spectrum of the individual subcarrier and, for example, $I_0(\epsilon)$ is shown in Fig. 5.4 as a function of ϵ.

In the case of the AWGN channel with negligible noise power, cf. Fig. 5.4, the even and odd elements of $\tilde{\mathbf{Y}}$ are obtained as a linear combination of the source data symbols $S_\kappa, \kappa = 0, \ldots, N_\mathrm{c} - 1$, weighted by the CFO coefficients. For example, for the odd value Y_1 in Fig. 5.4 one can write

$$Y_1 = d_0 I_{-1/2}(\epsilon) + d_1 I_{1/2}(\epsilon) + d_2 I_{3/2}(\epsilon) + \ldots + d_{N_\mathrm{c}-1} I_{N_\mathrm{c}-1/2}(\epsilon). \tag{5.44}$$

The same linear combinations can be written for every element $Y_{\kappa'}, \kappa' = 0, \ldots, 2N_\mathrm{c} - 1$, of the vector $\tilde{\mathbf{Y}}$.

These linear dependencies can be written for frequency-selective mobile radio channel in the vector-matrix form. In the following text, we consider N_c source data symbols $S_\kappa, \kappa = 0, \ldots, N_\mathrm{c} - 1$, which form source vector $\mathbf{S}$ and the channel is described by its frequency domain channel matrix $\underline{\mathbf{H}}$, as defined in Sec. 2.2.6. With this notation, the received vector $\tilde{\mathbf{Y}}$ is given by

$$\tilde{\mathbf{Y}} = \underline{\mathbf{\Psi H}}\mathbf{S} + \underline{\mathbf{\Psi}}\mathbf{N}, \tag{5.45}$$

where $2N_c \times N_c$-dimensional matrix $\underline{\mathbf{\Psi}}$ describes linear dependance between $\underline{\mathbf{H}}\mathbf{S}$ and $\tilde{\mathbf{Y}}$, and $\mathbf{N}$ denotes the vector of AWGN samples of length N_c. The variance of the AWGN noise is σ^2, as indicated in Sec. 2.2.6.

For every even row $2n, n = 0, \ldots, N_c - 1$, the elements $\Psi_{n,l}, l = 0, \ldots, N_c - 1$, of the matrix $\underline{\mathbf{\Psi}}$ describe the CFO coefficients which form the even elements of $\tilde{\mathbf{Y}}$ and are given by

$$\Psi_{2n,l} = I_{l-n}(\epsilon). \tag{5.46}$$

Note that if the frequency offset ϵ is zero, then every even row $2n$ has only one non-zero element $\Psi_{2n,2n} = I_0(\epsilon)$.

For every odd row $2n + 1, n = 0, \ldots, N_c - 1$, the elements $\Psi_{n,l}, l = 0, \ldots, N_c - 1$, denote CFO coefficients which form odd elements of $\tilde{\mathbf{Y}}$ and are given by

$$\Psi_{2n+1,l} = I_{(2(l-n)-1)/2}(\epsilon). \tag{5.47}$$

Vector $\underline{\mathbf{\Psi}}\mathbf{N}$ in (5.45) is a noise vector, which cross-correlation matrix is given by $\sigma^2\underline{\mathbf{\Psi}}\mathbf{\Psi}^H$, where $(.)^H$ denotes Hermitian transpose. Clearly, vector $\underline{\mathbf{\Psi}}\mathbf{N}$ is not a vector of the white Gaussian noise, since $\sigma^2\underline{\mathbf{\Psi}}\mathbf{\Psi}^H$ is not a diagonal matrix. At first, we convert (5.45) into equivalent form with the

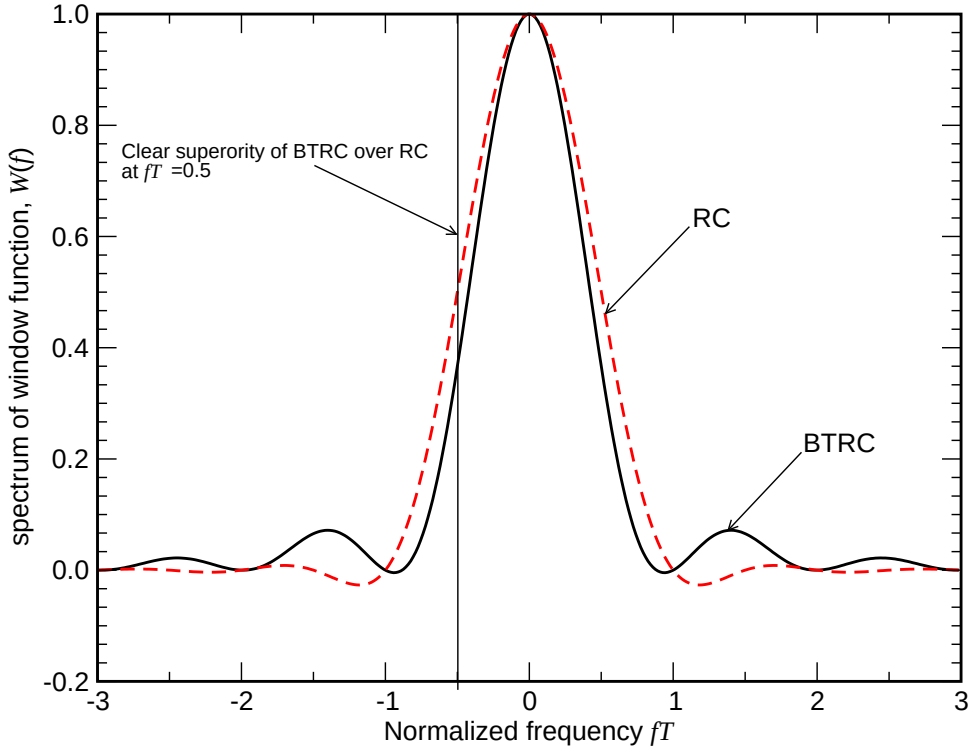

Figure 5.6: Spectra of BTRC and RC windows versus normalized frequency fT_c; $\beta = 1.0$.

white noise. In doing so, we multiply the left and right sides of (5.45) by the matrix $(\underline{\mathbf{\Psi}}^H\underline{\mathbf{\Psi}})^{-1}\underline{\mathbf{\Psi}}^H$. Bearing in mind that

$$(\underline{\mathbf{\Psi}}^H\underline{\mathbf{\Psi}})^{-1}\underline{\mathbf{\Psi}}^H\underline{\mathbf{\Psi}} = \underline{\mathbf{1}}, \tag{5.48}$$

where $\underline{\mathbf{1}}$ is a unity matrix of size $N_c \times N_c$, (5.45) can be rewritten as

$$(\underline{\mathbf{\Psi}}^H\underline{\mathbf{\Psi}})^{-1}\underline{\mathbf{\Psi}}^H\tilde{\mathbf{Y}} = \underline{\mathbf{H}}\mathbf{S} + \mathbf{N}. \tag{5.49}$$

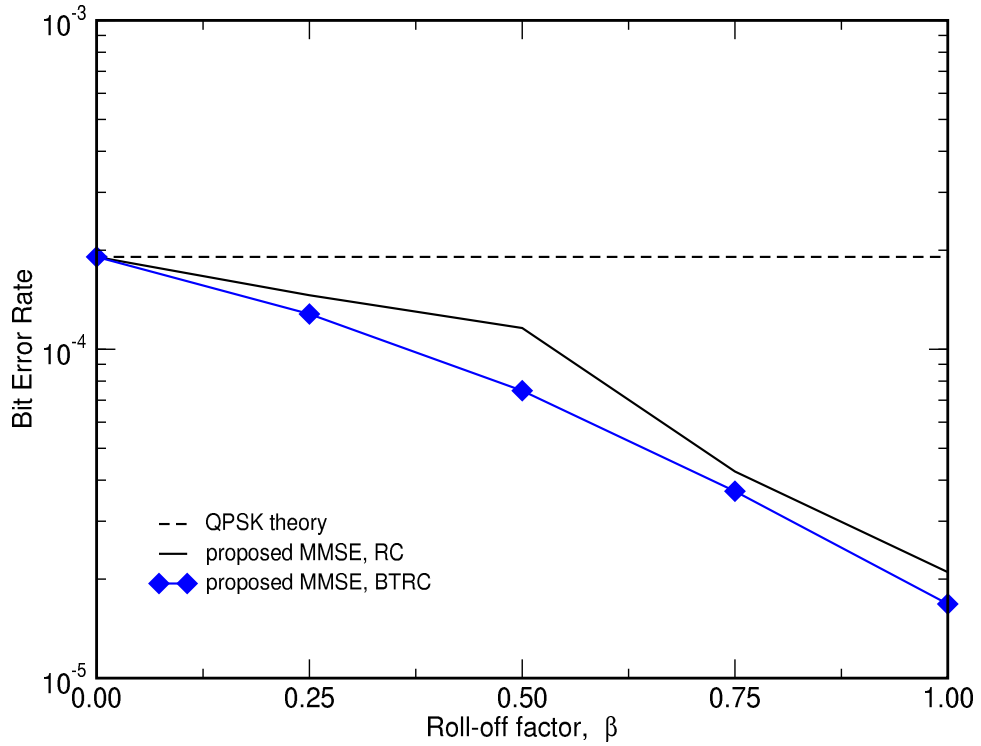

Figure 5.7: BER versus roll-off factor β for the BTRC and RC windows function; SNR = 8 dB.

The noise is white in (5.49). Thus, the multiplication of $\tilde{\mathbf{Y}}$ by the $N_c \times 2N_c$-dimensional matrix $(\underline{\mathbf{\Psi}}^H \underline{\mathbf{\Psi}})^{-1} \underline{\mathbf{\Psi}}^H$ transfers (5.45) into the equivalent form with the white noise (5.49) and can be considered as an application of whitening filter [Pro00] in frequency domain.

With (5.49), the MMSE estimation $\hat{\mathbf{S}}$ of the source vector $\mathbf{S}$ is straight forward [Hay86]

$$\hat{\mathbf{S}} = (\underline{\mathbf{H}}^H \underline{\mathbf{H}} + \sigma^2 \underline{\mathbf{1}})^{-1} \underline{\mathbf{H}}^H (\underline{\mathbf{\Psi}}^H \underline{\mathbf{\Psi}})^{-1} \underline{\mathbf{\Psi}}^H \tilde{\mathbf{Y}}. \tag{5.50}$$

The simulation results for the derived equalizer are given in Fig. 5.5 for the AWGN channel and for the frequency offset $\epsilon = 0$. The OFDM system with $N_c = 32$ subcarriers and QPSK modulation alphabet is used. The theoretical performance of the coherently detected QPSK is given as a reference. If rectangular windowing is utilized with the roll-off factor $\beta = 0$, or equivalently, the length of the prefix and postfix N_w is set to zero, the performance of the proposed equalizer is the same as the theoretical QPSK performance. With increasing β and investing more power into the prefix and postfix, the performance of the equalizer in (5.50) improves. The performance gain is about 0.5 dB for $\beta = 0.5$ and is approximately 1 dB if $\beta = 1$.

The performance of the equalizer depends on the window type, since matrix $\underline{\mathbf{\Psi}}$ is composed of CFO coefficients. The performance of the equalizer improves if window with better spectral properties is applied, for example, "better than" raised cosine (BTRC) window [TB04]. The spectra of individual subcarriers with BTRC and RC windows are shown in Fig. 5.6.

The BER performance of OFDM with the BTRC window is shown in Fig. 5.5 for $\beta = 1$. For BTRC, the cross correlation matrix $\sigma^2 \underline{\mathbf{\Psi}} \underline{\mathbf{\Psi}}^H$ approaches unity matrix and noise $\underline{\mathbf{\Psi}}\mathbf{N}$ in (5.45) is more "white" than for RC.

In Fig. 5.5, for large SNR values and $\beta = 1$, the BER performance gap between QPSK theory and BTRC curves is 1.8 dB, and is about 1 dB between BTRC and RC curves; QPSK performance is given as a reference.

In order to demonstrate the superiority of BTRC over RC, the BER performance of the OFDM system with these windows is shown in Fig. 5.7, as a function of β . The SNR is fixed and is equal to 8 dB. The BER of QSPK, which is independent of β, is given as a reference. Clearly, BTRC window outperforms RC window and allows obtaining the same BER performance by using the prefix and postfix with the length reduced by 5-10 %.

Note that proposed equalizer has the same BER performance even if received OFDM symbol has frequency offset. In this case, however, frequency offset ϵ must be exactly estimated.

The proposed MMSE equalizers improves BER. This BER improvement depends on the length of the prefix and postfix N_{w} and disappears if N_{w} is set to zero, i.e., rectangular window is applied. Thus, the proposed algorithm utilizes a part of the energy invested into the prefix and postfix for the data equalization and, therefore, improves the spectral efficiency of an OFDM system described in Chapter 2.

Chapter 6

IFDMA Uplink System Evaluation

6.1 Introduction

In this Chapter, IFDMA uplink system is developed and compared with the conventional OFDMA and OFDMA-CDM systems. At first, system design is performed which assumes simulation of out-of-band radiation power, passband interference and BER performance of all considered multi-carrier systems with the non-linear power amplifier (NLA). Then, optimum IFDMA uplink system is developed and its performance is studied in the mobile radio channel.

The content and the most important contributions and results of the investigations which are performed in this chapter are shortly summarized as follows:

- The basic system parameters and frame structure are identified in Sec. 6.2.1 for IFDMA, MSK-IFDMA, GOQPSK-IFDMA, OFDMA-CDM and OFDMA systems. As a result, all multi-carrier systems have the same bandwidth efficiency and data rate.

- The NLA model is described in Sec. 6.2.2.

- The out-of-band radiation power of considered multi-carrier systems is compared in Sec. 6.2.3. In Sec. 6.2.4, passband interference caused by NLA is investigated, which appears as a non-linear noise-likely disturbance which depends on the multi-carrier system and PAPR.

- The BER performance of the considered multi-carrier systems in AWGN channel are given in Sec 6.2.5 for fixed SNR. Presented results make it possible to investigate the influence of the NLA on the performance of multi-carrier systems.

- In Sec. 6.3, the performance of the IFDMA uplink system is simulated in the frequency selective mobile radio channel. The BER performance of the IFDMA BS receiver with NLA is presented. The BS receiver employs the frequency domain algorithm, described in Chapter 4. As a reference, performance of the OFDMA uplink system is given. The proposed simulation results verify superiority of the IFDMA with proposed frame structure over the existing techniques.

6.2 System Design

6.2.1 System Parameters

The simulated IFDMA, MSK-IFDMA, GOQPSK-IFDMA, OFDMA-CDM and OFDMA systems have

$$N_{\mathrm{c}} = 1024 \tag{6.1}$$

subcarriers. The carrier frequency is

$$f_{\mathrm{c}} = 5 \text{ GHz} \tag{6.2}$$

and the transmission bandwidth is

$$BW = 20 \text{ MHz}. \tag{6.3}$$

The maximum number of users is K. For OFDMA-CDM and IFDMA, the spreading length is L. For OFDMA, no spreading is applied. The parameters L and K are variable and an expression

$$N_{\mathrm{c}} = LK \tag{6.4}$$

always holds true. In order to variate the data rate per user the M-modification is applied. The total number of subcarriers occupied by each user is given as the product LM. Four different scenarios are considered: $M = 1$, $M = 4$, $M = 16$ and $M = 32$. Only one user is active, i.e.,

$$N_{\mathrm{u}} = 1. \tag{6.5}$$

If $L = K = 32$ and $M = 32$, the considered systems are fully loaded and all N_{c} subcarriers are occupied. An oversampling rate is

$$N_{\mathrm{ov}} = 16 \tag{6.6}$$

and perfect time and frequency synchronization at the BS receiver is assumed. The roll-off factor α of the RC pulse-shaping function is chosen as

$$\alpha = 0.25 \tag{6.7}$$

and the normalized bandwidth of the Gaussian pulse-shaping function defined in (2.77) is given by

$$BT_{\mathrm{c}} = 0.3. \tag{6.8}$$

The length of the RC pulse-shaping function is

$$N_{\mathrm{f}} = 3, \tag{6.9}$$

which results in a filter with 96 taps. The Gaussian and MSK pulse-shaping functions $g(t)$ in (2.75) and (2.77), respectively, are truncated symmetrically around zero and the length of these functions is $N_{\mathrm{f}} = 2$ for both cases. As are result, MSK and Gaussian pulse-shaping filters have 64 taps each. All filters are modeled as FIR filters. For the BER simulations, a convolutional code is chosen with the code rate of

$$R_{\mathrm{c}} = 1/2 \tag{6.10}$$

and memory 6. In OFDMA, OFDMA-CDM and IFDMA systems, QPSK is used as a modulation alphabet. For the MSK-IFDMA and GOQPSK-IFDMA, the modulation is chosen as described in Sec. 2.3.5. Therefore, all multi-carrier systems have the same bandwidth efficiency and data rate. Table 6.1 briefly summarizes the parameters of the IFDMA/OFDMA/OFDMA-CDM/GOQPSK-IFDMA/MSK-IFDMA systems used in simulations.

Table 6.1: Parameters of the uplink IFDMA/OFDMA/OFDMA-CDM/GOQPSK-IFDMA/MSK-IFDMA systems

Carrier frequency	$f_{\mathrm{c}} = 5$ GHz
Number of subcarriers	$N_{\mathrm{c}} = 1024$
Transmission bandwidth	$BW = 40$ MHz
Subcarrier spacing	$\Delta f = 39.06$ kHz
Chip duration	$T_{\mathrm{c}} = 25\ \mu$s
Number of OFDM symbols in an OFDM frame	$N_{\mathrm{frame}} = 24$
Window type	rectangular
Modulation alphabet for IFDMA, OFDMA-CDM and OFDMA	QPSK with Gray coding
Spreading length (except OFDMA)	L, variable
Maximum allowed number of users	K, variable
Useful OFDM symbol duration	$T = 25.6\ \mu$s
Discrete length of guard interval	$N_{\Delta} = 485$
Length of guard interval	$T_{\Delta} = 12.13\ \mu$s
Window function	Raised cosine
Roll-off factor of the window function	$\beta = 0.25$
Channel coding type	Convolutional
Channel code rate	$R_{\mathrm{c}} = 1/2$
Channel code memory length	6
Channel decoder	Viterbi
Linear equalizer	MMSE
Roll-off factor of the RC pulse-shaping function	$\alpha = 0.25$
Length of the RC pulse-shaping function	$N_{\mathrm{f}} = 3$
Oversampling coefficient	$N_{\mathrm{ov}} = 16$
Filter type	FIR
Number of taps of the RC filter	96
Number of taps of Gaussian filter and MSK filters	64

6.2.2 Nonlinear Power Amplifier Model

The nonlinear power amplifier (NLA) is modeled as a memoryless device, which amplifies power of the transmit signal $x(t)$. Let $x(t) = |x(t)|e^{j\varphi(t)}$ be a NLA complex input signal with amplitude $|x(t)|$ and phase $\varphi(t)$. At the output of NLA, signal $x_{\mathrm{amp}}(t)$ can be written by

$$x_{\mathrm{amp}}(t) = |x_{\mathrm{amp}}(t)|e^{j(\varphi(t)+\varphi_{\mathrm{amp}}(t))}, \tag{6.11}$$

where $\varphi_{\mathrm{amp}}(t)$ is an additional phase modulation introduced by the NLA.

The NLA can be described by the input back-off (IBO) and output back-off (OBO) characteristics. The IBO characteristics, IBO, is given by

$$IBO = \frac{|x(t)|^2}{P_{\mathrm{sat}}}, \tag{6.12}$$

where P_{sat} is an input saturation power of the NLA and $|x(t)|^2$ is the instantaneous power of the transmit signal.

The OBO characteristics, OBO, is defined by

$$OBO = \frac{|x_{\text{amp}}(t)|^2}{P_{\text{satout}}}, \tag{6.13}$$

where P_{satout} is the output saturation power of the NLA. In this Chapter, typical linearized traveling wave tube amplifier (LTWTA) is considered. The OBO versus IBO for LTWTA is represented in Fig. 6.1. The dependance of $\varphi_{\text{amp}}(t)$ on IBO is called phase characteristic of the NLA and is shown in Fig. 6.2. The relationship between IBO and OBO as well as the relationship between $\varphi_{\text{amp}}(t)$ and IBO are the design characteristics of the NLA and are independent of $x(t)$ and $x_{\text{amp}}(t)$. With definitions (6.12), (6.13) and Fig. 6.1, is is possible to establish a relationship between $|x_{\text{amp}}(t)|$ and $|x(t)|$ and with (6.12) and Fig. 6.2 to calculate additional phase modulation $\varphi_{\text{amp}}(t)$.

We introduce an average power P of the transmit signal $x(t)$ which is equal to

$$P = \frac{1}{T}\int_0^T |x(t)|^2 dt = \frac{LM}{N_{\text{c}}} E\{|d_q|^2\}, \tag{6.14}$$

where $E\{|d_q|^2\}$ denotes the average power of the complex-valued data symbol d_q, T is an OFDM symbol duration and M is the coefficient of the M-modification, cf. Chapter 2.

A working point of the amplifier is defined as a ratio P/P_{sat} and denotes how close the average power P of the transmit signal $x(t)$ can approach the saturation power P_{sat}. If multi-carrier system operates at low value of P/P_{sat}, then cheap power amplifier can be applied with the small input saturation power P_{sat}. In this case, good NLA efficiency is achieved as well, since low value of P_{sat} means low consumption power of NLA [FK00]. However, if P/P_{sat} is low, the amplitude peaks $|x(t)|$ might lie in the highly non-linear area of OBO characteristic, which results in strong non-linear distortions of $x_{\text{amp}}(t)$.

The output saturation power P_{satout} normalizes power of $x_{\text{amp}}(t)$ in our simulations. For simplicity, P_{satout} is chosen such that expression

$$\int_0^T |x(t)|^2 dt = \int_0^T |x_{\text{amp}}(t)|^2 dt \tag{6.15}$$

holds true.

6.2.3 Out-Of-Band Radiation

In this subsection, transmit spectra of IFDMA, OFDMA, OFDMA-CDM, GOQPSK-IFDMA and MSK-IFDMA are compared. The NLA working point is equal to $P/P_{\text{sat}} = -1$ dB, which means that amplifier operates near saturation point and the transmit signal $x(t)$ experiences strong non-linear distortions. Such a low value of P/P_{sat} are chosen deliberately in order to compare the out-of-band radiation power of the considered multi-carrier system.

The normalized SEDs versus normalized frequency fT_{c} for IFDMA, OFDMA, and OFDMA-CDM, GOQPSK-IFDMA and MSK-IFDMA are shown in Fig. 6.3, Fig. 6.4, Fig. 6.5 and Fig. 6.6 for different number of occupied subcarriers ML. All spectra are normalized so that each subcarrier carries data with the power of 0 dB. The spectra of individual subcarriers is not shown for the purpose of clarity. Only an envelope of each transmit spectrum is depicted in order to get an impression of the influence

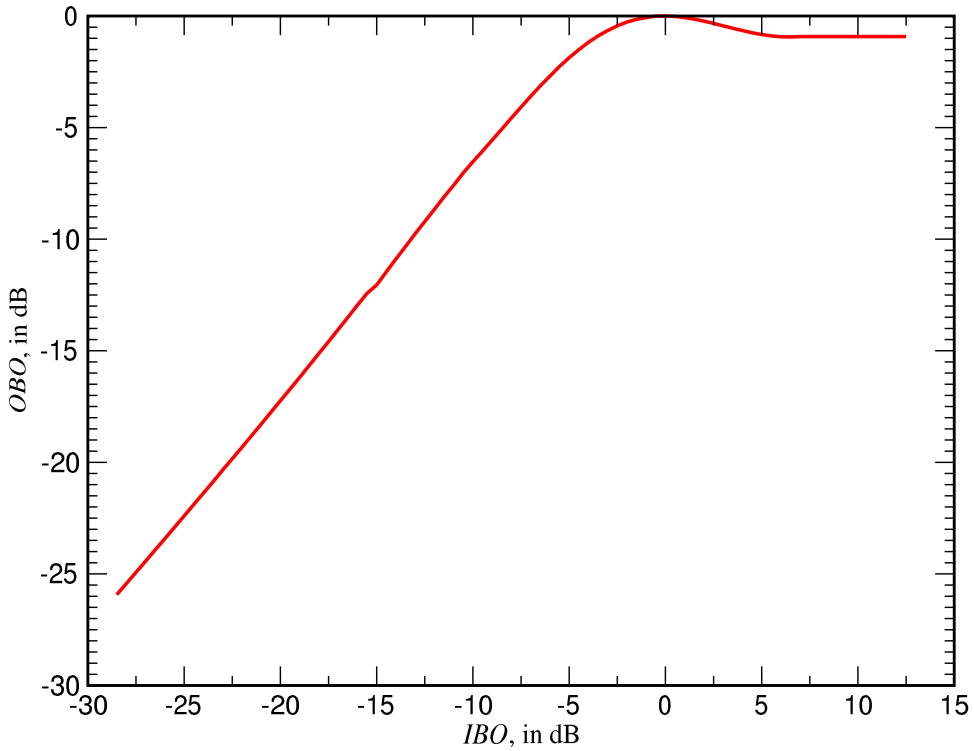

Figure 6.1: The output back-off OBO of the LTWTA NLA versus input back-off IBO.

of the NLA on the power emitted in the out-of-band frequency range, which is defined for normalized frequencies $|fT_{\mathrm{c}}| > 0.5$. The analysis of Fig. 6.3, Fig. 6.4, Fig. 6.5 and Fig. 6.6 reveals that out-of-band radiation power increases with an increasing of number of occupied subcarriers ML since sidelobes of each individual subcarrier sum up constructively.

The normalized SEDs for IFDMA, OFDMA, OFDMA-CDM, GOQPSK-IFDMA and MSK-IFDMA are shown in Fig. 6.3 for $M = 1$. Note that IFDMA with Nyquist pulse-shaping has the same out-of-band radiation power as a conventional OFDMA and OFDMA-CDM. The amplitude peaks in Fig. 2.10c lead to the poor PAPR of the IFDMA transmit signal and are responsible for the high out-of-band radiation. Because of the sinusoidal pulse-shaping function in (2.75), MSK-IFDMA has maximum radiation power in the out-of-band frequency range. As a result of the Gaussian pulse-shaping function, defined in (2.77), and PAPR equal to 0 dB, GOQPSK-IFDMA has the smallest out-of-band radiation power among all considered systems. The gap between MSK-IFDMA and IFDMA curves is more than 10 dB at the normalized frequency $fT_{\mathrm{c}} = 1$.

The normalized SEDs for IFDMA, OFDMA, OFDMA-CDM, GOQPSK-IFDMA and MSK-IFDMA are shown in Fig. 6.4 for the case of $M = 4$. The curves for IFDMA, OFDMA and OFDMA-CDM are coincide, which reveals that these three system experience the same non-linear distortions. Again, GOQPSK-IFDMA outperforms all considered systems and has the lowest out-of-band radiation power. The gap between GOQPSK and IFDMA curves is equal to 8 dB and is smaller than in Fig. 6.3.

The normalized SED for IFDMA, OFDMA, OFDMA-CDM, GOQPSK-IFDMA and MSK-IFDMA are shown in Fig. 6.5 and Fig. 6.6 for $M = 16$ and $M = 32$, respectively. The amount of the out-of-band radiation is equal for IFDMA, OFDMA and OFDMA-CDM and out-of-band radiation

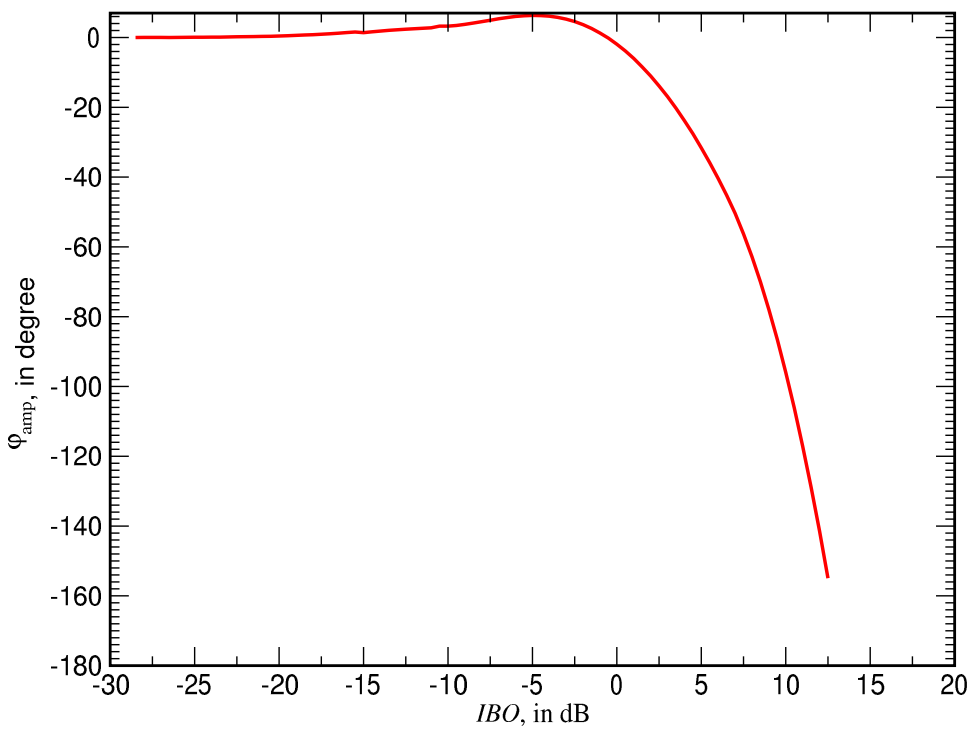

Figure 6.2: The phase characteristics, $\varphi_{\text{amp}}(t)$, of the NLA versus input back-off, IBO.

of MSK-IFDMA is the worst. The GOQPSK-IFDMA outperforms all existing techniques and the performance gap is more than 10 dB for the normalized frequency $fT_{\text{c}} = 1$.

Modern OFDMA based system are scalable, e.g. WiMAX [For06]. The scalability is achieved by adjusting the DFT size to the transmission bandwidth while fixing the sub-carrier frequency spacing. By fixing the subcarrier spacing and OFDM symbol duration, the basic unit of physical (time and frequency) resource remains constant. Therefore, the impact to higher layers is minimal when scaling the bandwidth. The scalability was introduced in WiMAX, since it was developed to perform in the different frequency bands and is able to support a wide range of bandwidths. The scalable OFDMA based system should have minimum interference with existing transmission system, thus, minimization of out-of-band radiation is an important requirement. With GOQPSK-IFDMA introduced in this thesis, the out-of-band radiation power can be suppressed in the most efficient way.

6.2.4 Scatter Plots

It was shown in the previous section that NLA causes non-linear distortions of the transmit signal $x(t)$, which influence transmit spectrum and cause strong out-of-band radiation. In this section, it is demonstrated that NLA is responsible for the non-linear distortions in the passband, i.e., in the normalized frequency range $-0.5 \leq fT_{\text{c}} \leq 0.5$.

The example of a negative impact of the NLA on the transmit signal is shown in Fig. 6.7 where the distortions of the QPSK constellation are presented. An OFDMA system is utilized with $M = 4$. The working point P/P_{sat} of the NLA is set to 2.5 dB and SNR is infinity. Large filled circles denote original non-distorted constellation points, whereas small dots designate constellation points after the NLA. Four ”clouds” in Fig. 6.7 are obtained as a result of non-linear distortions caused by the NLA, which are referred to as a passband interference in the following text. It is seen that

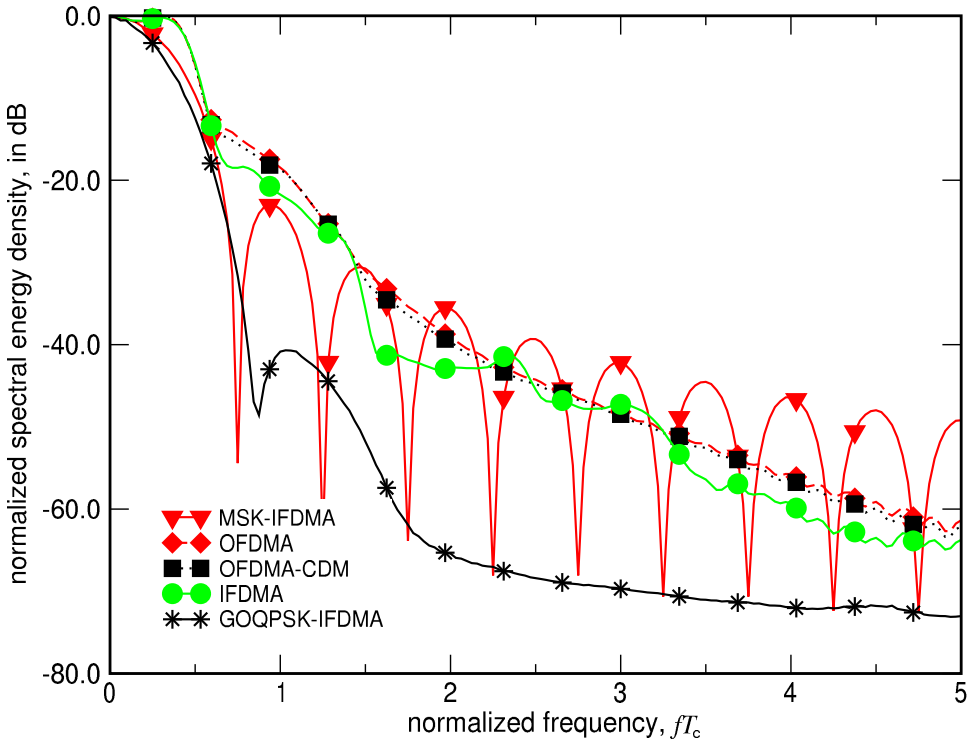

Figure 6.3: Normalized spectral energy density versus normalized frequency fT_c for $M = 1$; $P/P_{sat} = -1$ dB; $L = 32$; $K = 32$.

passband interference appears as noise-like distortion of the transmit constellation which cannot be compensated at the transmitter or receiver. Note that the whole constellation is rotated by the angle of additional phase modulation φ. This angle is equal to the angle φ_{amp}, which can be obtained as the ordinate value of the NLA phase characteristics shown in Fig. 6.2, for IBO equal to P/P_{sat}. Since the average power P of the transmit signal is known at the transmitter, the angle of additional phase modulation φ is also known and is precompensated in the following.

In order to quantize the effects of NLA on the received constellation, we introduce minimum square error (MSE) of constellation distortions which is calculated as an expectation of the Euclidian distance between the transmit d_q and receive $\hat{d}_q$ data symbols. The MSE of constellation distortions is given by

$$MSE = E\{|d_q - \hat{d}_q|^2\}. \tag{6.16}$$

The MSE of the received QPSK constellation versus working point P/P_{sat} of the NLA is shown in Fig. 6.8. The coefficient of the M-modification is $M = 1$. It is seen that MSK-IFDMA and IFDMA with the Nyquist pulse-shaping can be ideally precompensated and their signals are passed unaffected through the NLA. The MSE is equal to zero and is independent of P/P_{sat} for MSK-IFDMA and IFDMA. MSK-IFDMA and IFDMA have PAPR equal to zero when $M = 1$ and their transmit signals are the repetition of the data sequence, as described in Chapter 3. These data symbols are transmitted with a constant power in time domain and NLA rotates each transmit data symbol by a constant angle φ, which can be precompensated and, therefore, the negative impact of the NLA is eliminated completely. Since the complex-valued envelopes of OFDMA and OFDMA-CDM are not constant, thus, negative impact of the NLA cannot be eliminated, the MSE performance of OFDMA and OFDMA-

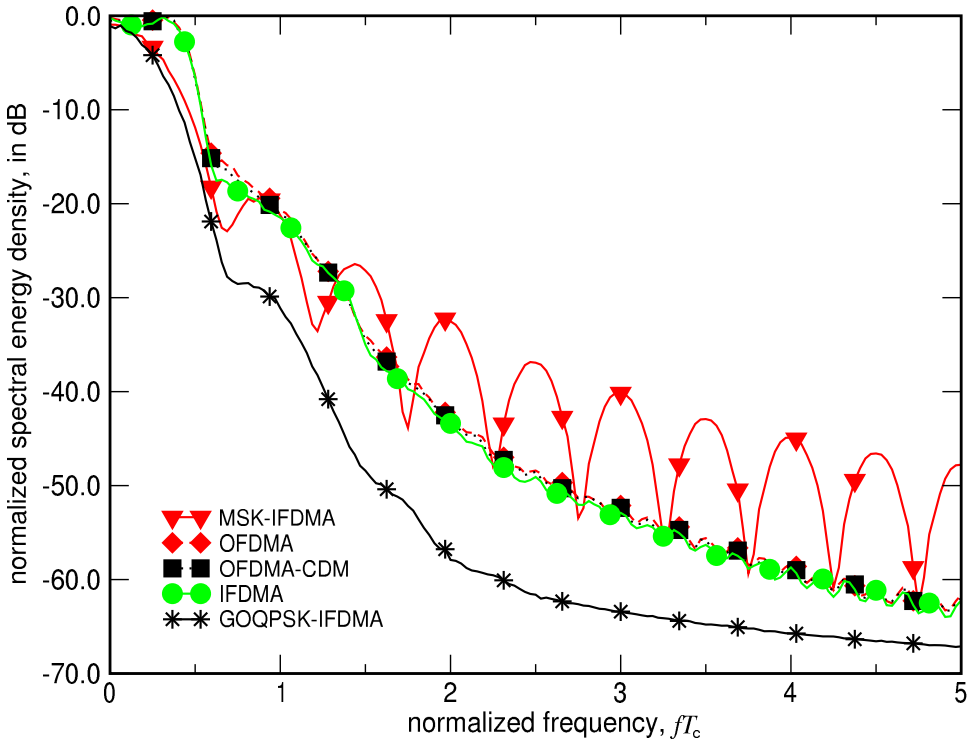

Figure 6.4: Normalized spectral energy density versus normalized frequency fT_c for $M = 4$; $P/P_{sat} = -1$; $L = 32$; $K = 32$.

CDM is significantly worse than MSE performance of IFDMA based systems and decreases with an increasing P/P_{sat}.

The MSE of the received QPSK constellation versus working point P/P_{sat} of the NLA is shown in Fig. 6.9 for $M = 4$. As expected, the constellation points of IFDMA and MSK-IFDMA are less scattered than constellation points of OFDMA and OFDMA-CDM.

The MSEs of the received QPSK constellation versus working point P/P_{sat} of the NLA are shown in Fig. 6.10 and Fig. 6.11 for $M = 16$ and $M = 32$, respectively. For large values of M, the passband interference is approximately equal for all considered systems which results in the same MSE performance for all considered multi-carrier systems. For IFDMA systems, however, passband interference can be minimized by minimizing coefficient M.

6.2.5 BER Performance

It was concluded in Chapter 3 that application of IFDMA is practical only for small values of M when IFDMA results in the reduced PAPR comparing to OFDMA and OFDMA-CDM. The impact of PAPR on the system performance is shown in Fig. 6.12 for $M = 1$ and in Fig. 6.13 for $M = 4$, where BER simulation results are presented for differen multi-carrier systems. The BER curves are plotted versus working point P/P_{sat} of NLA. The SNR per bit μ_b is set to 4 dB.

As shown in Fig. 6.12, IFDMA and MSK/GOQPSK-IFDMA outperform OFDMA and OFDMA-CDM. IFDMA and MSK/GOQPSK-IFDMA have approximately the same, constant performance which is independent of P/P_{sat}. For OFDMA and OFDMA-CDM, the BER performance gets worse if P/P_{sat} increases. This effect can be explained as follows. For $M = 1$, the IFDMA and MSK/GOQPSK-

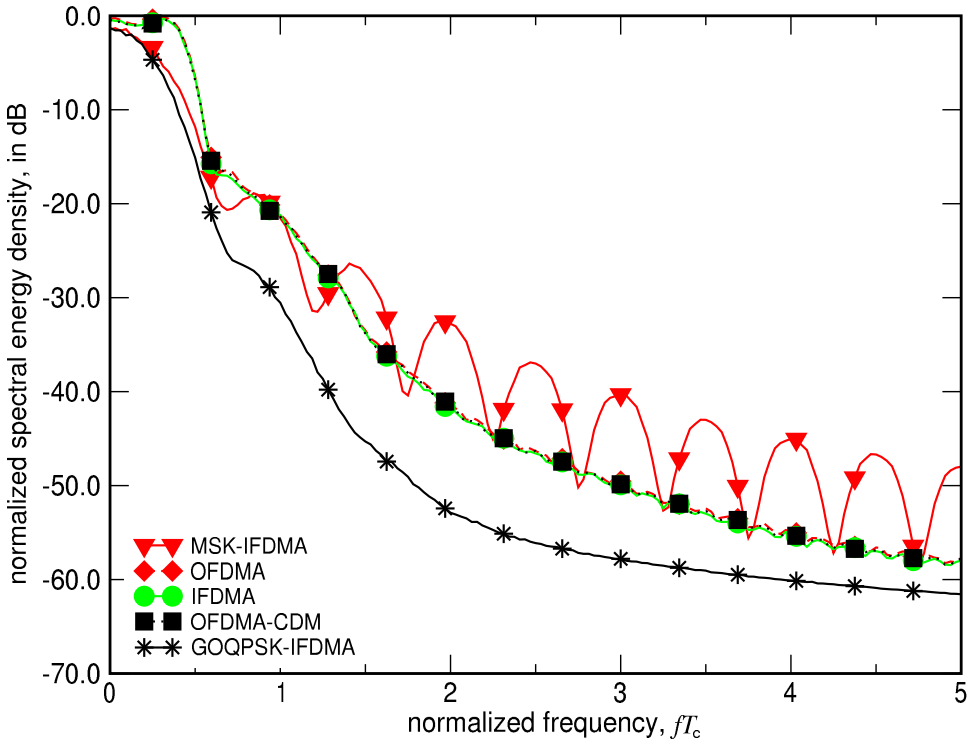

Figure 6.5: Normalized spectral energy density versus normalized frequency fT_c for $M = 16$; $P/P_{sat} = -1$ dB; $L = 32$; $K = 32$.

IFDMA transmit signal is composed of the repeated data sequence, as shown in Chapter 3. Therefore, all data symbols are transmitted with the same power and are equally influenced by the NLA. This influence results is an additional phase modulation φ_{amp} which can be easily precompensated as described in Sec. 6.2.4 and, thus, the negative impact of NLA can be completely eliminated. The time domain signal of OFDMA does not have constant envelope and amplitude variations create non-linear passband interference. Clearly, this passband radiation increases with increasing P/P_{sat} and BER gets worse.

In Fig. 6.13, the BER of the same multi-carrier systems are simulated versus P/P_{sat}. The M-modification coefficient is chosen $M = 4$, which results in an increased PAPR for OFDMA and IFDMA. Again, IFDMA and MSK/GOQPSK-IFDMA outperform OFDMA and OFDMA-CDM, however, the performance gain is smaller than in Fig. 6.12. As shown in Fig. 3.4, the PAPR performance gap between IFDMA and OFDMA is about 1 dB, which corresponds to the BER performance gap between IFDMA and OFDMA presented in Fig. 6.13.

6.3 Simulation Results and Discussion

In this subsection, performance of the IFDMA uplink system is studied. C1 urban macro-cell clustered channel model is used [Con06c] which simulates urban propagation scenario without line-of-sight component with the cell size of 200 meters. The maximum MT velocity is equal to 70 km/h and new velocity values are generated for every frame. The maximum frequency offset comprises 0.82% of the subcarrier spacing.

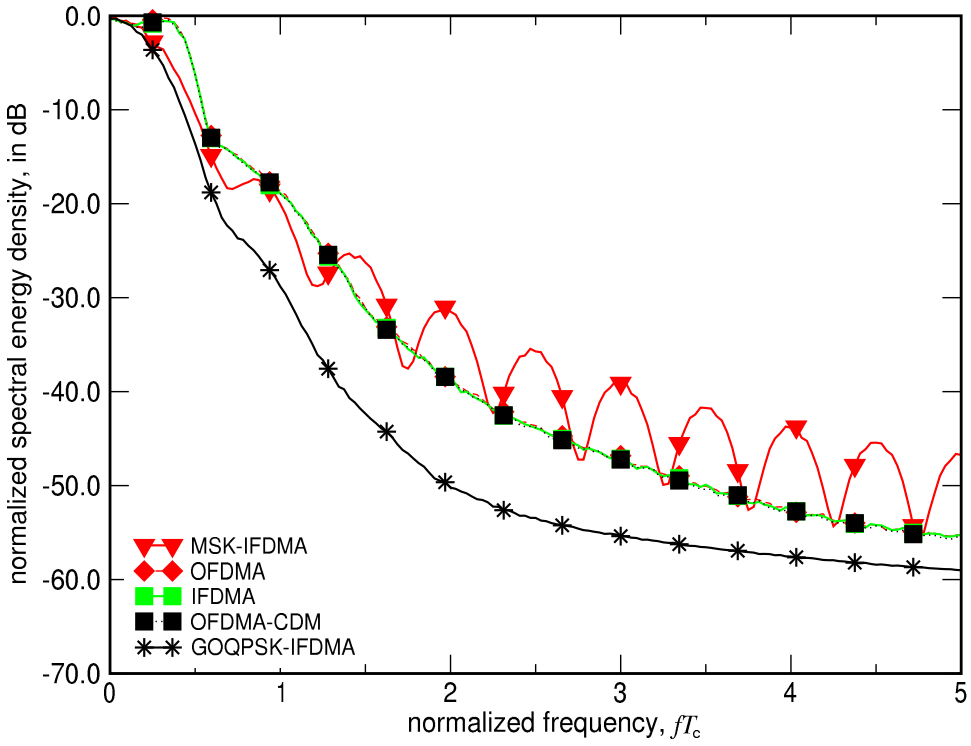

Figure 6.6: Normalized spectral energy density versus normalized frequency fT_c for $M = 32$; $P/P_{sat} = -1$ dB; $L = 32$; $K = 32$.

Propagation delay of the transmit signal of each individual user is a normally distributed random variable which might be as great as 0.66μs which is only 2% of the chip interval duration. However, oscillators's frequencies at the BS and MT are not synchronized. Therefore, transmit signals of different users are modeled to arrive at the BS receiver with the random time delay equal to the chip interval duration T_c.

The combination of GOQPSK and IFDMA, introduced in Chapter 3, shows some advantages over conventional IFDMA, while demonstrating the same BER performance. GOQPSK can be used as an alternative to the QPSK and, unfortunately, cannot be combined with 16- or 64-QAM, which are widely used in a variety of multi-carrier standards [Wim07, Wir99].

In Fig. 6.14, BER performance of the fully loaded IFDMA uplink system is presented. The number of active users is $K = 32$. Perfect channel estimation is utilized and no power loss due to the insertion of the guard interval, postfix and prefix are assumed. As shown in the previous section, advantages of the IFDMA over other multi-carrier techniques are remarkable only for small values of the M-modification coefficient M, thus, M is equal to four in the following text.

As a reference, performance of the OFDMA uplink system is given. Both systems have the same frame structure and the same data rate. OFDMA and IFDMA utilize algorithms described in Chapter 4 and Chapter for frequency and estimation.

It is seen that IFDMA outperforms OFDMA and the performance gain is about 8 dB. Several factors are responsible for this performance gain. At first, IFDMA demonstrates smaller PAPR than OFDMA, which results in the smaller passband interference due to NLA. Second, non-linear distortions caused by NLA influences the frequency time offset estimation algorithm, however, for IFDMA the negative impact is less.

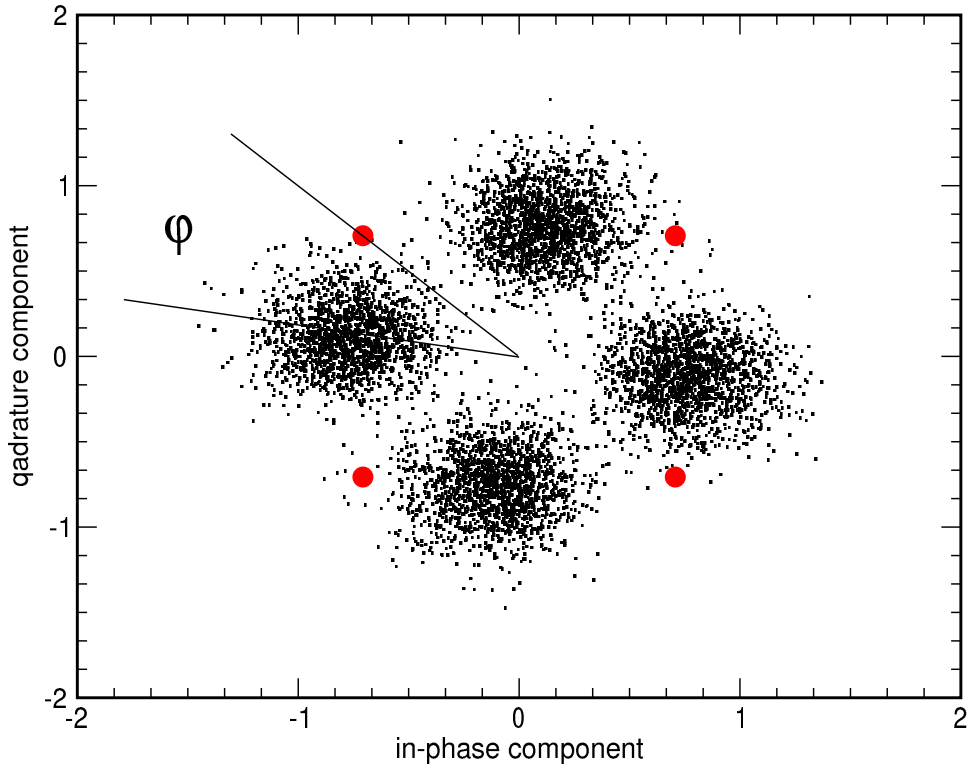

Figure 6.7: Scatter plot of received QSPK constellation in the case of OFDMA; $P/P_{\text{sat}} = 2.5$ dB; $L = 32$; $K = 32$; $M = 4$.

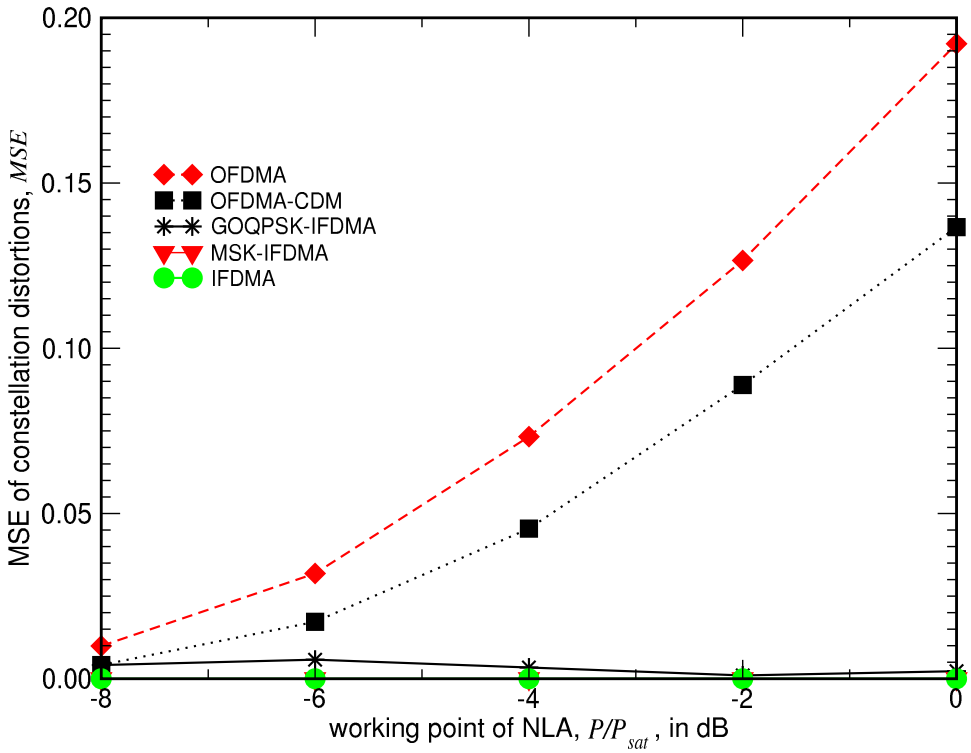

Figure 6.8: MSE of the constellation distortions versus working point P/P_{sat} of the NLA for IFDMA, OFDMA, OFDMA-CDM, MSK-IFDMA and GOQPSK-IFDMA; $M = 1$; $L = 32$; $K = 32$.

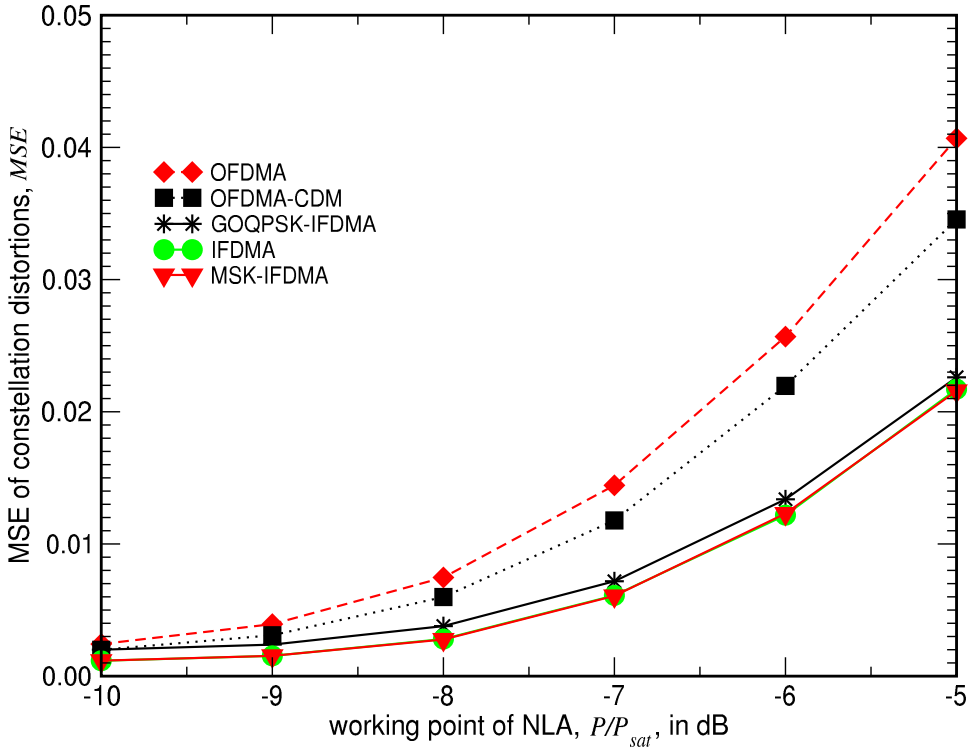

Figure 6.9: MSE of the constellation distortions versus working point P/P_{sat} of the NLA for IFDMA, OFDMA, OFDMA-CDM, MSK-IFDMA and GOQPSK-IFDMA; $M = 4$; $L = 32$; $K = 32$.

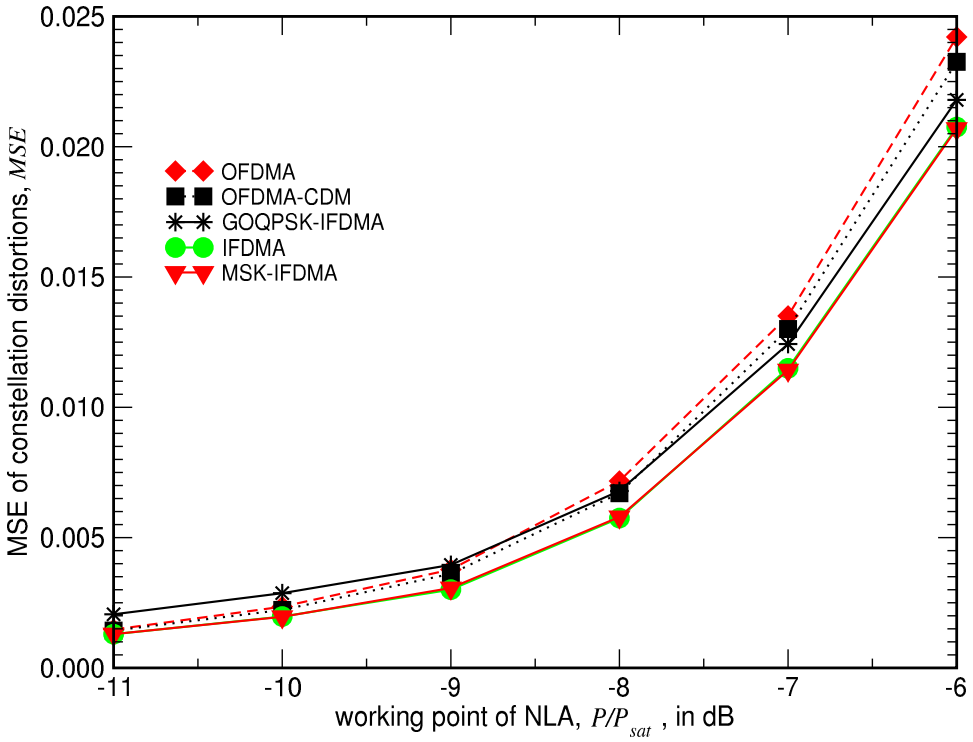

Figure 6.10: MSE of the constellation distortions versus working point P/P_{sat} of the NLA for IFDMA, OFDMA, OFDMA-CDM, MSK-IFDMA and GOQPSK-IFDMA; $M = 16$; $L = 32$; $K = 32$.

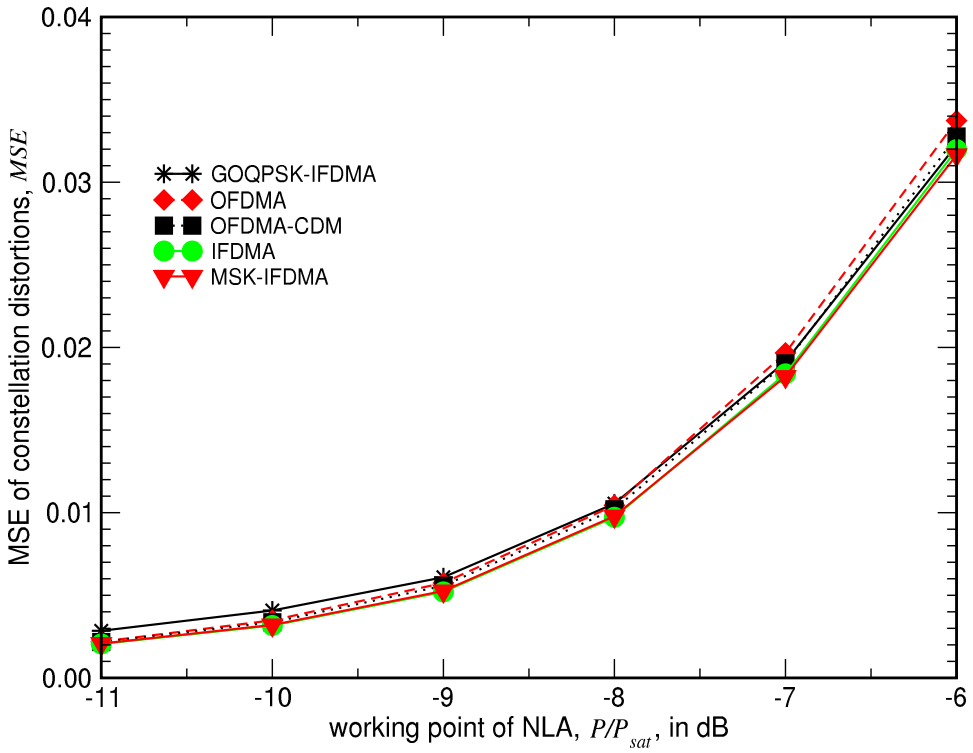

Figure 6.11: MSE of the constellation distortions versus working point P/P_{sat} of the NLA for IFDMA, OFDMA, OFDMA-CDM, MSK-IFDMA and GOQPSK-IFDMA; $M = 32$; $L = 32$; $K = 32$.

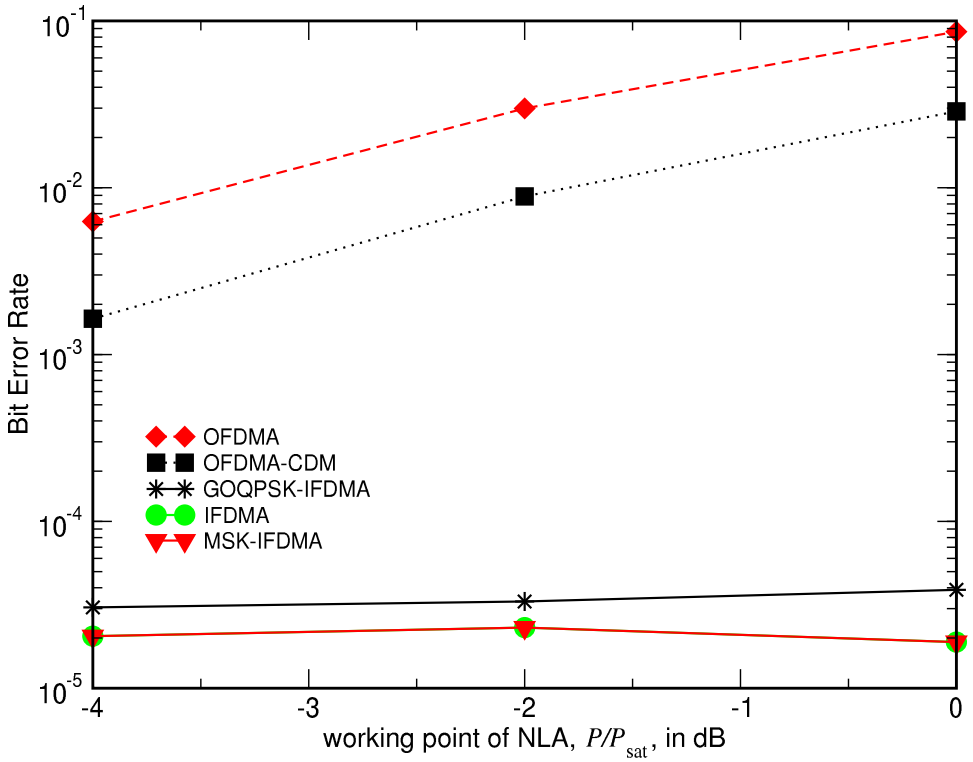

Figure 6.12: BER versus working point P/P_{sat} of NLA for IFDMA, OFDMA, OFDMA-CDM, MSK-IFDMA and GOQPSK-IFDMA; $M = 1$; $L = 32$; $K = 32$.

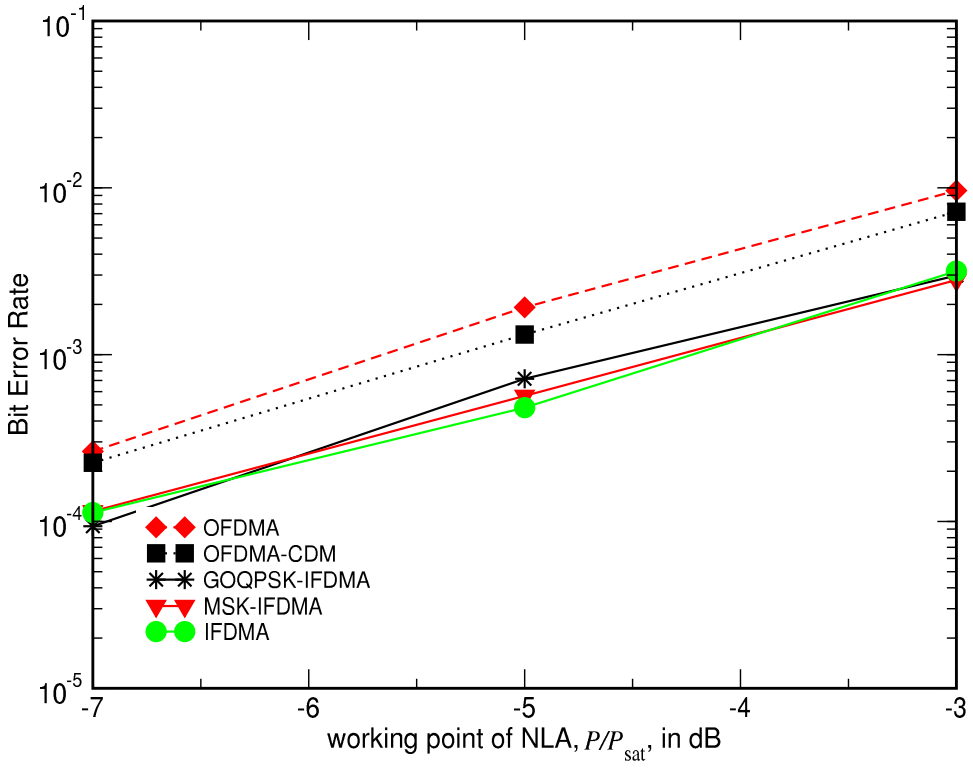

Figure 6.13: BER versus working point P/P_{sat} of NLA for IFDMA, OFDMA, OFDMA-CDM, MSK-IFDMA and GOQPSK-IFDMA; $M = 4$; $L = 32$; $K = 32$.

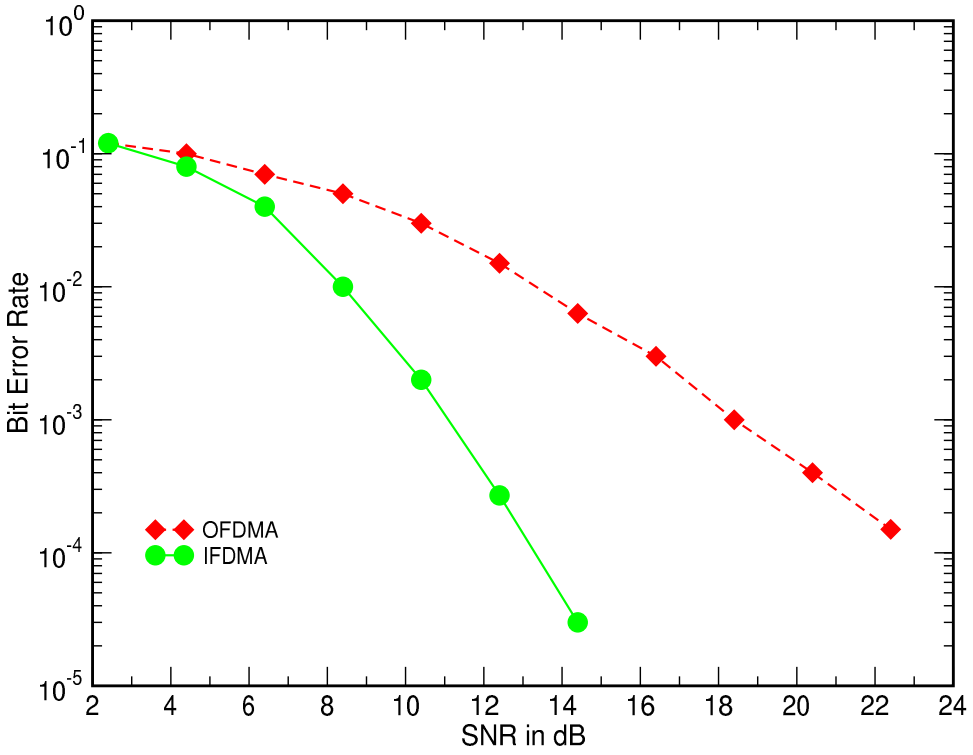

Figure 6.14: BER versus SNR per bit for IFDMA and OFDMA; $M = 4$; $L = 32$; $K = 32$.

Chapter 7

Abstract

The first objective of this thesis is to develop the interleaved frequency-division multiple-access (IFDMA) receiver with frequency domain equalization, low complexity and possibility to separate users in the frequency domain. Note that at the time the work on this thesis was started, the efficient IFDMA receiver was not developed and relationship between OFDMA and IFDMA systems were not yet understood.

The IFDMA technique is introduced as a special case of the orthogonal frequency-division multiple-access code division multiplexing (OFDMA-CDM). The proposed IFDMA transmitter does not have the computationally intensive discrete Fourier transform (DFT) operation and, thus, is more preferable than the conventional OFDMA and OFDMA-CDM transmitters.

The concept of minimum shift keying (MSK) and Gaussian-shaped offset QPSK (GOQPSK) IFDMA is proposed. As a result of GOQPSK and MSK combination with IFDMA, the MSK/GOQPSK-IFDMA transmit signal is generated without phase transitions and has better spectral properties than the conventional OFDMA transmit signal.

The peak-to-average power ratio (PAPR) of the OFDMA, IFDMA and newly introduced GOQPSK- and MSK-IFDMA are compared. The cumulative distribution function of PAPR distribution is analyzed for the GSMK/MSK-IFDMA. As a reference, the conventional OFDMA and OFDMA-CDM systems are used. Finally, the circumstances under which PAPR distribution of GOQPSK-IFDMA outperforms the PAPR distribution of the conventional IFDMA are identified. The most valuable results is that IFDMA based systems can achieve the PAPR of single-carrier systems providing any required data rate for data transmission.

The effect of frequency offsets on the performance of IFDMA uplink system is investigated using raised cosine (RC) window. It is shown that MAI caused by the frequency offsets can be reduced significantly if the RC window is applied instead of conventional rectangular window.

Generally, frequency offset estimation in the uplink of multi-carrier systems is a complicated task, since the received signal at the BS comprises of the received signals from many users and each user can have its own frequency offset. Moreover, received signals from different users are distorted by different transmission channels which makes the problem of channel estimation complicated.

A frequency domain algorithm for frequency offset estimation is proposed and its performance is investigated in the mobile radio channel. This algorithm utilizes pilot symbols and provides joint frequency offset and channel estimation. A special construction of pilot symbols with additional spreading in the time domain is proposed which allows reduction of the frequency offset estimation error.

A practical time domain (TD) algorithm is evaluated which uses repetitive structure of the IFDMA transmit signal in the time domain. The TD algorithm is independent of the transmission channel and modulation alphabet. Statistical properties of the estimate are analyzed and proven analytically and by Monte-Carlo simulations. As a result, the obtained estimate is unbiased and is able to provide a reliable result at the SNR of practical interest. The proposed algorithm is compared with existing techniques and its superiority is proven.

The optimum MMSE equalization technique for OFDM and IFDMA with windowing at the receiver is presented. As shown in literature, the application of the window in the receiver changes the received spectrum of each individual subcarrier. Varying the roll-off factor of the DFT window function and, therefore, changing the length of the prefix and postfix, MAI caused by the frequency offset can be reduced.

The minimum mean square error algorithm which utilizes part of the energy invested into prefix and postfix for the equalization is proposed which allows to improve the BER of OFDM system with windowing. For simplicity, the proposed algorithm is presented for OFDM but can also be applied for IFDMA.

Additionally, The SI of IFDMA systems is investigated in an independent Rayleigh channel and it is shown that IFDMA has significantly less SI than the conventional OFDMA-CDM.

The IFDMA uplink system with non-linear amplifier is investigated and compared with OFDMA and OFDMA-CDM techniques in terms of passband interference, out-of-band radiation and BER performance. Finally, the performance of IFDMA system is simulated in the mobile radio channel.

Appendix

A.1 DFT Operation at the Receiver

This Appendix shows that the windowing operation and a DFT of size $2N_{\mathrm{c}}$ make possible an interference-free reception of source data symbols $S_\kappa, \kappa = 0, \ldots, N_{\mathrm{c}} - 1$, under the condition that the window function $w(t)$ satisfies Nyquist criterion in the frequency domain.

We introduce the transmit sequence $\bar{x}_\upsilon, \upsilon = 0, \ldots, 2N_{\mathrm{c}} - 1$, as a sequence in (2.25) with appended $N_{\mathrm{c}} - 2N_{\mathrm{w}}$ zeros

$$\bar{x}_\upsilon = \begin{cases} \frac{1}{\sqrt{N_{\mathrm{c}}}} \sum_{\kappa=0}^{N_{\mathrm{c}}-1} S_\kappa e^{j2\pi\kappa(\upsilon - N_{\mathrm{w}})/N_{\mathrm{c}}} & \text{if } \upsilon = 0, \ldots, N_{\mathrm{c}} + 2N_{\mathrm{w}} - 1 \\ 0 & \text{if } \upsilon = N_{\mathrm{c}} + 2N_{\mathrm{w}}, \ldots, 2N_{\mathrm{c}} - 1. \end{cases} \tag{A.1}$$

In the same way, we introduce sequence $\bar{h}_\upsilon, \upsilon = 0, \ldots, 2N_{\mathrm{c}} - 1$, which is obtained by appending $2N_{\mathrm{c}} - M_{\mathrm{ch}}$ zeroes to the complex-valued CIR sequence $h_m, m = 0, \ldots, M_{\mathrm{ch}} - 1$, defined in Sec. 2.2.3, so that

$$\bar{h}_\upsilon = \begin{cases} h_\upsilon & \text{if } \upsilon = 0, \ldots, M_{\mathrm{ch}} - 1 \\ 0 & \text{if } \upsilon = M_{\mathrm{ch}}, \ldots, 2N_{\mathrm{c}} - 1. \end{cases} \tag{A.2}$$

The sequence of AWGN $\bar{n}_\upsilon, \upsilon = 0, \ldots, 2N_{\mathrm{c}} - 1$, is obtained as

$$\bar{n}_\upsilon = \begin{cases} n_{\mathrm{w},\upsilon} & \text{if } \upsilon = 0, \ldots, N_{\mathrm{c}} + 2N_{\mathrm{w}} - 1 \\ 0 & \text{if } \upsilon = N_{\mathrm{c}} + 2N_{\mathrm{w}}, \ldots, 2N_{\mathrm{c}} - 1. \end{cases} \tag{A.3}$$

Due to the guard interval, the sequence $y_\upsilon, \upsilon = 0, \ldots, 2N_{\mathrm{c}} - 1$, can be represented as a cyclic convolution of the transmit sequence $\bar{x}_\upsilon$ and $\bar{h}_\upsilon$ plus additive white Gaussian noise $\bar{n}_\upsilon$ [NP02]

$$y_\upsilon = \sum_{k=0}^{2N_{\mathrm{c}}-1} \bar{x}_k \bar{h}_{(k-\upsilon) \bmod 2N_{\mathrm{c}}} + \bar{n}_\upsilon. \tag{A.4}$$

The windowing operation is a multiplication of y_υ by the samples $w_\upsilon, \upsilon = 0, \ldots, 2N_{\mathrm{c}} - 1$, of the window function $w(t)$. Note that sequence w_υ is non-zero only within interval $\upsilon = 0, \ldots, N_{\mathrm{c}} + 2N_{\mathrm{w}} - 1$, as shown in Fig. 2.6b. The obtained sequence $y_{\mathrm{w},\upsilon}, \upsilon = 0, \ldots, 2N_{\mathrm{c}} - 1$, is given by

$$y_{\mathrm{w},\upsilon} = y_\upsilon w_\upsilon = \sum_{k=0}^{2N_{\mathrm{c}}-1} \underbrace{w_k \bar{x}_k}_{I} \underbrace{\bar{h}_{(k-\upsilon) \bmod 2N_{\mathrm{c}}}}_{II} + \underbrace{w_\upsilon \bar{n}_\upsilon}_{III}, \tag{A.5}$$

which is a cyclic convolution of the sequences I,

$$w_\upsilon \bar{x}_\upsilon, \upsilon = 0, \ldots, 2N_{\mathrm{c}} - 1, \tag{A.6}$$

and sequence II,

$$\bar{h}_\upsilon, \upsilon = 0, \ldots, 2N_\mathrm{c} - 1, \tag{A.7}$$

plus noise term, sequence III

$$w_\upsilon \bar{n}_\upsilon, \upsilon = 0, \ldots, 2N_\mathrm{c} - 1. \tag{A.8}$$

The DFT of the sequence I is introduced by

$$X_{\kappa'} = \frac{1}{\sqrt{2N_\mathrm{c}}} \sum_{\upsilon=0}^{2N_\mathrm{c}-1} w_\upsilon \bar{x}_\upsilon e^{-j\frac{2\pi}{2N_\mathrm{c}}\upsilon\kappa'}, \kappa' = 0, \ldots, 2N_\mathrm{c} - 1, \tag{A.9}$$

whereas the DFT of sequence II is given by

$$\bar{H}_{\kappa'} = \frac{1}{\sqrt{2N_\mathrm{c}}} \sum_{\upsilon=0}^{2N_\mathrm{c}-1} \bar{h}_\upsilon e^{-j\frac{2\pi}{2N_\mathrm{c}}\upsilon\kappa'}, \kappa' = 0, \ldots, 2N_\mathrm{c} - 1, \tag{A.10}$$

and DFT of the noise term is denoted by

$$N_{\kappa'} = \frac{1}{\sqrt{2N_\mathrm{c}}} \sum_{\upsilon=0}^{2N_\mathrm{c}-1} w_\upsilon \bar{n}_\upsilon e^{-j\frac{2\pi}{2N_\mathrm{c}}\upsilon\kappa'}, \kappa' = 0, \ldots, 2N_\mathrm{c} - 1. \tag{A.11}$$

At the output of DFT block in Fig 2.4, one obtains a frequency domain sequence $Y_{\kappa'}, \kappa' = 0, \ldots, 2N_\mathrm{c} - 1$,

$$Y_{\kappa'} = \frac{1}{\sqrt{2N_\mathrm{c}}} \sum_{\upsilon=0}^{2N_\mathrm{c}-1} w_\upsilon y_{\mathrm{w},\upsilon} e^{-j\frac{2\pi}{2N_\mathrm{c}}\upsilon\kappa'}. \tag{A.12}$$

According to the theorem of the cyclic convolution [PM96], the convolution of the sequences I and II is equivalent to the multiplication of their DFTs. Thus, frequency-domain sequence $Y_{\kappa'}, \kappa = 0, \ldots, 2N_\mathrm{c} - 1$, is given by

$$Y_{\kappa'} = \bar{H}_{\kappa'} X_{\kappa'} + N_{\kappa'}, \tag{A.13}$$

The sequence $X_{\kappa'}, \kappa' = 0, \ldots, 2N_\mathrm{c} - 1$, can be further developed as

$$\begin{aligned}
X_{\kappa'} &= \frac{1}{\sqrt{2N_\mathrm{c}}} \sum_{\upsilon=0}^{2N_\mathrm{c}-1} w_\upsilon \bar{x}_\upsilon e^{-j\frac{2\pi}{2N_\mathrm{c}}\upsilon\kappa'} \\
&= \frac{1}{\sqrt{2N_\mathrm{c}}} \sum_{\upsilon=0}^{N_\mathrm{c}+2N_\mathrm{w}-1} w_\upsilon x_\upsilon e^{-j\frac{2\pi}{2N_\mathrm{c}}\upsilon\kappa'} \\
&= \frac{1}{\sqrt{2N_\mathrm{c}}} \sum_{\upsilon=0}^{N_\mathrm{c}+2N_\mathrm{w}-1} \left[w_\upsilon \frac{1}{\sqrt{N_\mathrm{c}}} \sum_{\kappa=0}^{N_\mathrm{c}-1} S_\kappa e^{j2\pi\kappa(\upsilon-N_\mathrm{w})/N_\mathrm{c}} \right] e^{-j\frac{2\pi}{2N_\mathrm{c}}\upsilon\kappa'} \\
&= \frac{1}{N_\mathrm{c}\sqrt{2}} \sum_{\kappa=0}^{N_\mathrm{c}-1} S_\kappa \left[\sum_{\upsilon=0}^{N_\mathrm{c}+2N_\mathrm{w}-1} w_\upsilon e^{j2\pi\kappa(\upsilon-N_\mathrm{w})/N_\mathrm{c}} \right] e^{-j\frac{2\pi}{2N_\mathrm{c}}\upsilon\kappa'} = \\
&= \frac{1}{N_\mathrm{c}\sqrt{2}} \sum_{\kappa=0}^{N_\mathrm{c}-1} S_\kappa \left[\sum_{\upsilon=0}^{N_\mathrm{c}+2N_\mathrm{w}-1} w_\upsilon e^{j\frac{4\pi\kappa(\upsilon-N_\mathrm{w})-2\pi\upsilon\kappa'}{2N_\mathrm{c}}} \right] = \\
&= \sum_{\kappa=0}^{N_\mathrm{c}-1} S_\kappa e^{j2\pi\frac{N_\mathrm{w}}{N_\mathrm{c}}\kappa} \frac{1}{N_\mathrm{c}\sqrt{2}} \left[\sum_{\upsilon=0}^{N_\mathrm{c}+2N_\mathrm{w}-1} w_\upsilon e^{j\pi\upsilon\frac{(2\kappa-\kappa')}{N_\mathrm{c}}} \right].
\end{aligned} \tag{A.14}$$

The properties of the last sum in (A.14) can be better understood if we consider the spectrum function $I_0(f)$ which denotes spectrum of each individual subcarrier. $I_0(f)$ is given by

$$I_0(f) = \frac{1}{N_c\sqrt{2}} \sum_{\upsilon=0}^{N_c+2N_w-1} w_\upsilon e^{j\pi\upsilon\frac{f}{N_c}} \tag{A.15}$$

and is depicted in Fig. A.1 as a function of the frequency f. The requirement for the interference-

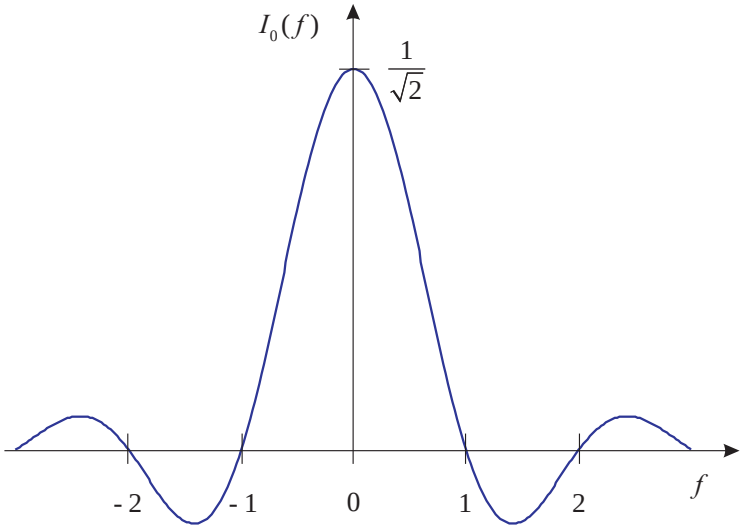

Figure A.1: The spectrum function $I_0(f)$ of the RC window; $\alpha = 0.25$.

free reception of transmit source data symbols $S_\kappa, \kappa = 0, \ldots, N_c - 1$, is that $w(t)$ satisfies Nyquist criterion in the frequency domain, i.e., for every $n = 1, 2...$, the expression

$$I_0(n) = \begin{cases} \frac{1}{\sqrt{2}} & \text{if } n = 0 \\ 0 & \text{otherwise} \end{cases} \tag{A.16}$$

holds true

Bearing in mind that RC window satisfies conditions given in (A.16), the last sum in (A.14) becomes

$$\frac{1}{N_c\sqrt{2}} \sum_{\upsilon=0}^{N_c+2N_w-1} w_\upsilon e^{j\pi\upsilon\frac{2\kappa-\kappa'}{N_c}} = \begin{cases} 0 & \text{if } 2\kappa - \kappa' \neq 0 \text{ and } \kappa' \text{ is even} \\ \frac{1}{\sqrt{2}} & \text{if } 2\kappa - \kappa' = 0 \text{ and } \kappa' \text{ is even.} \end{cases} \tag{A.17}$$

One can choose only even elements of the sequence $X_{\kappa'}, \kappa' = 2\kappa, \kappa = 0, \ldots, N_c - 1$, in (A.14). In doing so, $X_{\kappa'}$ simplifies to

$$X_{\kappa'} = \frac{1}{\sqrt{2}} e^{2\pi\frac{N_w}{N_c}\kappa} S_\kappa. \tag{A.18}$$

Note that the exponent $e^{j2\pi\frac{N_w}{N_c}\kappa} = e^{j\pi\frac{N_w}{N_c}\kappa'}$ appears due to the prefix of the length N_w. This exponent represents additional linear phase rotation of the transmit source symbols S_κ, which is transmitted on the the κth subcarrier. This linear phase rotation can be easily eliminated in the channel estimation process.

The fading coefficient $H_{\kappa'}$ on the κth subcarrier is defined as even element $\kappa' = 2\kappa$, of the sequence

$$\begin{aligned} H_{\kappa'} &= \frac{1}{\sqrt{2}} \bar{H}_{\kappa'} e^{j\pi \frac{N_{\mathrm{W}}}{N_{\mathrm{c}}} \kappa'} \\ &= \frac{1}{\sqrt{2}} e^{j\pi \frac{N_{\mathrm{W}}}{N_{\mathrm{c}}} \kappa'} \sum_{m=0}^{M_{\mathrm{ch}}-1} h_m e^{-j\frac{\pi}{N_{\mathrm{c}}} m\kappa'}. \end{aligned} \tag{A.19}$$

Bearing in mind (A.19) and (A.18), expression (A.13) can be represented as

$$Y_{\kappa'} = H_{\kappa'} S_{\kappa} + N_{\kappa'}. \tag{A.20}$$

Note that the exponent $e^{j\pi \frac{N_{\mathrm{W}}}{N_{\mathrm{c}}} \kappa'}$ and normalization coefficients $1/\sqrt{2}$ from (A.18) are explicitly included into the fading coefficient $H_{\kappa'}$.

Only even elements, $\kappa' = 2\kappa, \kappa = 0, \ldots, N_{\mathrm{c}} - 1$, of the sequence $Y_{\kappa'}, \kappa = 2\kappa', \kappa = 0, \ldots, N_{\mathrm{c}} - 1$, represent the received values on the subcarriers $\kappa = 0, \ldots, N_{\mathrm{c}} - 1$. Each element $Y_{\kappa'}$ is equal to the multiplication of the fading coefficient $H_{\kappa'}$ and transmit source symbol S_{κ} plus additive white Gaussian noise sample $N_{\kappa'}$.

A.2 CFO Coefficients

To derive the expression for carrier frequency offset (CFO) coefficients $I_\kappa(\epsilon)$, we consider a conventional OFDM system with N_c subcarriers, which are used for the transmission of source symbols $S_\kappa, \kappa = 0, \ldots, N_\mathrm{c} - 1$. The considered system has a prefix and postfix of length N_w. For simplicity, we consider an AWGN channel with negligible noise power.

After IDFT operation and addition of the prefix and postfix, the OFDM discrete signal $x_\upsilon, \upsilon = 0, \ldots, N_\mathrm{c} + 2N_\mathrm{w} - 1$, is given in (2.25). With the frequency offset ϵ and without guard interval it is given by

$$x_\upsilon = \frac{1}{\sqrt{N_\mathrm{c}}} \sum_{\kappa=0}^{N_\mathrm{c}-1} S_\kappa e^{j2\pi\kappa(\upsilon - N_\mathrm{w} + \epsilon)/N_\mathrm{c}}. \tag{A.21}$$

At the receiver, after guard interval removal windowing operation is performed. Windowing operation is a multiplication of $x_\upsilon, \upsilon = 0, \ldots, N_\mathrm{c} + 2N_\mathrm{w} - 1$ by the samples $w_\upsilon, \upsilon = 0, \ldots, N_\mathrm{c} + 2N_\mathrm{w} - 1$. After DFT of size $2N_\mathrm{c}$, the received sequence $Y_{\kappa'}, \kappa' = 0, \ldots, N_\mathrm{c} + 2N_\mathrm{w} - 1$, is represented by

$$\begin{aligned}
Y_{\kappa'} &= \frac{1}{\sqrt{2N_\mathrm{c}}} \sum_{\upsilon=0}^{N_\mathrm{c}+2N_\mathrm{w}-1} w_\upsilon x_\upsilon e^{-j\frac{2\pi}{2N_\mathrm{c}}\upsilon\kappa'} \qquad (A.22)\\
&= \frac{1}{\sqrt{2N_\mathrm{c}}} \sum_{\upsilon=0}^{N_\mathrm{c}+2N_\mathrm{w}-1} \left[w_\upsilon \frac{1}{\sqrt{N_\mathrm{c}}} \sum_{\kappa=0}^{N_\mathrm{c}-1} S_\kappa e^{j2\pi\kappa(\upsilon - N_\mathrm{w} + \epsilon)/N_\mathrm{c}} \right] e^{-j\frac{2\pi}{2N_\mathrm{c}}\upsilon\kappa'}\\
&= \frac{1}{N_\mathrm{c}\sqrt{2}} \sum_{\kappa=0}^{N_\mathrm{c}-1} S_\kappa \left[\sum_{\upsilon=0}^{N_\mathrm{c}+2N_\mathrm{w}-1} w_\upsilon e^{j2\pi\kappa(\upsilon - N_\mathrm{w} + \epsilon)/N_\mathrm{c}} \right] e^{-j\frac{2\pi}{2N_\mathrm{c}}\upsilon\kappa'} =\\
&= \frac{1}{N_\mathrm{c}\sqrt{2}} \sum_{\kappa=0}^{N_\mathrm{c}-1} S_\kappa \left[\sum_{\upsilon=0}^{N_\mathrm{c}+2N_\mathrm{w}-1} w_\upsilon e^{j\frac{4\pi\kappa(\upsilon - N_\mathrm{w} + \epsilon) - 2\pi\upsilon\kappa'}{2N_\mathrm{c}}} \right] =\\
&= \sum_{\kappa=0}^{N_\mathrm{c}-1} S_\kappa e^{j2\pi\frac{N_\mathrm{w}}{N_\mathrm{c}}\kappa} \frac{1}{N_\mathrm{c}\sqrt{2}} \left[\sum_{\upsilon=0}^{N_\mathrm{c}+2N_\mathrm{w}-1} w_\upsilon e^{j\frac{2\pi\upsilon(2\kappa + 2\epsilon - \kappa')}{2N_\mathrm{c}}} \right].
\end{aligned}$$

If the frequency offset is $\epsilon = 0$, the last sum in (A.22) becomes

$$\frac{1}{N_\mathrm{c}\sqrt{2}} \sum_{\upsilon=0}^{N_\mathrm{c}+2N_\mathrm{w}-1} w_\upsilon e^{j\frac{2\pi\upsilon(2\kappa - \kappa')}{2N_\mathrm{c}}} = \begin{cases} 0 & \text{if } 2\kappa - \kappa' \neq 0 \text{ and } \kappa' \text{ is even} \\ \frac{1}{\sqrt{2}} & \text{if } 2\kappa - \kappa' = 0 \text{ and } \kappa' \text{ is even.} \end{cases} \tag{A.23}$$

Only even elements of the sequence $Y_{\kappa'}, \kappa' = 2\kappa, \kappa = 0, \ldots, N_\mathrm{c} - 1$, represent the data received on the κth subcarrier. If $\kappa' = 2\kappa$, the received value $Y_{\kappa'}$ is given by

$$Y_{\kappa'} = \frac{1}{\sqrt{2}} S_\kappa e^{j2\pi\frac{N_\mathrm{w}}{N_\mathrm{c}}\kappa}, \tag{A.24}$$

where the exponent $e^{j(2\pi N_\mathrm{w}/N_\mathrm{c})\kappa}$ appears in due to the prefix of the length N_w.

If ϵ is not equal to zero, the CFO coefficient $I_{\kappa-\kappa'}(\epsilon)$ is given by

$$I_{\kappa-\kappa'}(\epsilon) = \frac{1}{N_\mathrm{c}\sqrt{2}} \sum_{\upsilon=0}^{N_\mathrm{c}+2N_\mathrm{w}-1} w_\upsilon e^{j\frac{2\pi\upsilon(2\kappa + 2\epsilon - \kappa')}{2N_\mathrm{c}}}. \tag{A.25}$$

The expression (A.25) for the CFO coefficient $I_{\kappa-\kappa'}(\epsilon)$ can be simplified for the rectangular window. If window is rectangular, the length of the prefix and postfix N_{w} is equal to zero and window samples are given by

$$w_\upsilon = 1, \upsilon = 0, \ldots, N_{\mathrm{c}} - 1. \tag{A.26}$$

Therefore, (A.25) can be rewritten as

$$I_{\kappa-\kappa'}(\epsilon) = \frac{1}{N_{\mathrm{c}}\sqrt{2}} \sum_{\upsilon=0}^{N_{\mathrm{c}}-1} e^{j\frac{\pi\upsilon(2\kappa+2\epsilon-\kappa')}{N_{\mathrm{c}}}}. \tag{A.27}$$

Bearing in mind the formula for the sum of a geometric series

$$1 + t + t^2 + \ldots + t^{N_{\mathrm{c}}-1} = \frac{1 - t^{N_{\mathrm{c}}}}{1 - t}, \tag{A.28}$$

the equation in (A.27) can be represented as

$$I_{\kappa-\kappa'}(\epsilon) = \frac{1}{N_{\mathrm{c}}\sqrt{2}} \frac{1 - e^{j\pi(2\kappa-2\epsilon+\kappa')}}{1 - e^{j\frac{\pi}{N_{\mathrm{c}}}(2\kappa+2\epsilon-\kappa')}}. \tag{A.29}$$

Taking into account the identity [OS89]

$$\frac{1 - e^{-j\omega N_{\mathrm{c}}}}{1 - e^{-j\omega}} = \frac{\sin\left(\frac{\omega N_{\mathrm{c}}}{2}\right)}{\sin\left(\frac{\omega}{2}\right)} e^{-j(1-N_{\mathrm{c}})\frac{\omega}{2}}, \tag{A.30}$$

the equation in (A.29) can be developed

$$I_{\kappa-\kappa'} = \frac{\sin\left(\pi\left(\kappa - \kappa'/2 + \epsilon\right)\right)}{N_{\mathrm{c}}\sqrt{2}\sin(\frac{\pi}{N_{\mathrm{c}}}(\kappa - \kappa'/2 + \epsilon))} e^{j\pi\left(1-\frac{1}{N_{\mathrm{c}}}\right)(\kappa-\kappa'/2+\epsilon)}. \tag{A.31}$$

If the frequency offset ϵ is not equal to zero and κ' is even, the expressions (A.31) and (A.25) represent the influence of the κth subcarrier on the received element κ'.

A.3 Statistical Properties of the Estimate

To investigate the statistical properties of the frequency offset estimate $\hat{\epsilon}$ we consider the elements $\zeta_{2,k}$ and $\zeta_{1,k}$ of the vectors $\boldsymbol{\zeta}_1$, and $\boldsymbol{\zeta}_2, k = 0, \ldots, \frac{N_c}{2} - 1$. First, we represent each element $\zeta_{1,k}$ as a sum of two elements

$$\zeta_{1,k} = \tilde{r}_{1,k} + \tilde{n}_{1,k}, \tag{A.32}$$

where $\tilde{r}_{1,k}$ is a noise-free part of the $\zeta_{1,k}$ and $\tilde{n}_{1,k}$ is the AWGN component with the variance σ^2.

The elements $\zeta_{2,k}, k = 0, \ldots, \frac{N_c}{2} - 1$ of the vector $\boldsymbol{\zeta}_2$ are given as

$$\zeta_{2,k} = \tilde{r}_{2,k} + \tilde{n}_{2,k}, \tag{A.33}$$

where $\tilde{r}_{2,k}$ is a noise-free part of the $\zeta_{2,k}$ and $\tilde{n}_{2,k}$ is the AWGN component.

The noise elements $\tilde{n}_{2,k}$ and $\tilde{n}_{1,k}$ are statistically independent and the following expression is valid

$$E\{|\tilde{n}_{1,k}|^2\} = E\{|\tilde{n}_{2,k}|^2\} = \sigma^2. \tag{A.34}$$

Bearing in mind the ML solution in (4.37), the tangent of the estimation error $\hat{\epsilon} - \epsilon$ is given

$$\tan(\pi(\hat{\epsilon} - \epsilon)) = \frac{\sum_{k=0}^{\frac{N_c}{2}-1} \Im\left\{(\tilde{r}_{2,k} + \tilde{n}_{2,k})(\tilde{r}^*_{1,k} + \tilde{n}^*_{1,k})e^{-j\pi\epsilon}\right\}}{\sum_{k=0}^{\frac{N_c}{2}-1} \Re\left\{(\tilde{r}_{2,k} + \tilde{n}_{2,k})(\tilde{r}^*_{1,k} + \tilde{n}^*_{1,k})e^{-j\pi\epsilon}\right\}}. \tag{A.35}$$

For the large values of SNR, the products containing $\tilde{n}^*_{2,k}\tilde{n}_{1,k}$ can be neglected. If $|\hat{\epsilon} - \epsilon| \ll \frac{1}{2\pi}$, the tangent can be approximated by its argument so that

$$\hat{\epsilon} - \epsilon \approx \frac{1}{\pi} \frac{\sum_{k=0}^{\frac{N_c}{2}-1} \Im\left\{(\tilde{r}_{2,k}\tilde{n}^*_{1,k} + \tilde{r}^*_{1,k}\tilde{n}_{2,k})e^{-j\pi\epsilon}\right\}}{\sum_{k=0}^{\frac{N_c}{2}-1} \Re\{\tilde{r}_{2,k}\tilde{r}^*_{1,k}e^{-j\pi\epsilon}\}}. \tag{A.36}$$

Close inspection of (A.36) reveals that addends in the nominator are multiplied by the noise elements $\tilde{n}^*_{1,k}$ and $\tilde{n}_{2,k}$, which have a mean value equal to zero. Therefore, the conditional expectation [Pap02] of the estimation error $\hat{\epsilon} - \epsilon$ is given by

$$E\left\{\hat{\epsilon} - \epsilon|\epsilon\right\} = 0, \tag{A.37}$$

which proofs that the frequency offset estimate $\hat{\epsilon}$ is conditionally unbiased for the small values of ϵ.

Thus, the conditional variance of the frequency offset estimate $\hat{\epsilon}$ can be expressed

$$\sigma^2_\epsilon = E\{\hat{\epsilon}^2|\epsilon\} \approx \left(\frac{1}{\pi}\right)^2 \frac{\sum_{k=0}^{\frac{N_c}{2}-1} \left(E\{|\tilde{r}_{2,k}|^2\}\frac{E\{|\tilde{n}_{1,k}|^2\}}{2} + E\{|\tilde{r}_{1,k}|^2\}\frac{E\{|\tilde{n}_{2,k}|^2\}}{2}\right)}{\sum_{k=0}^{\frac{N_c}{2}-1} E\{|\tilde{r}_{2,k}|^2|\}E\{|\tilde{r}_{1,k}|^2\}}. \tag{A.38}$$

Bearing in mind that

$$E\{(\tilde{r}_{2,k})^2\} = E\{|\tilde{r}_{1,k}|^2\} = P \cdot E\{|d_q|^2\}/K, \tag{A.39}$$

$N_{\mathrm{c}} = KL$ and taking into account (A.34), the expression (A.38) can be simplified

$$\sigma_\epsilon^2 = E\{\hat{\epsilon}^2|\epsilon\} \approx \left(\frac{1}{\pi}\right)^2 \frac{1}{\frac{E\{|d_q|^2\}}{\sigma^2} LP}. \tag{A.40}$$

The SNR per data symbol is defined as $\mu = \frac{E\{|d|^2\}}{\sigma^2}$ in (5.15). Therefore, the conditional variance of the frequency offset estimate σ_ϵ^2 can be expressed as

$$\sigma_\epsilon^2 \approx \left(\frac{1}{\pi}\right)^2 \frac{1}{\mu LP}. \tag{A.41}$$

Bibliography

[4MO06] IST 4MORE project, 2006. web site: http://www.ist-4more.org.

[AL87] M. Alard and R. Lassalle. Principles of modulation and channel coding for digital broadcasting for mobile receivers. *EBU Technical Review*, (224):168–190, Aug. 1987.

[Ala98] S.M Alamouti. A simple transmit diversity techniques for wireless communications. *IEEE Journal on Selected Areas in Communications*, 16:1451–1458, Oct. 1998.

[AMAS02] H. Atarashi, N. Maeda, S. Abeta, and M. Sawahashi. Broadband packet wireless access based on VSF-OFCDM and MC/DS-CDMA. *IEEE International Symposium on Personal, Indoor and Mobile Radio Communications (PIMPRC'02), Lisboa, Portugal*, 3:992– 997, Sep. 2002.

[Arm01] A.G. Armada. Understanding the effects of phase noise in orthogonal frequency division multiplexing (OFDM). *IEEE Transactions on Broadcasting*, 47:153–159, Jun. 2001.

[AS03] H. Atarashi and M. Sawahashi. Broadband wireless access based on VSF-OFCDM and VSCRF-CDMA and its experiments. *Multi-Carrier Spread Spectrum & Related Topics Workshop (MC-SS'03), Oberpfaffenhofen, Germany*, Sep. 2003.

[BDN05] F. Berens, Y. Durand, and F. Nouvel. Designing a multiple antenna MC-CDMA SoC for beyond 3G applications. *Embedded System Conference - 2005, San Francisco, CA, USA*, Mar. 2005.

[BEL03] A. Bury, J. Egle, and J. Lindner. Diversity comparison of spreading transforms for multicarrier spread spectrum transmission. *IEEE Transactions on Communications*, 51(5):774–787, May 2003.

[Bin90] J.A.C. Bingham. Multicarrier modulation for data transmission: An idea whose time has come. *IEEE Communications Magazine*, 28:5–14, May 1990.

[BL00] A. Bury and J. Lindner. Comparison of amplitude distribution for Hadamard spreading and Fourier spreading in multi-carrier code division multiplexing. *IEEE Global Telecommunications Conference (GLOBECOM'00), San Francisco, CA, USA*, pages 857–860, Nov./Dec. 2000.

[BR98] K. Bruninghaus and H. Rohling. Multi-carrier spread-spectrum and its relation to single-carrier transmission. *IEEE Vehicular Technology Conference (VTC-Fall'98), Ottawa, Canada*, 1998.

[Bro03] I. De Broeck. *Untersuchung von Interleaved FDMA in der Mobilfunkübertragung*. Dissertation, Technische Universität Darmstadt, Sep. 2003.

[BS99] A.R.S. Bahai and B.R. Salzberg. *Multi-carrier digital communications: theory and applications of OFDM*. Kluwer Academic/Plenum, 1999.

[BT07] N.C. Beaulieu and P. Tan. On the effects of receiver windowing on OFDM performance in the presence of carrier frequency offset. *IEEE Transactions on Wireless Communications*, 6:202–209, Jan. 2007.

[Bur01] A. Bury. *Efficient Multi-Carrier Spread Spectrum Transmission*. PhD thesis, Düsseldorf: VDI Verlag, Fortschritt-Berichte VDI, series 10, no. 685, 2001.

[BV98] J. Boutros and E. Viterbo. Signal space diversity: a power- and bandwidth-efficient diversity technique for the Rayleigh fading channel. *IEEE Transactions on Information Theory*, 44:1453–1467, Jul. 1998.

[Ċ05] I. Ċosovič. *Uplink Multi-Carrier CDMA Mobile Radio Systems*. Mediagraf 2005, Belgrade, 2005.

[Cen05] IEEE History Center. *Popov's Contribution to the Development of Wireless Communication*. IEEE, 2005. web page: http://www.ieee.org/web/aboutus/history_center/popov.html.

[Cen06] IEEE History Center. *Nikola Tesla*. IEEE, 2006. web page: http://www.ieee.org/web/aboutus/history_center/tesla.html.

[CEPA02] S. Coleri, M. Ergen, A. Puri, and A.Bahai. Channel estimation techniques based on pilot arrangement in OFDM systems. *IEEE Transactions on Broadcasting*, 48(3):223–229, Sep. 2002.

[Con06a] 4MORE Consortium. Further theoretical studies on MIMO MC-SS techniques. *4MORE Deliverable D1.5*, Jun. 2006.

[Con06b] WINNER Consortium. The WINNER II air interface: Refined multiple access concepts. *WINNER Deliverable D4.6.1*, Nov. 2006. web site: https://www.ist-winner.org/WINNER2-Deliverables/D4.6.1.pdf.

[Con06c] WINNER Consortium. Winner II interim channel models. *WINNER Deliverable D1.1.1 V1.1*, Nov. 2006. web site: https://www.ist-winner.org/WINNER2-Deliverables/D1.1.1.pdf.

[Cou93] Leon W. Couch. *Digital And Analog Communication Systems*. Macmillian Publishing Company, New York; 4th edition, 1993.

[CSM95] F. Classen, M. Speth, and H. Meyr. Channel estimation unit for an OFDM system suitable for mobile communications. *ITG Conference on Mobile Radio, Neu-Ulm, Germany*, pages 5–14, Sep. 1995.

[CTY03] Z. Cao, U. Tureli, and Y.Yao. Efficient structure-based carrier frequency offset estimation for interleaved OFDMA uplink. *IEEE International Conference on Communications (ICC'03), Anchorage, USA*, May 2003.

[DK99] A. Dekorsy and K.-D. Kammeyer. A new OFDMA-CDMA uplink concept with M-array orthogonal modulation. *European Transaction on Telecommunications (ETT)*, 10, Jul/Aug. 1999.

[DK01] A. Dammann and S. Kaiser. Standard conformable antenna diversity techniques for OFDM and its application to the DVB-T system. *IEEE Global Telecommunications Conference (GLOBECOM'01), San Antonio, TX, USA*, 5:3100–3105, Nov. 2001.

[FA02] D. Falconer and S. L. Ariyavisitakul. Frequency domain equalization for single-carrier broadband wireless systems. *White Paper*, Feb. 2002. web page: http://www.sce.carleton.ca/bbw/papers/whitepaper2.pdf.

[Fet03] G. Fettweis. WIGWAM- wireless gigabit with advanced multimedia support. *Wireless World Research Forum (WWRF), New York, USA*, Oct. 2003.

[FK00] K. Fazel and S. Kaiser. *Multi-carrier and spread spectrum systems*. John Wiley and Sons, 2000.

[For06] WiMAX Forum. Mobile WiMAX part I: A technical overview and performance evaluation. Aug. 2006. web site: http://www.wimaxforum.org/technology/downloads/.

[GA02] D.L. Goeckel and G. Ananthaswamy. On the design of multidimensional signal set for OFDM systems. *IEEE Transactions on Communications*, 50(3):442–452, Mar. 2002.

[GR00] D. Galda and H. Rohling. A low complexity transmitter structure for OFDMA-FDMA uplink systems. *IEEE Global Telecommunications Conference (GLOBECOM'00), San Francisco, CA, USA*, pages 857–860, Nov./Dec. 2000.

[GSM07] GSMA. *How to realize the benefits of mobile broadband today*. GSM Association, Feb. 2007. web page: http://hspa.gsmworld.com/upload/news/files/26022007162724.pdf.

[Haa03] E. Haas. *Design, Evaluation and Implementation of a Multi-Carrier Transmission System for Aeronautical Communications*. PhD thesis, Herbert Utz Verlag GmbH, Munich, Germany, 2003.

[Hay86] S. Haykin. *Adaptive filter theory*. Prentice-Hall, Englewood Cliffs, New Jersey, 1986.

[HL05] D. Huang and K.B Letaief. An interference-cancellation scheme for carrier frequency offsets correction in OFDMA systems. *IEEE Transactions on Communications*, 53(7):1155– 1165, Jul. 2005.

[HSR97] P. Höher, S.Kaiser, and P. Robertson. Pilot-symbol-aided channel estimation in time and frequency. *IEEE Global Telecommunications Conference (GLOBECOM'97), Phoenix, USA*, pages 90–96, Nov. 1997.

[ITU03] ITU. *Framework and overall objectives of the future development of IMT and systems beyond IMT-2000*. ITU Recommendation ITU-R M.1645, Jun. 2003. web page: http://www.ieee802.org/18/Meeting_documents/2007_Jan/R-REC-M.1645-0-200306-I!!MSW-E.doc.

[Kai95] S. Kaiser. Analytical performance evaluation of OFDM-CDMA mobile radio systems. *European Personal and Mobile Communication Conference (EPMCC'95), Bologna, Italien*, Nov. 1995.

[Kai98] S. Kaiser. *Multi-Carrier CDMA Mobile Radio Systems - Analysis and Optimization of Detection, Decoding and Channel Estimation*. PhD thesis, Düsseldorf: VDI Verlag, Fortschritt-Berichte VDI, series 10, no. 531, 1998.

[Kai00a] S. Kaiser. Spatial transmit diversity techniques for broadband OFDM systems. *IEEE Global Telecommunications Conference, (GLOBECOM'00), San Francisco, CA, USA*, 3:1824–1828, Nov. 2000.

[Kai00b] S. Kaiser. OFDM with code division multiplexing and transmit antenna diversity for mobile communications. *IEEE International Symposium on Personal, Indoor and Mobile Radio Communications (PIMRC'00), London, UK*, 3:804–808, Sep. 2000.

[Kai02] S. Kaiser. OFDM code division multiplexing in fading channels. *IEEE Transactions on Communications*, 50, no. 8:1266–1273, Aug. 2002.

[KDL+04] S. Kaiser, Y. Durand, L.Herault, I.-F. Helard, D.Mottier, A.Gameiro, J.Rodriguez, C.Barquinero, F.Berenz, F.Bauer, R.Rabineau, and F.J. Casajus. 4G MC-CDMA multi antenna system on chip for radio enhancements (4MORE). *IST Mobile & Wireless Communications Summit (IST'04), Lyon, France*, Jun. 2004.

[LH05] L.Cariou and J.-F. Hélard. MIMO frequency hopping spread spectrum multi-carrier multiple access: a novel uplink system for B3G cellular networks. *Telecommunications Systems*, 30(1-3):193–214, Nov. 2005. http://4more.av.it.pt/publications/IETR_journal06.pdf.

[LXG02] Z. Liu, Y. Xin, and G. Giannakis. Space-time-frequency coded OFDM over frequency-selective fading channels. *IEEE Transactions on Signal Processing*, 50(10):2465–2476, 2002.

[MAT03] IST MATRICE project, 2003. web site: http://www.ist-matrice.org.

[MM99] M. Morelli and U. Mengali. An improved frequency offset estimator for OFDM applications. *IEEE Communications Letters*, 3(3):75–77, Mar. 1999.

[Moo94] P.H. Moose. A technique for orthogonal frequency division multiplexing frequency offset correction. *IEEE Transactions on Communications*, 42:2908–2914, Oct. 1994.

[Mor04] M. Morelli. Timing and frequency synchronization for the uplink of an OFDMA system. *IEEE Transactions on Communications*, 52, no. 2:286–306, Feb. 2004.

[Mus96] C. Muschallik. Improving an OFDM reception using an adaptive Nyquist windowing. *IEEE Transactions on Consumer Electronics*, 42:259–269, Aug. 1996.

[MW01] S.H Muller-Weinfurtner. Optimum Nyquist windowing in OFDM receivers. *IEEE Transactions on Communications*, 49:417–420, Mar. 2001.

[MZB00] H. Minn, M. Zeng, and V.K. Bhargava. On timing offset estimation for OFDM systems. *IEEE Communications Letters*, 4(7):242–244, Jul. 2000.

[NHM02] S. Nobilet, J.-F. Helard, and D. Mottier. Spreading sequences for uplink and downlink MC-CDMA systems: PAPR and MAI reduction. *European Transactions on Telecommunications (ETT)*, 13:465–474, Sep./Oct. 2002.

[NP02] R.V. Nee and R. Prasad. *OFDM for Wireless Multimedia Communications*. Artech House, 2002.

[Ono07] S. Onoe. *4G in Japan, Status and Performance Prospects. 4G - the road ahead. Plenary Session*. IST Mobile and Wireless Communications Summit (IST'07), Budapest, Hungary, Jul. 2007.

[OS89] A. Oppenheim and R. Schafer. *Digital Signal Processing*. Prentice-Hall, 1989.

[Pae02] M. Paetzold. *Mobile Fading Channels*. John Wiley and Sons, 2002.

[Pap02] A. Papoulis. *Probability, Random Variables, and Stochastic Processes*. McGraw-Hill, New York; 4th edition, 2002.

[PM96] J.G Proakis and D.G. Manolakis. *Digital Signal Processing. Principles, Algorithms and Applications*. Prentice-Hall, Inc., 1996.

[PMK05] M.O. Pun, M. Morelli, and C.-C. J. Kuo. A novel iterative receiver for uplink OFDMA. *IEEE Global Telecommunications Conference, (GLOBECOM'05), St. Louis, MI, USA*, 6:2669–2673, Nov. 2005.

[Pro00] J. Proakis. *Digital Communications*. McGraw Hill Higher Education, Dec. 2000.

[PSM94] T. Pollet, P. Spruyt, and M. Moeneclaey. The BER performance of OFDM systems using non-synchronized sampling. *IEEE Global Telecommunications Conference, 1994. (GLOBECOM'94), San Francisco, CA* , 1:253–257, Dec. 1994.

[PTK04] M.O. Pun, S.H. Thai, and C.-C. J. Kuo. Joint maximum likelihood estimation of carrier frequency offset and channel for uplink OFDMA systems. *IEEE Global Telecommunications Conference, (GLOBECOM'04), Dallas, TX*, 6:3748–3752, Nov. 2004.

[Pur87] M. B. Pursley. The role of spread-spectrum in packet radio networks. *Proceedings of the IEEE*, 75(1):116–134, Jan. 1987.

[RD05] R. Raulefs and A. Dammann. Exploiting rotated spreading features for MC-CDMA. *International OFDM Workshop 2005, Hamburg, Germany*, Sep. 2005.

[RE05] D. Radovic and M. Eric. Channel impact on subspace CFO estimation for interleaved OFDMA uplink. *International OFDM Workshop 2005, Hamburg, Germany*, 6, Sep. 2005.

[SA00] M. K. Simon and M.-S. Alouini. *Digital Communications over Fading Channels*. John Wiley and Sons, Inc, 2000.

[SBS98] U. Sorger, I.De Broeck, and M. Schnell. Interleaved FDMA - a new spread-spectrum multiple-access scheme. *IEEE International Conference on Communications (ICC'98), Atlanta,GA,USA*, pages 1013–1017, June.1998.

[SBS99] M. Schnell, I. De Broeck, and U. Sorger. A promising new wideband multiple-access scheme for future mobile communications systems. *European Transactions on Telecommunications (ETT)*, 10, No. 4:417–427, Jul./Aug. 1999.

[SC97] T.M. Schmidl and D.C. Cox. Robust frequency and timing synchronization for OFDM. *IEEE Transactions on Communications*, 45:1613–1621, Dec. 1997.

[Sch02] L.L. Scharf. *Statistical Signal Processing. Detection Estimation and Time Series Analysis*. Addison-Wesley Publishing Company, 2002.

[SFF+07] T. Svensson, T. Frank, D. Falconer, M. Sternad, E. Costa, and A. Klein. B-IFDMA - a power efficient multiple access scheme for non-frequency-adaptive transmission. *IST Mobile & Wireless Communications Summit (IST'07), Budapest, Hungary*, Jul. 2007.

[SFSA05] M. Sternad, S. Falahati, T. Svensson, and D. Aronsson. Adaptive TDMA/OFDMA for wide-area coverage and vehicular velocities. *IST Mobile & Wireless Comminication Summit (IST'05), Dresden, Germany*, Jun. 2005.

[SL05] R. Song and S.-H. Leung. A novel OFDM receiver with second order polynomial Nyquist function. *IEEE Communications Letters*, 9(5):391–393, May 2005.

[Ste94] R. Steele. *Mobile Radio Communications*. Pentech Press, London, 1994.

[Ste00] H. Steendam. *The Effect of Synchronization Errors on Multicarrier Systems*. PhD thesis, Ghent University, Netherlands, 2000.

[Str06] *Beyond 3G: Looking for True Mobile Broadband*. Strategy Analytics, Nov. 2006.

[TB04] P. Tan and N.C Beaulieu. Reduced ICI in OFDM systems using the "better than" raised cosine pulse. *IEEE Communications Letters*, 8(3):135–137, Mar. 2004.

[TC99] TIA/EIA/IS-CDMA2000. *Physical layer standard for CDMA2000 spread spectrum systems*. Aug. 1999.

[THC99] V. Tarokh, H. H.Jafarkhani, and A.R. Calderbank. Space-time block codes from orthogonal designs. *IEEE Transactions on Information Theory*, 45:1456–1467, Jun. 1999.

[TLP00] A. M. Tonello, N. Laurenti, and S. Pupolin. On the effect of time and frequency offsets in the up-link of an asynchronous multi-user DMT OFDMA system. *International Conference on Telecommunications (ICT'00), Acapulco, Mexico*, pages 614–618, Jan. 2000.

[Vit90] A.J. Viterbi. Very low rate convolutional codes for maximum theoretical performance of spread-spectrum multiple-access channels. *IEEE Journal on Selected Areas in Communications*, 8:641–649, May 1990.

[Vit95] A. J. Viterbi. *CDMA Principles of Spread Spectrum Communication*. 1995.

[WE71] S. Weinstein and P. Ebert. Data transmission by frequency-division multiplexing using the discrete Fourier transform. *IEEE Transactions on Communications*, 19(5):628–634, Oct. 1971.

[Wig07] WIGWAM project, 2007. web site: http://www.wigwam-project.com/.

[Wim07] IEEE 802.16 Published Standards and Drafts, 2007. web site: http://grouper.ieee.org/groups/802/16/published.html.

[WIN03] IST WINNER project, 2003. web site: http://www.ist-winner.org/.

[Wir99] IEEE Std 802.11a/D7.0-1999, 1999. Part 11: Wireless LAN Medium Access Control (MAC) and Physical Layer (PHY) specifications: High Speed Physical Layer in the GHz Band.

[XZG03] P. Xia, S. Zhou, and G. B. Giannakis. Bandwidth- and power-efficient multi-carrier multiple access. *IEEE Transactions on Communications*, 51(11):1828–1837, Nov. 2003.

[YH03] H. Yoo and D. Hong. Edge sidelobe suppressor scheme for OFDMA uplink systems. *IEEE Communications Letters*, 7(11):534–536, Nov. 2003.

[ZF04] E. Zimmermann and G. Fettweis. Scenario specification for gigabit wireless. *Wireless World Research Forum (WWRF), Beijing, China*, Feb. 2004.

Publications of the Author

[ARS05a] A. Arkhipov, R. Raulefs, and M. Schnell. Advantages of superimposed packets allocation for CDM-OFDMA. *IEEE Vehicular Technology Conference (VTC-Spring'05), Stockholm, Sweden*, May. 2005.

[ARS05b] A. Arkhipov, R. Raulefs, and M. Schnell. Combination of H-ARQ and iterative multiuser detection for OFDMA-CDM. *5th. International Workshop Multi-Carrier Spread Spectrum & Related Topics (MC-SS'05), Oberpfaffenhofen, Germany*, pages 371–382, Sep. 2005.

[ARS06] A. Arkhipov, R. Raulefs, and M. Schnell. OFDMA-CDM performnce enhancement by combining H-ARQ and interference cancellation. *IEEE Journal on Selected Areas in Communications*, 24(6):1199–1207, Jun. 2006.

[AS] A. Arkhipov and M. Schnell. Frequency offset estimation for IFDMA uplink systems. *IEEE Global Telecommunications Conference (GLOBECOM'06), San Francisco, California, USA.*

[AS03] A. Arkhipov and M. Schnell. The influence of user frequency offset on the up-link performance of SS-MC-MA. *European Conference on Wireless Technology (ECWT'03), Munich, Germany*, 2003.

[AS04a] A. Arkhipov and M. Schnell. Performance evaluation of SS-MC-MA up-link transmission with user frequency offsets. *European Wireless (EW'04), Barcelona, Spain*, Oct. 2004.

[AS04b] A. Arkhipov and M. Schnell. Interleaved frequency-division multiple-access system with frequency domain equalization. *International OFDM Workshop 2004, Dresden, Germany*, Sep. 2004.

[AS06] A. Arkhipov and M. Schnell. Practical algorithm for sampling time offset estimation in IFDMA uplink systems. *IEEE Transactions on Wireless Communications*, 2006. Submitted.

[AS07a] A. Arkhipov and M. Schnell. Sampling time offset estimation in IFDMA uplink systems. *IST Mobile & Wireless Communications Summit (IST'07), Budapest, Hungary*, Jul. 2007.

[AS07b] A. Arkhipov and M. Schnell. Suppression of ISI caused by sampling time offset in IFDMA systems. *IST Mobile & Wireless Communications Summit (IST'07), Budapest, Hungary*, Jul. 2007.

[CAS04] I. Cosovic, A. Arkhipov, and M. Schnell. Pre-equalization in combination with transmit diversity for OFDMA code-division multiplexing systems in fading channels. *IEEE Vehicular Technology Conference VTC-Spring'04, Milan, Italy*, May 2004.

[EARK05] R. Elliott, A. Arkhipov, R. Raulefs, and W.A. Krzymien. Effective SINR mapping for an MC-CDMA system. *5th. Workshop Multi-Carrier Spread Spectrum & Related Topics (MC-SS'05), Oberpfaffenhofen, Germany*, pages 361–370, Sep. 2005.

[HAB+02] E. Haas, A.Arkhipov, B.Kunz, H.Lang, F.Pupeter, and M.Schnell. Der "Advanced Airport Data Link" - Konzept und Demonstrator für einen modernen Flughafen-Datenlink. *DGLR-Workshop Data Link und Informationsmanagement, Münich, Deutschland*, Mai 2002.

[HKH+01] E. Haas, B. Kunz, H.Lang, F.Pupeter, A.Arkhipov, and M.Schnell. Demonstration: Multicarrier CDMA system for aeronautical communications. *3rd. International Workshop on Multi-Carrier Spread-Spectrum & Related Topics (MC-SS'01), Oberpfaffenhofen, Germany*, Sep 2001.

Abbreviations and Symbols

Abbreviations

3GPP	3rd Generation Partnership Project
4MORE	4G MC-CDMA Multiple Antenna System on Chip for Radio Enhancement
BER	bit error rate
BS	base station
CDF	cumulative distribution function
CDM	code-division multiplexing
CDMA	code-division multiple-access
CFO	carrier frequency offset
DFE	decision-feedback equalizer
DFT	discrete Fourier transform
DS-CDMA	direct sequence CDMA
EGC	equal gain combining
EV-DO	Evolution- Data Optimized
FD	frequency domain
FDM	frequency-division multiplexing
FDMA	frequency-division multiple-access
FFT	fast Fourier transform
FIR	finite impulse response
FOMA	Freedom Of Mobile multimedia Access
GOQPSK	Gaussian-shaped offset QPSK
HSDPA	High Speed Downlink Packet Access

HSOPA	High Speed OFDM Packet Access
HSPA	High Speed Packet Access
HSUPA	High Speed Uplink Packet Access
IBO	input back-off
IDFT	inverse discrete Fourier transform
IEEE	institute of electrical and electronics engineers
IFDMA	interleaved frequency-division multiple-access
IFFT	inverse fast Fourier transform
IMT-2000	International Mobile Telecommunications-2000
IST	European Information Society Technology
ITU	International Telecommunications Union
LE	linear equalization
LTE	Long Term Evolution
LTWTA	linearized traveling wave tube amplifier
MC-CDMA	Multi-Carrier CDMA
MIMO	multiple-input multiple-output
MRC	maximum ratio combining
MSK	minimum shift keying
MT	mobile terminal
NLA	non-linear power amplifier
OBO	output back-off
OFDMA	orthogonal frequency-division multiple-access
OFDMA-CDM	OFDMA code-division multiplexing
PAPR	peak-to-average power ratio
QAM	quadrature amplitude modulation
QPSK	quadrature phase-shift keying
RC	raised cosine
S/P	serial-to-parallel
SC-FDE	single-carrier with frequency domain equalization

SED	spectral energy density
SI	self-interference
SIC	soft interference cancelation
SIR	signal-to-interference ratio
SNR	signal-to-noise ratio
TD	time domain
TD-SCDMA	Time Division - Synchronous CDMA
TDMA	time-division multiple-access
UMB	Ultra Mobile Broadband
UMTS	Universal Mobile Telecommunication System
VSF-CDMA	Variable Spreading Factor CDMA
VSF-OFCDM	Variable Spreading Factor Orthogonal Frequency and Code Division Multiplexing
W-CDMA	Wideband CDMA
WH	Walsh-Hadamard
WIGWAM	WIreless Gigabit With Advanced Multimedia
WSSUS	wide sense stationary uncorrelated scattering
ZF	zero forcing

Symbols

$(.)^*$	complex conjugation
$(.)^H$	Hermitian transpose of a vector or a matrix
$(.)^T$	transposition of a vector or a matrix
$(.)^{(i)}$	value of ith user
$(.)^{-1}$	inversion
$*$	linear convolution
$\Im\{.\}$	imaginary part of a complex number
∞	infinity
$\lceil x \rceil$	smallest integer larger or equal to x

$\max\{.\}$	maximum value in an array or in a function
$\Pr\{x\}$	probability of x
$\Re\{.\}$	real part of a complex number
$E\{.\}$	mean value

Variables

B	3 dB bandwidth of the Gaussian pulse-shaping function
BW	bandwidth of an OFDM symbol
$\mathbf{b}^{(i)}$	bit sequence of the ith user at the output of a channel encoder
β	roll-off factor of the window function $w(t)$
$\bar{C}_{\mu}^{(i \bmod P_\mathrm{p})}$	μth element of the vector $\bar{\mathbf{C}}_{\mu}^{(i \bmod P_\mathrm{p})}$
$\underline{\mathbf{C}}_L$	WH matrix of the size $L \times L$
$\mathbf{C}_n$	Fourier code of length L
$\bar{\mathbf{C}}^{(i \bmod P_\mathrm{p})}$	$(i \bmod P_\mathrm{p})$th WH code of length P_p
$\hat{d}_q^{(i)}$	estimate of the qth data symbol of the ith user
$d_n^{(i)}$	nth complex-valued data symbol of the ith user
$\mathbf{d}^{(i)}$	vector representing L data symbols $d_q^{(i)}$ of the ith user transmitted within one OFDM symbol
$\delta(t)$	Kronecker delta function
$\epsilon^{(i)}$	frequency offset of the ith user normalized to the subcarrier spacing Δf
ϵ_max	maximum frequency offset
$\hat{\epsilon}$	estimation of the normalized frequency offset ϵ
$\tilde{\epsilon}$	trial variable
$\varepsilon^{(i)}$	frequency offset of the ith user (Hz)
E_κ	κth diagonal element of $\underline{\mathbf{E}}$
E_rx	energy of the useful part of equalized symbol
$\underline{\mathbf{E}}^{(i)}$	equalization matrix of the ith user
$f_l^{(i)}$	lth diagonal element of the matrix $\underline{\mathbf{f}}^{(i)}$

$\underline{\mathbf{f}}^{(i)}$	diagonal matrix of user frequency offset of the ith user
Δf	subcarrier spacing
f_κ	the κth subcarrier frequency
$g(t)$	pulse-shaping function
$G(f)$	frequency domain representation of $g(t)$
$h(\tilde{t}, t)$	time-variant channel impulse response
$h_m^{(i)}$	mth element of the CIR vector $\breve{\mathbf{h}}^{(i)}$
$H_{\mathrm{r},n}$	nth element of the vector $\mathbf{H}_\mathrm{r}$
$\mathbf{H}_\mathrm{r}$	vector of fading coefficients of the ith user
$\underline{\mathbf{H}}^{(i)}$	channel matrix in the frequency domain
$\breve{\mathbf{h}}^{(i)}$	channel impulse response of the ith user
$\hat{\mathbf{H}}$	estimation of the vector $\mathbf{H}_\mathrm{r}$
$I_\kappa(\epsilon)$	CFO coefficient as a function of ϵ
IBO	input back-off
K	maximum allowed number of users
L	spreading length
μ_b	SNR per bit
μ	SNR per data symbol
M	M-modification coefficient
MSE	minimum square error
N_f	length of the pulse-shaping function $g(t)$
N_ov	oversampling coefficient
N_u	number of active users
N_w	length of the prefix and postfix
$n(t)$	additive white gaussian noise
N_Δ	length of the guard interval
N_κ	frequency domain noise component on the κth subcarrier
N_frame	number of OFDM symbols in an OFDM frame
$\mathbf{N}$	frequency domain representation of the vector $\mathbf{n}$

$\mathbf{n}$	noise vector before detection
OBO	output back-off
$\mathbf{\Omega}$	modulation alphabet
P	average power of $x(t)$
P_{b}	BER of the uncoded system
P_{p}	number of pilot symbols
P_{satout}	output saturation power
P_{sat}	input saturation power
$\varphi_{\mathrm{amp}}(t)$	additional phase modulation caused by the NLA
$\Psi_{n,l}$	element of the matrix $\underline{\mathbf{\Psi}}$
$\underline{\mathbf{\Psi}}$	matrix of CFO coefficients
R_{c}	code rate
R_κ	κth element of $\mathbf{R}$
$\mathbf{R}$	vector representing the received sequence at the output of linear equalization block
σ^2	variance of the noise
$\sigma^2_{\mathrm{noise}}$	variance of the noise after linear equalization
$\sigma^2_{\mathrm{SI,OFDMA\text{-}CDM}}$	variance of the SI in OFDMA-CDM
σ^2_{SI}	variance of the SI in IFDMA
SIR	signal-to-interference ratio
$\sigma^2{}_\epsilon$	conditional variance of the estimate $\hat{\epsilon}$
$\bar{S}_\kappa^{(i)}$	pilot symbol of the ith user transmitted on the κth subcarrier
$S_\kappa^{(i)}$	κth source symbol of the ith user
τ_{max}	maximum delay of the channel impulse response $h(\tilde{t}, t)$
T	OFDM symbol duration excluding prefix, postfix and guard interval
T'	OFDM symbol duration including prefix, postfix and guard interval
T_{e}	duration of spreading code element
T_{frame}	OFDM frame duration
$\underline{\mathbf{\Theta}}(\tilde{\epsilon})$	$2L \times L$-dimensional matrix composed of CFO coefficients
T_Δ	duration of the guard interval

w_υ	υth sample of the window function $w(t)$
V_g	energy loss due to the guard interval, postfix and prefix
$W(f)$	frequency domain representation of $w(t)$
$w(t)$	window function
$\underline{\mathbf{w}}$	diagonal matrix representing the window function $w(t)$
$X_\mathrm{w}(t)$	frequency domain representation of $x(t)$ with $\delta(t)$ as a pulse-shaping function
$X(f)$	frequency domain representation (transmit spectrum) of $x(t)$
$x(t)$	complex-valued envelope of an OFDM symbol
x_υ	υth sample of $x(t)$
$x_\infty(t)$	infinite complex-valued envelope of an OFDM symbol
$x_\mathrm{amp}(t)$	signal at the output of NLA
x_max	maximum amplitude value of an IFDMA signal
$\bar{x}_{\mu,l}^{(i)}$	lth element of $\bar{\mathbf{x}}_\mu^{(i)}$
$\bar{x}_l^{(i)}$	lth element of $\bar{\mathbf{x}}^{(i)}$
$x_{\mathrm{w},\upsilon}$	υth sample obtained after IDFT operation in the OFDM transmitter
$\mathbf{x}^{(i)}$	vector representing transmit time domain signal of the ith user
$\bar{\mathbf{X}}$	vector representing the known pilot sequence of the ith user in the frequency domain
$\bar{\mathbf{x}}^{(i)}$	vector representing the known transmitted pilot sequence of the ith user
$\bar{y}_k^{(i)}$	kth element of the vector $\bar{\mathbf{y}}^{(i)}$
$y(t)$	received complex-valued waveform
y_υ	υth sample of $y(t)$
$\mathbf{Y}$	frequency domain representation of the received vector $\mathbf{y}$
$y_{\mathrm{w},\upsilon}$	υth sample obtained after windowing operation and adding of zeros in the OFDM receiver
$\tilde{\mathbf{Y}}$	received vector composed of $2N_\mathrm{c}$ values $Y_{\kappa'}$
$\bar{Y}_{nK+i}^{(i)}$	$(nK+i)$th element of the vector $\bar{\mathbf{Y}}^{(i)}$
$\mathbf{y}$	vector representing the received time domain signal
$\bar{\mathbf{y}}_\mu$	vector representing the μth received pilot in time domain
$\bar{\mathbf{Y}}^{(i)}$	vector representing the received pilot sequence of the ith user after reduction of MAI

$\bar{\mathbf{y}}^{(i)}$	vector representing the known received pilot sequence of the ith user
$\bar{\mathbf{Y}}_{\mu}$	vector representing the μth received pilot in frequency domain
$\bar{\mathbf{Y}}_{\mathrm{r}}$	auxiliary vector of length $2L$ composed of the received values of users i and $i+1$
$\zeta_{1,k}$	kth element of the vector $\boldsymbol{\zeta}_1$
$\zeta_{2,k}$	kth element of the vector $\boldsymbol{\zeta}_2$
$\boldsymbol{\zeta}_1$	vector composed of the first $\frac{N_{\mathrm{c}}}{2}$ elements of the vector $\bar{\mathbf{y}}^{(i)}$
$\boldsymbol{\zeta}_2$	vector composed of the last $\frac{N_{\mathrm{c}}}{2}$ elements of the vector $\bar{\mathbf{y}}^{(i)}$